

Old Dominion University

## ODU Digital Commons

---

Mechanical & Aerospace Engineering Theses & Dissertations

Mechanical & Aerospace Engineering

---

Summer 8-2022

# The Effect of Soft Tissue and Bone Morphology on the Stresses in the Foot and Ankle

Jinhyuk Kim

*Old Dominion University*, [jinhyuk.kim06@gmail.com](mailto:jinhyuk.kim06@gmail.com)

Follow this and additional works at: [https://digitalcommons.odu.edu/mae\\_etds](https://digitalcommons.odu.edu/mae_etds)



Part of the [Biomedical Engineering and Bioengineering Commons](#), and the [Mechanical Engineering Commons](#)

---

### Recommended Citation

Kim, Jinhyuk. "The Effect of Soft Tissue and Bone Morphology on the Stresses in the Foot and Ankle" (2022). Doctor of Philosophy (PhD), Dissertation, Mechanical & Aerospace Engineering, Old Dominion University, DOI: 10.25777/j92k-hd59

[https://digitalcommons.odu.edu/mae\\_etds/352](https://digitalcommons.odu.edu/mae_etds/352)

This Dissertation is brought to you for free and open access by the Mechanical & Aerospace Engineering at ODU Digital Commons. It has been accepted for inclusion in Mechanical & Aerospace Engineering Theses & Dissertations by an authorized administrator of ODU Digital Commons. For more information, please contact [digitalcommons@odu.edu](mailto:digitalcommons@odu.edu).

**THE EFFECT OF SOFT TISSUE AND BONE MORPHOLOGY ON THE  
STRESSES IN THE FOOT AND ANKLE**

by

Jinhyuk Kim

B.S.M.E. May 2014, Old Dominion University  
M.S.M.E. August 2017, Old Dominion University

A Dissertation Submitted to the Faculty of  
Old Dominion University in Partial Fulfillment of the  
Requirements for the Degree of

DOCTOR OF PHILOSOPHY

MECHANICAL ENGINEERING

OLD DOMINION UNIVERSITY  
August 2022

Approved by:

Stacie I. Ringleb (Director)

Sebastian Y. Bawab (Member)

Hunter Jared Bennett (Member)

Krishnanand N. Kaipa (Member)

## **ABSTRACT**

### **THE EFFECT OF SOFT TISSUE AND BONE MORPHOLOGY ON THE STRESSES IN THE FOOT AND ANKLE**

Jinhyuk Kim

Old Dominion University, 2022

Director: Dr. Stacie I. Ringleb

The foot and ankle interface with the ground, thus they absorb reaction forces and initiate load distribution through the body. The plantar fascia (PF) is a flexible structure that absorbs reaction forces and distributes loading across the foot. It is frequently a source of foot pain especially when people have plantar fasciitis and/or diabetes mellitus. Finite element (FE) models of the foot and ankle were created to examine the function however, the plantar fascia is frequently modeled as a 1D tension only spring, which does not represent variations caused by injury and/or disease.

As models move toward being patient specific, understanding what components of a model can be generic versus what should be patient specific is critical when minimizing the time to create and simulate results. The purpose of this dissertation was to develop 3D finite element foot and ankle models including different thickness of 3D solid plantar fascia (i.e., 3mm, 4mm, and 5mm) and different ankle positions (i.e., neutral position, 10° dorsiflexion, and 10° plantarflexion). Additionally, the effect of different thicknesses of cartilage (i.e., 0.5mm, 1.0mm, and 1.7mm) and bone morphology (health and injured) was investigated in a model of the talocrural joint. As the thickness of plantar fascia increased, the strains of plantar fascia were increased, and the peak plantar pressure moved from hindfoot to forefoot. Also, the peak plantar pressures were highest when the foot was in 10° of plantarflexion and lowest in the neutral position. Finally, contact area decreased with decreasing cartilage thickness, with a greater decrease in contact area in healthy ankles. In 3 models, contact stress increased as cartilage thickness decreased. The fourth model

had little decrease in contact area, thus the contact pressures may have been affected more by bone morphology. In conclusion, in models of the foot and ankle, the plantar fascia can be generic if it is less than 4 mm thick, a variety of foot positions should be considered, and specific bone morphologies should be included in the ankle if there is a known pathology.

Copyright, 2022, by Jinhyuk Kim, All Rights Reserved.

This dissertation is dedicated to my loving family who has been a constant support and encouragement during the changes of graduate school and life.

## ACKNOWLEDGEMENTS

I would like to thank Dr. Statrice Ringleb for her noble guidance and support with full encouragement and enthusiasm. She encouraged me to be a highly motivated scientist with enthusiasm. Also, she gave me in my research project the guidance and continued support for my research project.

I would also like to thank Dr. Sebastian Bawab for his encouragement, constant support, and guidance throughout my dissertation.

I would like to thank my committee member, Dr. Kaipa and Dr. Bennett, for contributing their time and expertise to writing the strong this dissertation.

I would like to thank my parents. I cannot express in some words how much my parent supported me through the past years. My accomplishment and success are because they believed in me.

I would like to thank my wife Minju , and my children, Justina and Olivia, for love and constant support. Without you, I would not be the person I am today.

## TABLE OF CONTENTS

	Page
LIST OF TABLES .....	ix
LIST OF FIGURES .....	x
Chapter	
INTRODUCTION .....	1
1.1 BACKGROUND .....	1
1.2 ANATOMY OF FOOT AND PLANTAR FASCIA .....	3
1.3 COMPUTATIONAL MODELING OF FOOT AND ANKLE .....	6
1.4 STATEMENT OF PURPOSE .....	10
THE EFFECT OF THE DIFFERENT PLANTAR FASCIA THICKNESS AND TENDON LOADING IN 3-D FINITE ELEMENT FOOT MODEL .....	13
2.1 INTRODUCTION .....	13
2.2 STATEMENT OF PURPOSE .....	14
2.3 METHODS .....	14
2.4 RESULTS .....	20
2.5 DISCUSSION .....	22
2.6 CONCLUSION .....	23
THE EFFECT OF PLANTAR FASCIA THICKNESS AT VARIOUS FOOT POSITION IN A 3-D FINITE ELEMENT FOOT MODEL .....	25
3.1 INTRODUCTION .....	25
3.2 STATEMENT OF PURPOSE .....	27
3.3 METHODS .....	28
3.4 RESULTS .....	38
3.5 DISCUSSION .....	45
3.6 CONCLUSION .....	47
THE EFFECT OF PATIENT SPECIFIC BONE GEOMETRY ON CONTACT STRESS IN 3D- FINITE ELEMNET HINDFOOT MODEL .....	49
4.1 INTRODUCTION .....	49



4.2 STATEMENT OF PURPOSE ..... 51

4.3 METHODS ..... 51

4.4 RESULTS ..... 56

4.5 DISCUSSION ..... 63

4.6 CONCLUSION..... 65

DISCUSSION AND CONCLUSION ..... 66

    5.1 LIMITATIONS..... 68

    5.2 PILOT WORKED TOWARD FUTURE WORK ..... 70

REFERENCES ..... 77

VITA..... 83

## LIST OF TABLES

Table	Page
1 The parameters for the second-order polynomial plantar soft tissue .....	7
2 The linear elastic material properties for bones, cartilage, ligament, and plantar fascia .....	8
3 The coefficients of the second order polynomial material.....	9
4 The linear elastic material properties for bones, cartilage, ligaments, and plantar fascia.....	9
5 Material properties and element types .....	19
6 The thickness of plantar fascia between control group and patient with plantar fasciitis or diabetes, which was measured in Sonographic and MRI.....	27
7 The 3D FE foot model contained a total of 542595 elements. The Each segment showed a different number of elements.....	30
8 Material properties and element types for bone, cartilage, plantar fascia, and plantar soft tissue .....	36
9 The peak stress at heel and at forefoot with three different thickness of plantar fascia in various foot positions .....	39
10 The peak stresses in the segments of FE foot model with three different thickness of plantar fascia (e.g., 3mm, 4mm, and 5mm) in three different foot positions .....	42
11 The thickness of cartilage at ankle including the measurement methods. ....	50
12 The mean thickness of cartilages in two groups, healthy and patient with ankle injuries. ....	50
13 The information about the two patients .....	52
14 The articular cartilage thickness at tibia and talus was measured in previous research.....	54
15 The material properties for all tissues .....	67
16 Linear and non-linear material properties for plantar fascia.....	69

**LIST OF FIGURES**

Figure	Page
1 The bone structure segments model of the foot. Medical and lateral view of the foot segment (a). Anatomy of the foot bone can be divided into three parts such as hind foot including talus and calcaneus, mid foot including navicular, medial cuneiform, internal cuneiform, lateral cuneiform, and cuboid and forefoot including five metatarsal and five phalanges (b). .....	4
2 Anatomic dissection showing foot bone structure, the tendons, and ligaments; Achilles tendon and plantar fascia. (a) The transverse plane foot view with plantar fascia and transverse arch. (b) The lateral view of the foot with plantar fascia and Achilles tendon with the medial longitudinal arch [44]. .....	5
3 The medical view of bone structure is similar with triangle truss structure. Two upward forces on the metatarsal head and toes, and on calcaneus show the ground reaction force, and the downward arrow shows the body weight. ....	6
4 CT scan image of cadaver foot. The foot cadaver was fixed at neutral position on foot holding devices. (a) the CT scan image in the axial plane; (b) The CT scan image in the lateral axial plane; (c) the CT scan image in the sagittal; (d) the CT scan image in the coronal. ....	15
5 The pictures show how to create the foot bony segments from CT scan images. (a) on CT scan images, the bone was created separately. (b) the created bone segments were imported into Geomagic Design X to create geometric model as (C) figure. (d) Then, the geometric models were imported into Hypermesh to create meshed foot model. ....	16
6 The meshed foot segments imported into FE Bio software. The foot consisted of 15 segments including tibia, fibula, talus, calcaneus, navicular, cuboid, three cuneiforms, single segment metatarsal, and five segment phalanges. ....	17
7 The metatarsal was fused as a single segment (left). Also, the phalanges were also fused as 5 components of phalanges (right). ....	17
8 The CT scan images in three different views with bones (green) with cartilage segments (blue); (a) sagittal view, (b) axial view, and (c) coronal view. ....	18
9 3D geometric of the bones (green) with cartilage (blue). The bone segments created separately except metatarsal and phalanges. ....	18
10 The medial view of foot bones with cartilages (yellow) and plantar fascia (pink). ....	19
11 The 3D-FE foot model in midstance with rigid plate; bones, cartilage (aqua), 3mm thickness plantar fascia (green) and strain. The Achilles tendon force increased from 0 to 500N and 0 or 700N axial load was applied to the top surface of tibia and fibula. ....	20
12 The strain results based on three different thickness plantar fascia compared with an in vitro experiment, with increasing Achilles tendon loading. ....	21
13 The strain results based on three different thickness plantar fascia with a 700N axial load to the top surface of tibia and Achilles tendon loading from 0-500N applied to calcaneus, compared with: 1) an in vitro experiment with Achilles tendon loading from 0-500N to the calcaneus at 0-degree	

dorsiflexion and 2) with the various toe dorsiflexion at 15°, 30°, and 45°, with Achilles tendon loading from 0-500N [77].	22
14 The CT scan images in three views show cartilages (yellow for talus; red for tibia; blue for fibula) at ankle joint. (a) the axial view; (b) coronal view; (c) sagittal view.	29
15 The 3D solid cartilages were created in 3D Slicer (a), and exported into Geomagic Design X and Hypermesh to create geometric model (b). The FE model was imported into FEBio (c).	29
16 3D FE foot model including tibia, fibula, talus, calcaneus, cuboid, three naviculars, metatarsals, phalange is consisted of a one segment cartilage at each joint and plantar fascia. The cartilages at the ankle joint were created separately.	30
17 The 3-dimensional FE foot model at neutral position in sagittal and frontal view with a) 3mm, b) 4mm, and c) 5mm thick plantar fascia.	31
18 The 3-dimensional FE foot model at 10 degree dorsiflexion in sagittal and frontal view with a) 3mm, b) 4mm, and c) 5mm thick plantar fascia.	32
19 The 3-dimensional FE foot model at 10 degree plantar flexion in sagittal and frontal view with a) 3mm, b) 4mm, and c) 5mm thick plantar fascia.	33
20 The Computed Tomography (CT) scan was taken with lower limb cadaver in the three different foot angle like neutral position, 10-degrees dorsiflexion, and 10-degrees plantarflexion.	34
21 The 3D soft tissue of foot created on 3D Slicer (left). After that the 3D Solid foot model was imported into Geomagic Design X for creating geometric model and boolean intersection area between bones, cartilage, plantar fascia and soft tissue and Hypermesh for creating FE model (right).	35
22 The 3D soft tissue foot with Boolean intersection area between bones, cartilage, plantar fascia, and soft tissue.	35
23 The 3D FE foot model in various foot positions were developed with three different thickness of plantar fascia.	36
24 The 3D FE foot model was simulated under 700N axial load. The tibia and fibula only allowed to move in vertical movement. The phalanges were also fixed in all 6 degrees of freedom.	37
25 The tied contact method applied between foot and plate. The contact area was selected like the highlighted area on foot sole.	38
26 The plantar stresses at neutral position in axial views with a) 3mm, b) 4mm, and c) 5mm thick plantar fascia.	40
27 The plantar stresses at 10° dorsiflexion in axial views with a) 3mm, b) 4mm, and c) 5mm thick plantar fascia.	41
28 The plantar stresses at 10° dorsiflexion in axial views with a) 3mm, b) 4mm, and c) 5mm thick plantar fascia.	42
29 The peak von Mises stress of bones in 3D FE foot model at neutral position with three different thickness plantar fascia.	43

30	The peak von Mises stress of bones in 3D FE foot model at 10° dorsiflexion with three different thickness plantar fascia. ....	43
31	The peak von Mises stress of bones in 3D FE foot model at 10° plantar flexion with three different thickness plantar fascia. ....	44
32	The stresses at rearfoot and forefoot area are measured in various foot positions with three different thickness of plantar fascia. ....	44
33	The three CT scan images. One is from a death male cadaver foot (unknown age) and another two CT scan images were from two patients before ankle surgery.....	52
34	The 3D FE foot model including tibia, talus, and cartilage was created in three different thickness articular cartilage. ....	53
35	The articular cartilage was extruded along local bone surface normal between tibia and talus to a uniform thickness of 0.5mm, 1.0mm, and 1.7mm. (a) geometric model of the articular cartilage; (b) FE model of the articular cartilage.....	54
Figure 36	The 3D FE foot model was simulated under 600N axial load.....	55
Figure 37	The inferior view of talus. The talus at anterior and posterior calcaneal surface was fixed in six degrees of freedom.....	56
38	The peak stress at the tibial cartilage surface. The peak stress measured in two different group such as healthy group and patient group.....	58
39	The contact areas in various thickness of cartilage in the FE ankle models including tibia and talus... 58	
40	The distal view of the tibial articular cartilage in Model 1. The three different stress distributions showed similar stress distribution, but the peak stress was decreased when the thickness of cartilage increased. ....	59
41	The distal view of the tibial articular cartilage in Model 2. The peak stress and the stress distribution with 0.5mm and 1.0mm thick cartilage measured on the tibial articular cartilage. ....	60
42	The distal view of the tibial articular cartilage in Model 3. The peak stress and the stress distribution with 0.5mm and 1.0mm thick cartilage measured on the tibial articular cartilage. ....	61
43	The distal view of the tibial articular cartilage in Model 4. The peak stress and the stress distribution with 0.5mm and 1.0mm thick cartilage measured on the tibial articular cartilage. ....	62
44	The lateral view of CT scan. (a) CT scan taken from a death cadaver (Model 1); (b) the angle of tibia was perpendicular to the talus but bone spur was on the tibia (Model 3); (c) but the tibia in this picture was not perpendicular to the talus (Model 4).....	64
45	The FE model was developed based on CT scan images. As a first step, the rough solid model created in Slicer, then the geometric model developed by the Geomagic Design X software. Finally, the smooth FE model was created in Hypermesh. ....	65
46	The medial view of tibiotalar joint with ligaments (left) [111]. The medial and anterior view of foot with muscles.....	66

47 The 3D FE foot model including 18 bone segment, plantar fascia, ankle ligaments, short and long ligaments, soft tissue.....	71
48 The axial view of the metatarsal. The metatarsal consists of 5 segments, but one of metatarsal was developed as a single segment (left). Another metatarsal developed as individual segment (right)...	71
49 The stress at metatarsal was changed by the metatarsal structure.....	72
50 The plantar stress distribution and the peak plantar stress was affected by the bone structure like metatarsal and sesamoids.....	73
51 The single position control device developed using two servo motors and it tested under 66.6 lb. ....	74
52 The device tested with the cadaver. The device was operated from neutral position (left) to 20° plantar flexion (right).....	74
53 The 2nd generation foot and ankle positioning device designed with the five-servo motors.....	75
54 The 2nd generation device tested with 25lb 3D printer. ....	75
55 The 3D design device of the gear box including 25:1 worm gear and 1:7 spur gear box (Left) and the 3rd generation ankle positioning device with 5 gear boxes (Right).....	76
56 The real 3rd generation gear box (left) and the fully assembled foot and ankle loading device (right).	76

## CHAPTER I

### INTRODUCTION

#### 1.1 BACKGROUND

The human foot has several functions such as weight-bearing, absorption of shock, and transmitting thrust in motion [1]. The entire human foot experiences forces that are around five times higher than body weight in normal gait and thirteen times higher than body weight during activity movements such as running and jumping [2]. Thus, during the lifetime, the human foot experiences high plantar pressures, shear, and internal stresses [3-5]. Therefore, about 19 percent of the US population has an average of 1.4 foot problems every year [6]. Among the foot problems, heel pain is one of the most common foot problems [7]. In the US, over 1 million people who suffer from plantar heel pain visit physicians [8]. Heel pain varies depending on the age, body weight, sex, or running which is the most common activities in people and in athletes [9, 10]. Heel pain is frequently caused by plantar fasciitis and diabetes [11, 12]. Plantar fasciitis is related to several risk factors such as the high stress and higher plantar load over the rearfoot area [13, 14]. Furthermore, plantar fasciitis is not only related to the foot's mechanics such as a tight Achilles tendon or pes cavus and pes planus foot structures, but also related to the thickness of plantar fascia [15]. Specifically, as the plantar fascia thickness increases, the symptoms of the plantar heel pain level is increased [16]. Patients with diabetes face foot injuries in different forms than non-diabetic feet such as abrasions or blisters, nail extraction, stone bruise, ankle pain, and heel pain. Moreover, people with diabetes have more foot and ankle injuries such as foot ulcers, foot deformity, and plantar fasciitis than non-diabetics [17, 18]. Because diabetes can damage small and large blood vessels, diabetics have an increased risk of developing diabetic neuropathy [19]. Basically, foot injuries in patients with diabetes are typically greater than injuries in non-diabetic feet, which is frequently caused by the abnormally high plantar pressure [18]. The high plantar pressure can be

affected by the stiffness of plantar fascia [20]. The plantar fascia with high stiffness affects the high arch and the level of heel pain as well [21, 22]. The high stiffness of plantar fascia increasing thickness of plantar fascia measured up to 9.1mm thick plantar fascia lead to foot deformities like Pes cavus is characterized by high arch of the foot that does not flatten, and increases the foot pain level [23].

Previous studies have researched the relationship between heel pain and the thickness of the plantar fascia using ultrasonography and Magnetic Resonance Imaging (MRI) [24-27]. In [27], thirty patients participated to evaluate the relationship between heel pain and the thickening plantar fascia. In the first step, the patients measured pain with a visual analog scale (VAS) as well, the thickness of plantar fascia measured. Three weeks later, patients were treated and the thickness of plantar fascia was measured at the same time. After the treatment, around twenty-nine feet show a decreased thickness of plantar fascia and reduced the heel pain. Additionally, the thickness of plantar fascia was reduced from  $5.71 \pm 1.33$  mm to  $4.89 \pm 1.19$  mm [27]. Seventy-seven patients with heel pain and another seventy-seven subjects joined [24] study to compare the detection of plantar fasciitis between magnetic resonance imaging (MRI) and sonography. In [24], the patients with plantar fasciitis had increased the thickness of plantar fascia with pain duration in both examinations [24].

The plantar fascia is on the bottom of human foot and spreads from the heel to the toes and it is firmly joined to plantar muscle and skin [28]. Thus, the anatomical variability, functional morphology, and internal behavior of plantar fascia are not clearly understood. Nevertheless, the elastic properties of the plantar fascia were determined by the in vivo study with radiographic fluoroscopy system [29] and in vitro study with load deformation test [30]. However, the



deformations and strains of the plantar fascia during actual walking and daily activities have not been thoroughly studied yet.

Thus, 2-dimensional (2D) or 3-dimensional (3D) Finite Element Analysis (FEA) has also been used with other methods (e.g., ultrasonography and MRI) to understand internal behavior such as the internal stress, strain, or movement of foot elements in stance phase or in dynamic locomotion in athletes, diabetes, or plantar fasciitis [3, 31, 32]. In the previous studies, the 3D FE model were developed based on CT or MR images to simulate the biomechanical behavior of both a healthy and a diabetic foot [4, 33-35] and to analyzed the internal stress in the plantar fascia in patients with plantar fasciitis [36, 37]. The 3D FE models including bony structures, cartilage, ligaments, plantar fascia with 1D element or 3D solid element, and soft tissue have been simulated in the phases of the gait cycle and in the stance phase to understand the etiology of diabetic foot and the effect of plantar fascia stiffness during midstance of the gait cycle. In the previous 3D FE model, non-linear material properties (solid model) or linear material properties (1D tension only spring) was assigned to the plantar fascia. Thus, it contributed to understanding the effect of diabetes and plantar fasciitis in the plantar pressure distribution, the peak pressure, and arch height. However, the stiffness of plantar fascia was not considered in the 3D FE model with diabetes [4, 38] and with plantar fasciitis [39] even though the thickness of plantar fascia was increased in the patient with diabetes and with plantar fasciitis. It was not clearly explained how much increase the plantar pressure and peak pressure while increasing the thickness of plantar fascia.

## 1.2 ANATOMY OF FOOT AND PLANTAR FASCIA

The foot is an important body to absorb and transfer a load, so it supports body weight and body balance for activities such as walking, running, and jumping [40]. The foot and ankle joint

composed of 26 bones, 33 joints, more than 100 tendons, muscles, and ligaments are one of the most complex bony structures in the human body [41-43] (Figure 1). In feet, muscles, ligaments, and tendons are attached to bone to hold bones together and to maintain the arch of foot (Figure 2).

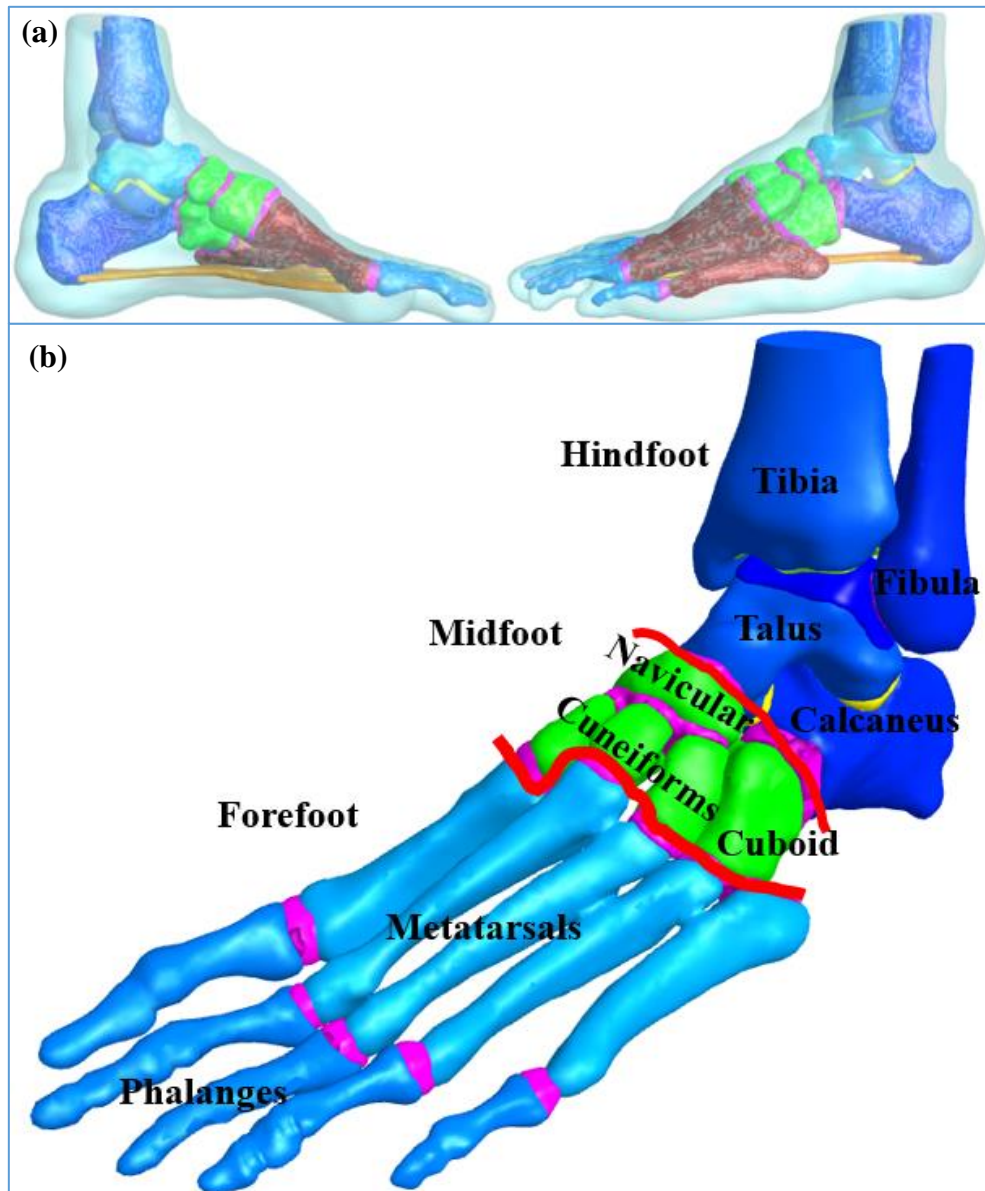


Figure 1 The bone structure segments model of the foot. Medical and lateral view of the foot segment (a). Anatomy of the foot bone can be divided into three parts such as hind foot including talus and calcaneus, mid foot including navicular, medial cuneiform, internal cuneiform, lateral cuneiform, and cuboid and forefoot including five metatarsal and five phalanges (b).

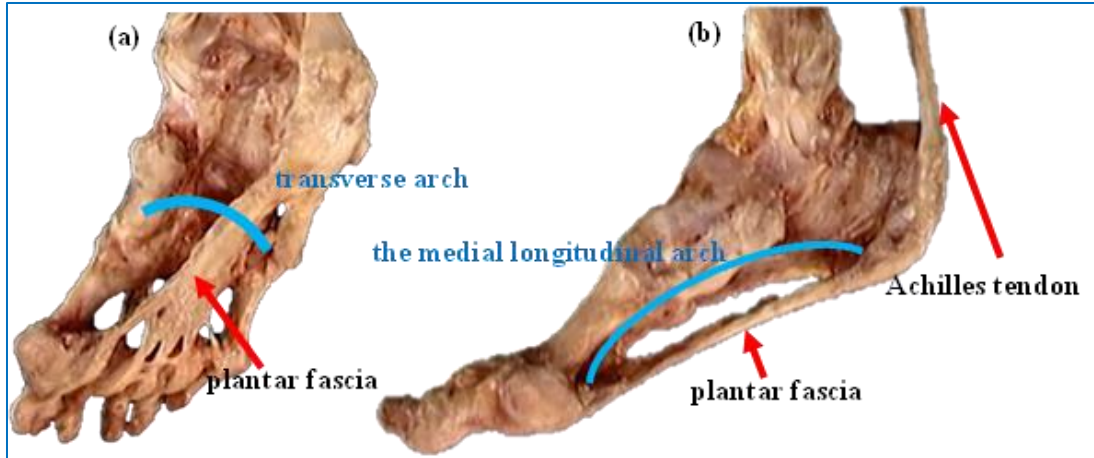


Figure 2 Anatomic dissection showing foot bone structure, the tendons, and ligaments; Achilles tendon and plantar fascia. (a) The transverse plane foot view with plantar fascia and transverse arch. (b) The lateral view of the foot with plantar fascia and Achilles tendon with the medial longitudinal arch [44].

The foot arch is described in two components are transverse arch and the medial longitudinal arch (Figure 2). The transverse arch is increasing the stiffness of foot [45] while the medial longitudinal arch transfers load from Achilles tendon to forefoot and absorbs the ground reaction force [40, 46]. The bones are oriented in an arch shape to support bending compressive stresses and to transfer the body weight to the ground during standing [47, 48].

The longitudinal arch is also supported by the plantar fascia. As shown in Figure 2, the plantar fascia is located beneath the skin on the sole, and it is the most important and strong ligament in structures of the foot and ankle to support an arch structure of the foot [21]. The plantar fascia acts as spring, so the plantar aponeurosis acts to resist tensile stress than compression [49]. Substantially, the plantar fascia transfers loads from the Achilles tendon to the forefoot and absorbs the ground reaction force during human locomotion [36, 50]. Thus, the arch height response to the loading during gait stance.

The primary role of plantar fascia is to support, transfer, and absorb the body weight and ground reaction forces during human locomotion. Consequently, the shape of the bone structure

with the plantar fascia can be simplified as a triangle (Figure 3) [51]. The windlass mechanism which was modeled by Hicks in 1954 [51], is a mechanical model of the foot during the gait cycle. It helps to explain the biomechanical factors and stresses during the weight bearing activities [52].

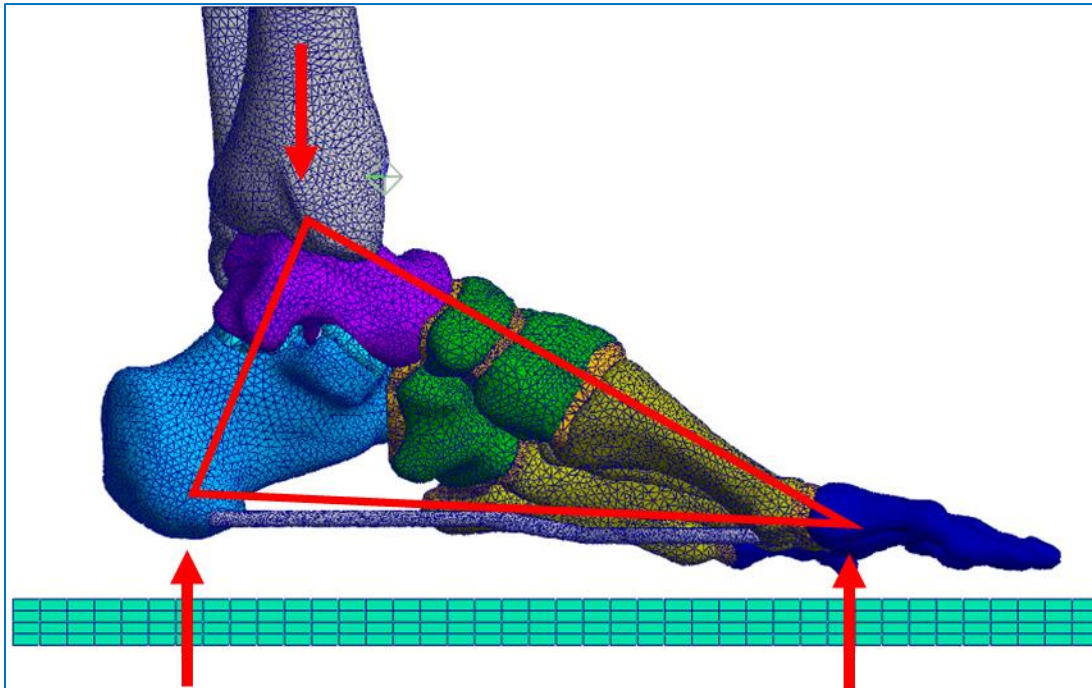


Figure 3 The medical view of bone structure is similar with triangle truss structure. Two upward forces on the metatarsal head and toes, and on calcaneus show the ground reaction force, and the downward arrow shows the body weight.

### 1.3 COMPUTATIONAL MODELING OF FOOT AND ANKLE

Finite element modeling and simulation analysis are widely used to understand the mechanical interaction between external and internal stresses and strains [4, 36]. In [4], the 3D FE model of a diabetic neuropathic and a healthy subject were developed including bones, cartilage, and plantar soft tissue to analyze and to compare the plantar pressure in four instants of the phase of gait like the static standing, heel strike, loading response, midstance, and push off phases. First,

[4] collected the physical plantar pressures data in four instants of the stance phase of gait from the two groups. After that, 30 bone segment models were built based on MRI data. The plantar fascia ( $E = 350$  MPa), short plantar ligament ( $E = 250$  MPa), and Achilles tendon ( $E = 250$  MPa) as 2-node cables with tension only were also generated to support the foot arch. The solid segments were imported into the Simpleware software (Synopsys Inc., Mountain view, CA) to generate the finite element model. ABAQUS FEA software (Simuleon Tech, Hertogenbosch, Netherlands) was used to simulate the 3D FE models. The 3D FE model simulated in the four-stance phase (i.e., heel strike, loading response, midstance, and push off) of gait. Additionally, the stiffness of the plantar ligament was tested incrementally by a factor of 2 and of 5. For the FE model, the homogeneous, isotropic, linear elastic materials used for plate, bones, cartilage, plantar fascia, tendons, and ligament. For the plantar soft tissue, the Hyperelastic, second-order polynomial parameters were used (Table 1). The simulation data was validated by comparing the results of experimentally measured the stress distribution.

Table 1 The parameters for the second-order polynomial plantar soft tissue

	$C_{10}$ (N/mm <sup>2</sup> )	$C_{01}$ (N/mm <sup>2</sup> )	$C_{20}$ (N/mm <sup>2</sup> )	$C_{11}$ (N/mm <sup>2</sup> )	$C_{02}$ (N/mm <sup>2</sup> )	$D_1$ (N/mm <sup>2</sup> )	$D_2$ (N/mm <sup>2</sup> )	Reference
Control Group	0.08556	-0.05841	0.03900	-0.02319	0.00851	3.65273	0.0000	[34]
Diabetic Group	0.17113	-0.11683	0.07800	-0.04638	0.01702	1.82636	0.0000	

[36] also created the 3D FE foot model including a 3D solid plantar fascia without plantar soft tissue to measure internal stress in plantar fascia during in stance phase of gait. The 3D FE foot and ankle model was developed using CT scan images. 3D solid model was created in Avizo

software (VSG SAS, Bordeaux, France). The solid model was imported into the ANSYS software (Swanson Analysis, Houston, PA, USA) to create FE model and to analyze the 3D FE model in stance phase of gait. The 3D FE model consisted of 27 bones, cartilage, ligaments, and a solid 2mm thick plantar fascia. The material properties of the 3D FE foot and ankle model were applied homogenous, isotropic, and linear elastic material for bones, cartilage, ligaments, and plantar fascia (Table 2). The bone segments were meshed with shell element and applied as rigid bodies in FE model. The gait stance phase was simulated by applying displacement to the midlines of the superior surface of the distal tibia and fibula. On the same time, the Achilles tendon force was applied to the posterior aspect of the calcaneus. The 3D FE model was validated by comparing the predicted tension and reaction force of plantar fascia with the cadaver study results [36].

Table 2 The linear elastic material properties for bones, cartilage, ligament, and plantar fascia

	Young's Modulus (MPa)	Poisson's Ratio	Thickness (mm)	Reference
Bones	7000	0.3	0.15	[36]
Cartilages	50	0.1	-	
Ligament	260	0.45	0.1	
Plantar fascia	350	0.45	2	

Furthermore, the computational modeling foot and ankle like FEM in [32] was developed to analyze the plantar pressure and internal stress in the metatarsal at the balance standing while increasing stiffness of soft tissue [32]. The FE model including plantar soft tissue was developed using MR images. The FE model consisted of 28 bones, 72 ligaments (two points tension only spring), cartilages, plantar fascia (two points tension only spring), and plantar soft tissue. The linear elastic materials applied for bones, cartilages ligaments, plantar fascia (

Table 4). The Hyperelastic, second-order polynomial parameters were used for plantar soft tissue (Table 3).

Table 3 The coefficients of the second order polynomial material

$C_{10}$ (N/mm <sup>2</sup> )	$C_{01}$ (N/mm <sup>2</sup> )	$C_{20}$ (N/mm <sup>2</sup> )	$C_{11}$ (N/mm <sup>2</sup> )	$C_{02}$ (N/mm <sup>2</sup> )	$D_1$ (N/mm <sup>2</sup> )	$D_2$ (N/mm <sup>2</sup> )
0.08556	-0.05841	0.03900	-0.02319	0.00851	3.65273	0.0000

Table 4 The linear elastic material properties for bones, cartilage, ligaments, and plantar fascia

Component	Young's modulus (MPa)	Poisson's ratio		Cross-sectional area (mm <sup>2</sup> )
Bones	7300	0.3		
Cartilage	1	0.4		
Ligaments	260	-		18.4
Plantar fascia	350	-		290.7

Moreover, the computational modeling of the ankle is applied to plan surgeries and test the function of foot structure [53]. The computational modeling is also used to understand subject specific foot injuries and pathology such as ankle replacement surgery [54]. The FE model developed to figure out the different of foot and ankle between the foot with total ankle replacement by comparing the contact pressure after total ankle replacement. Thus, the FE model was included 28 bones, 103 ligaments (tension only truss element), plantar fascia, nine groups of muscles, soft tissue, and total ankle arthroplasty consisted of three parts such as tibia plate, mobile bearing, and talar component. The linear elastic material properties were applied for bones, cartilage, ligament, plantar fascia, and total ankle arthroplasty (

Table 4). The second order hyperelastic polynomial material was used for plantar soft tissue (Table 3). The predicted plantar pressure and the vertical ground reaction force measured during the gait. Finite element analysis may improve our understanding of biomechanics behavior of foot supports such as the foot insole [55].

In this dissertation, a 3-dimensional (3D) finite element foot model was conducted to determine the effect of thickness of plantar fascia to the strain of plantar fascia, to the plantar pressure, and to the peak pressure. The 3D finite element foot model was developed based on the CT scan images. The CT scan images were taken from the cadaver of lower limb. The 3D FE foot and ankle model included 26 bones: tibia, fibula, talus, navicular, cuboid, 3 cuneiforms, 5 metatarsals, and 5 phalanges, cartilage, 3D solid plantar fascia, and plantar soft tissue.

#### 1.4 STATEMENT OF PURPOSE

The foot and ankle frequently experience pain like plantar fasciitis in people [56]. The foot injuries are caused by many reasons such as aging, overuse injuries, being overweight or fitting shoes [57-60]. Plantar fasciitis causes heel pain and is the most common foot injury. Previous studies had various approaches to model of the foot and ankle with patient specific models using in vivo [27, 61], in vitro [62, 63], or the computational models [64, 65] to analyze the dynamics between the plantar facial thickness and plantar fasciitis or between diabetes and plantar fasciitis. In vivo studies [27, 61] have used ultrasound to measure the thickness of plantar fascia because the thickness or the stiffness of plantar fascia was related to the heel pain. The average thickness of plantar fascia was 3.4mm in control group in both studies. However, the average symptomatic thickness of plantar fascia was  $5.71\text{mm} \pm 1.33\text{mm}$  in [27] and  $6.14\text{mm} \pm 1.4\text{mm}$  in [61]. Similarly, the thickness of plantar fascia in patient with asymptomatic plantar fasciitis was  $4.2\text{mm} \pm 0.5\text{mm}$



in [61]. Thus, over 4mm thick plantar fascia would be consistent with plantar fasciitis [27, 61]. In vitro study, the role of plantar fascia in foot stability [62] and the stiffness of plantar fascia [63] were determined by the measured the deformation plantar fascia. The stiffness of plantar was  $182.5 \pm 37.3$  N/mm in the lateral zone,  $232.5 \pm 53.1$  N/mm in the middle zone, and  $203.2 \pm 56.6$  N/mm. The overall average stiffness was  $209 \pm 51.9$  N/mm. In the computational studies, the 3D FE foot and ankle model including plantar fascia was developed to understand the effect of plantar fasciitis in plantar pressure and in internal stress at metatarsal. However, the plantar fascia was developed as a 1D spring [65] or solid model with 2mm thickness [64].

Nevertheless, the relationship between the thicker plantar fascia and plantar fasciitis was not clearly analyzed with the plantar pressure and the strain/stress of the plantar fascia in the literature. Also, it was studied in midstance or during gait. If we studied about the effect of the thicker plantar fascia at the different foot positions such as at 10-degree dorsiflexion and at 10-degree plantar flexion, we could be analyzed the difference of the transferred loading from Achille tendon (calcaneus) to plantar fascia (forefoot) during the changed ankle position. To determine how the thickness of the plantar fascia affects the plantar pressures and strains in the plantar fascia, three different approaches will be use in the assembly of a 3D finite element foot model.

As a first step, 3D FE foot and ankle model including various thick plantar fascia was developed without plantar soft tissue. The 3D FE foot and ankle model simulated to determine the effect of thicker plantar fascia on strain in the plantar fascia, three different thickness of the plantar fascia (e.g., 3mm, 4mm, and 5mm) measured by published literature [21, 22] will be included in the 3D finite element model without plantar soft tissue. Then, plantar soft tissue was developed, and it was imported into the 3D FE foot model to analyze the effect of thick plantar fascia to plantar pressure. Plantar pressure at forefoot and hindfoot should be impacted by the thicker plantar fascia

and diabetes according to the previously published literature [8, 66]. The 3D finite element foot model including plantar fascia and plantar soft tissue will be simulated to figure out the effect of thickness of plantar fascia to plantar pressure in three different foot positions such as neutral position, 10-degrees dorsiflexion and 10-degrees plantarflexion. In the last, the four FE foot models, two healthy models and two patient models including tibia, talus, and cartilage were developed to figure out the effect of bone morphology to the contact stress at ankle joint between tibial cartilage and talar cartilage. Also, the three different thickness of cartilages such as 0.5mm, 1.0mm and 1.7mm were applied to tibial cartilage and talar cartilage to figure out the changing of the location of the peak contact stress and the contact stress distribution.

## CHAPTER II

### THE EFFECT OF THE DIFFERENT PLANTAR FASCIA THICKNESS AND TENDON LOADING IN 3-D FINITE ELEMENT FOOT MODEL

#### 2.1 INTRODUCTION

The plantar fascia is a one of thickness ligaments in the human body. It connects from the calcaneus to the metatarsal heads to maintain the longitudinal arch of the foot, and absorb the body weight and ground reaction force [51]. The plantar fascia also transfers loads from the Achilles tendon to the forefoot during walking [46]. As a results, both Achilles tendon loading and plantar pressure may contribute to the strain in the plantar fascia. Additionally, a person with plantar fasciitis and/or diabetes mellitus can experience foot pain and arch collapse [28].

The two most common ailments that affect that plantar fascia are diabetes mellitus and plantar fasciitis. Diabetes mellitus can change soft tissue structure and function throughout the body, however, it has a significant impact in the foot [67]. Foot ulcerations are the most common foot pathology in diabetic patients, which are frequently cause by high peak plantar pressures [68]. The high plantar pressure in diabetic patients is related to the thickness of plantar fascia [20, 69].

Plantar fasciitis is the most common cause of heel pain [70]. The pain usually happens when asymptomatic person stands after rest. In 2017, approximately 10% of the people in the United States suffer from heel pain [66]. To reduce the heel pain, many physical therapy, steroid injections[71], stretching exercises [72], and heel inserts are used for treatment of plantar fasciitis [56]. The thickening of plantar fascia can be affected by the plantar fasciitis.

As a result, understanding the behavior of plantar fascia during gait, running, jumping, or the effect of foot pathology, many in vivo, in vitro studies, and computational method like finite

element analysis (FEA) are used to figure out the thickening of plantar fascia to plantar pressure or internal stress and strain in plantar fascia [24, 28, 69, 73].

Nowadays, Finite Element Analysis (FEA) is widely used to understand internal stress and strains of the plantar fascia during neutral standing, walking, or running [36, 64, 73]. Moreover, a two or three-dimensional finite element foot model has developed using computed tomography (CT) scan or magnetic resonance imaging (MRI) to figure out the effect of stiffness of plantar fascia to the strains of plantar fascia, the primary factor of plantar fasciitis, and the effect of diabetes in the plantar pressure and the stress/strains in plantar fascia [36, 38, 64].

## 2.2 STATEMENT OF PURPOSE

In the case of patients with plantar fasciitis and diabetes, the plantar fascia is typically thicker than healthy asymptomatic [27, 74]. Specifically, the average thickness of healthy plantar fascia is  $2.0 \pm 0.5$  mm or 2.3 – 4.3 mm with an average of approximately 3.4 mm [66], while plantar fasciitis and diabetic plantar fascia is  $5.71 \pm 1.3$  mm and  $3.1 \pm 1.0$  mm [20, 27], respectively.

Finite element models of the foot typically keep the plantar fascia at a constant thickness (i.e., 2mm or the cross-sectional area of  $3.2\text{mm}^2$ ) [46], while prior studies have shown increased thickness in patients with plantar fasciitis and diabetes mellitus. Therefore, the purpose of this study was to examine the strain of the plantar fascia with different plantar fascia thickness and Achilles tendon loading in 3-D finite element foot model during midstance of gait cycle.

## 2.3 METHODS

A 3-dimensional finite element foot model was developed using computed tomography images of foot cadaver. The CT scan images of cadaver foot were captured at 0.484 mm increments

in a neutral, unloaded position, and were processed using an open-source image computing platform called 3DSlicer(version 4.10.2) (Figure 4).

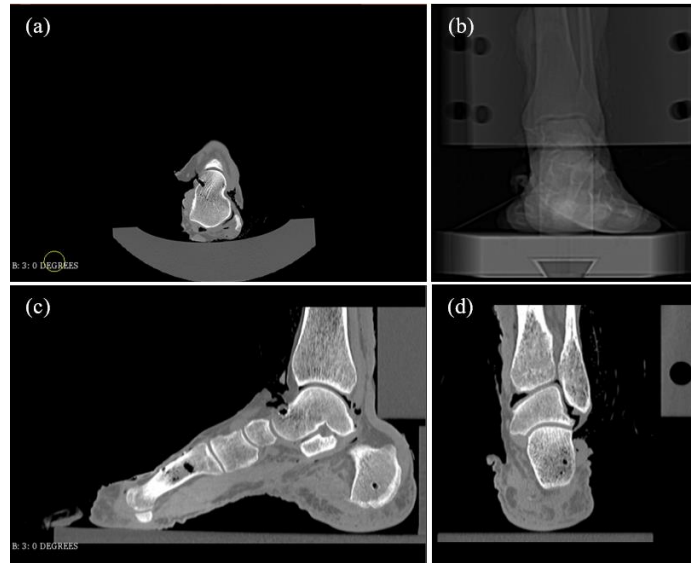


Figure 4 CT scan image of cadaver foot. The foot cadaver was fixed at neutral position on foot holding devices. (a) the CT scan image in the axial plane; (b) The CT scan image in the lateral axial plane; (c) the CT scan image in the sagittal; (d) the CT scan image in the coronal.

The bone segments created in 3D Slicer were imported into Geomagic Design X (3D Systems, Rock Hill, SC) to smooth the complex bony surfaces and to create geometric bone segments. The geometric bone segments were exported into Hypermesh (Altair, Troy, MI) (Figure 5) and FEBio (FEBio, Salt Lake City, UT) to mesh and simulate the foot in neutral position.

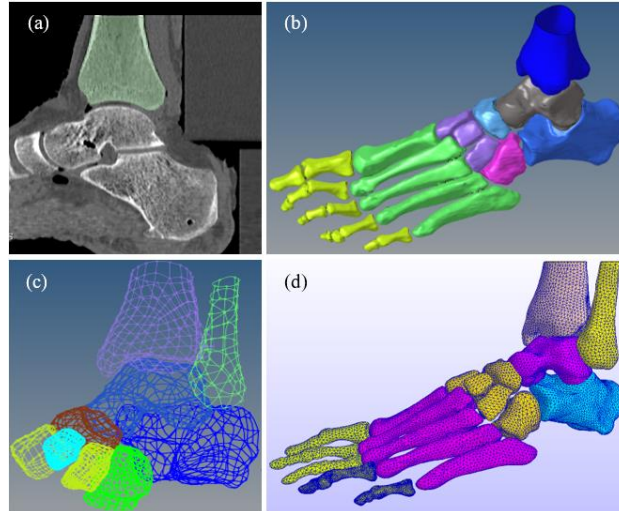


Figure 5 The pictures show how to create the foot bony segments from CT scan images. (a) on CT scan images, the bone was created separately. (b) the created bone segments were imported into Geomagic Design X to create geometric model as (C) figure. (d) Then, the geometric models were imported into Hypermesh to create meshed foot model.

The FE foot model contained 15-foot bony segments, including the tibia, fibula, talus, calcaneus, navicular, three cuneiforms, cuboid, metatarsals, and phalanges (Figure 6). The metatarsals and phalanges were fused as a single segment of metatarsals and 5 components of the phalanges (Figure 7).

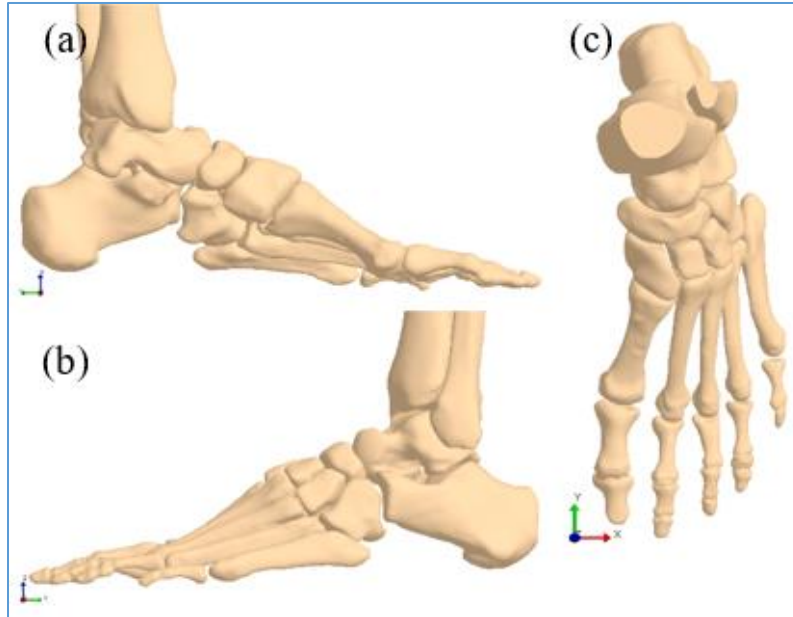


Figure 6 The meshed foot segments imported into FE Bio software. The foot consisted of 15 segments including tibia, fibula, talus, calcaneus, navicular, cuboid, three cuneiforms, single segment metatarsal, and five segment phalanges.

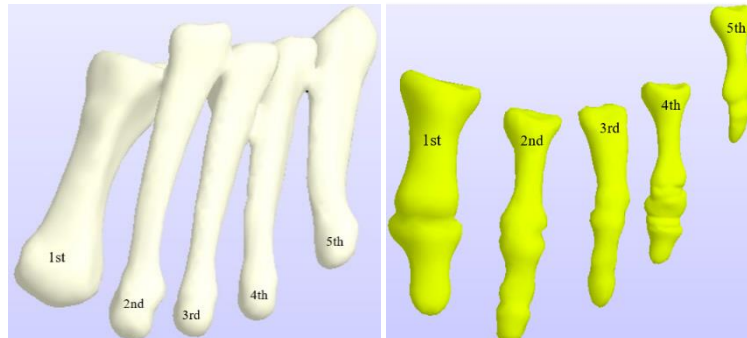


Figure 7 The metatarsal was fused as a single segment (left). Also, the phalanges were also fused as 5 components of phalanges (right).

The cartilages were created based on CT images using an open-source image computing platform called 3DSlicer(version 4.10.2). The cartilage was created from bone to bone to fill the gap at each join (Figure 8 and 9). After creating the cartilage in the 3DSlicer, the 3D geometry of the bones and cartilage are shown in Figure 9.

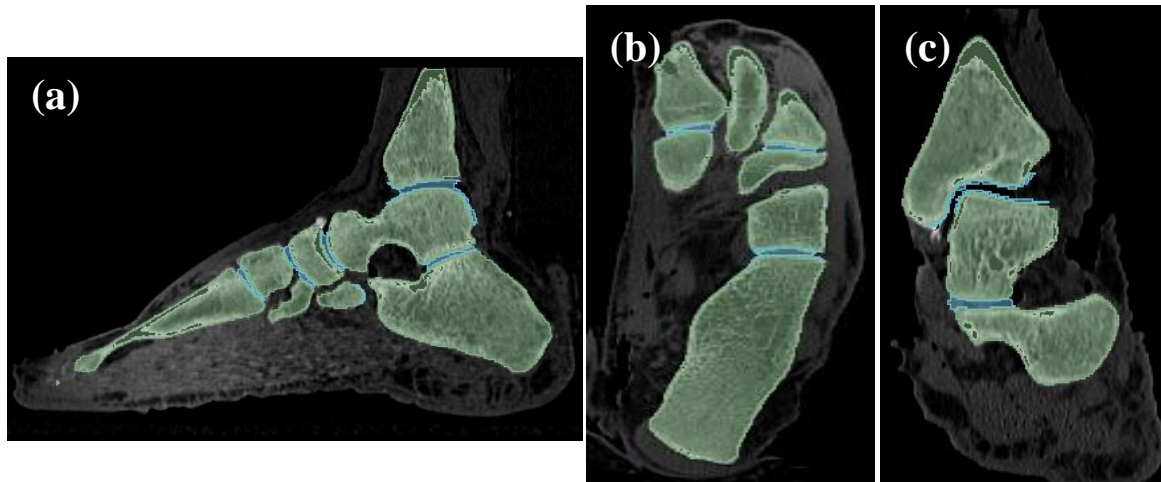


Figure 8 The CT scan images in three different views with bones (green) with cartilage segments (blue); (a) sagittal view, (b) axial view, and (c) coronal view.

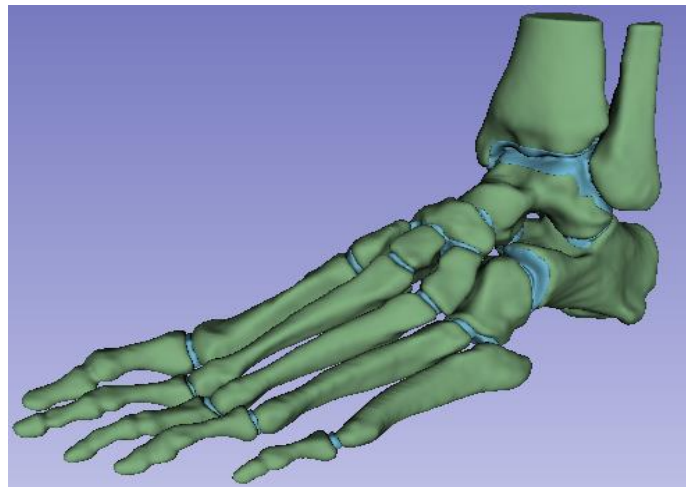


Figure 9 3D geometric of the bones (green) with cartilage (blue). The bone segments created separately except metatarsal and phalanges.

Fifteen cartilage segments (yellow) and the plantar fascia (pink) were also constructed the FE foot model (Figure 10) based on CT scan images. The cartilage was created from bone to bone to fill the gap at each joint including ankle joint between tibia and talus. The 3-dimensional plantar fascia was connected to the calcaneus and the heads of the metatarsals created based on measurements from the CT images. To understand the effect of thickening plantar fascia, three



different thickness plantar fascia (e.g., 3mm, 4mm, and 5mm) were simulated in the 3D FE foot model (Figure 10).

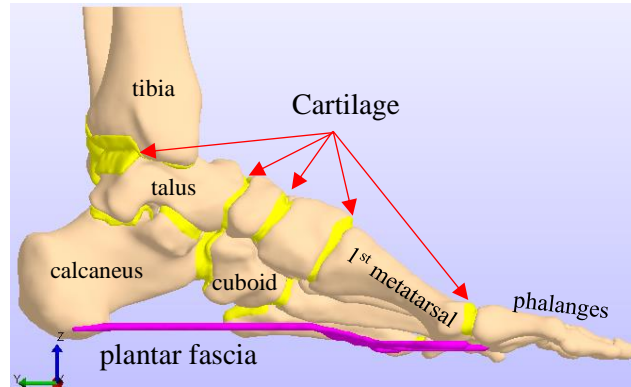


Figure 10 The medial view of foot bones with cartilages (yellow) and plantar fascia (pink).

The segments of FE foot model were idealized as linear elastic, homogeneous and isotropic including plantar fascia. The material properties obtained from previous literature [4, 31, 38, 75, 76] (Table 5).

Table 5 Material properties and element types

	Young's modulus (MPa)	Poisson's ratio	Element type
Bones	7300	0.3	Tetrahedral solid
Cartilage	100	0.4	Tetrahedral solid
Plantar fascia	350	0.3	Tetrahedral solid
Plate	Rigid body		

To evaluate the effects of the thickness of plantar fascia and Achilles tendon pulling force on plantar fascia responses, the cuboid and the medial cuneiform were fully fixed. The constraints has previously been established in the cadaver study by [77]. A 0 and 700N axial load was applied

to the top surface of the tibia and fibula, as the Achilles tendon force was increased from zero to 500N to simulate midstance (Figure 11). Tied surface to surface contact was applied to the bones, cartilages, and plantar fascia. Sliding surface to surface contact was used between the calcaneus and plate.

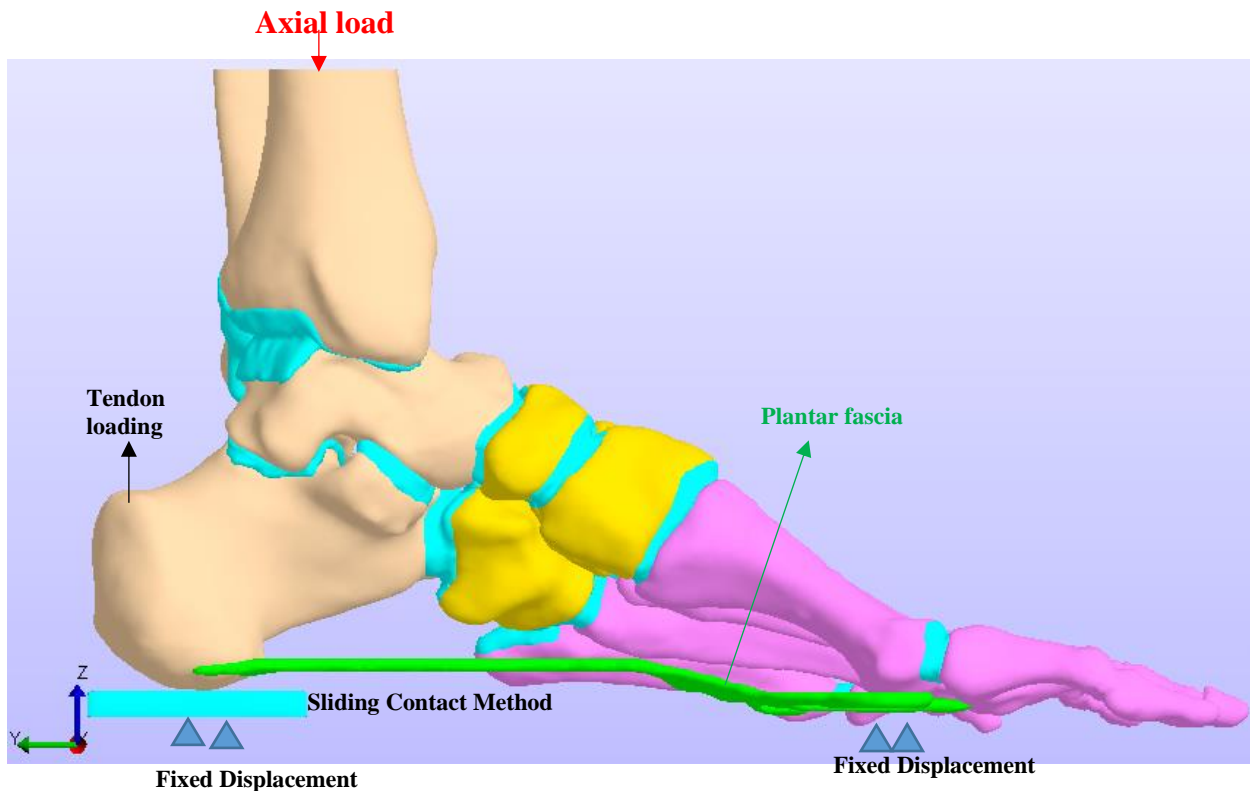


Figure 11 The 3D-FE foot model in midstance with rigid plate; bones, cartilage (aqua), 3mm thickness plantar fascia (green) and strain. The Achilles tendon force increased from 0 to 500N and 0 or 700N axial load was applied to the top surface of tibia and fibula.

## 2.4 RESULTS

The strain of the 3D FE models, when only the Achilles tendon was loaded from 0 to 500N, increased linearly with similar results when the plantar fascia was 3mm and 4mm thick, however, the strain with 5mm thick plantar fascia showed higher strain (Figure 12). The results were

compared with [78]'s experimental results and [64]'s simulate results. In the current results of strain, it indicated that when increased the thickness of the plantar fascia, the strain was also increased. In other words, the thick plantar fascia can affect to the plantar pressure in forefoot area.

With the 700N axial load and for Achilles tendon (AT) force varying from zero to 500N, the strain value ranged from 0.0214 to 0.0502. With 3mm plantar fascia, the strain measured from 0.0214 to 0.0324. With 4mm plantar fascia, the result of strain ranged from 0.0258 to 0.0355. The strain with 5mm plantar fascia measured from 0.0389 to 0.0502 (Figure 13). As a results, the strain on the plantar fascia was not only affected by Achilles tendon load, but also affected by the axial load like body weight.

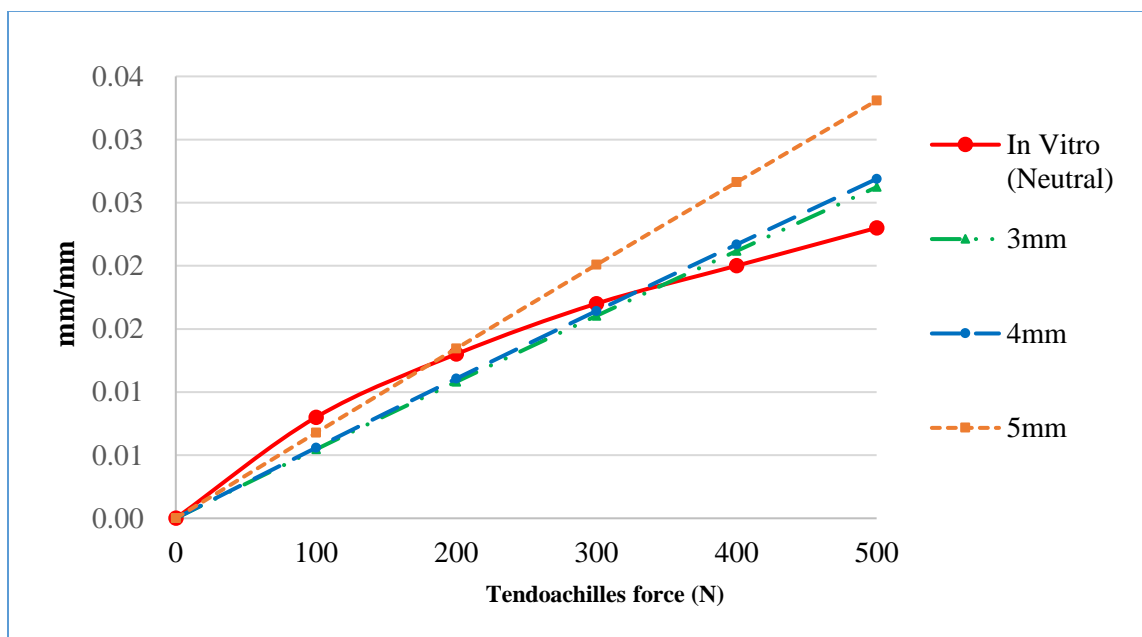


Figure 12 The strain results based on three different thickness plantar fascia compared with an in vitro experiment, with increasing Achilles tendon loading.

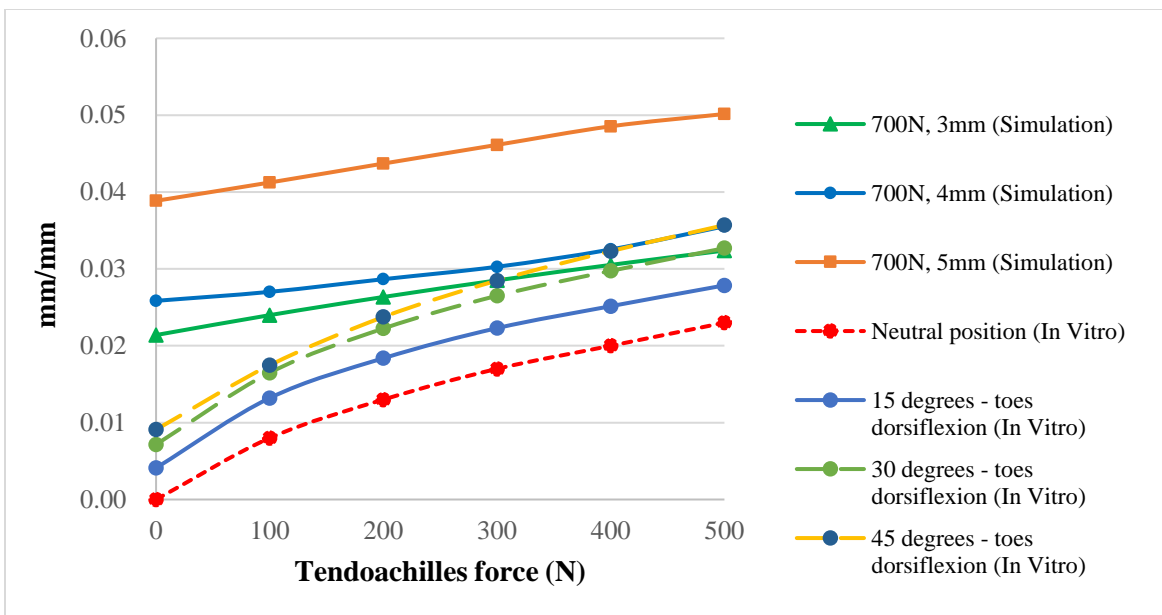


Figure 13 The strain results based on three different thickness plantar fascia with a 700N axial load to the top surface of tibia and Achilles tendon loading from 0-500N applied to calcaneus, compared with: 1) an in vitro experiment with Achilles tendon loading from 0-500N to the calcaneus at 0-degree dorsiflexion and 2) with the various toe dorsiflexion at 15°, 30°, and 45°, with Achilles tendon loading from 0-500N [77].

## 2.5 DISCUSSION

The purpose of this study was to create a 3D FE model to measure the relationship between loading and plantar fascia strain in simulated midstance phase. The three different thicknesses of plantar fascia were tested with various Achilles tendon forces with and without a 700N axial load applied to the tibia. The strain in the plantar fascia increased when the Achilles tendon force increased and the plantar fascia's thickness increased (Figure 12 and 13). However, the increase in plantar fascia strain did not increase proportionally with its thickness. Under 500N Achilles tendon force, the effect of thick plantar fascia with Achilles tendon force and axial load was 2.64% between 3mm and 4mm thick plantar fascia and 23.3% between 3mm and 5mm. The difference between the model and in vitro experiment from [77] at neutral position varied by 6-17% before reaching 300 N of loading. Because of the linear elastic properties of the model, the variation

increased to 36% difference from 300-500N of Achilles tendon loading at 5mm thickness plantar fascia (Figure 11). As shown in Figure 12, the strain was linearly increase in Achilles tendon forces and axial load. With the 700N axial load and for Achilles tendon force varying from zero to 500N, the strain value ranged from 0.0214 to 0.0502 (Figure 12). The percent increase in strain was also calculated 21.2% at 3mm thickness plantar fascia, 30.15% at 4mm thickness plantar fascia, and 62.8% at 5mm thickness plantar fascia. In [77] and [64] studies, when increase the angle of toe dorsiflexion with Achilles tendon force, the strain of plantar fascia was nonlinearly increased.

The modeling study, conducted by [64], did not apply axial loads, however, it increased loading on the plantar fascia by increasing the angle of dorsiflexing the toes, which increased strain, on the plantar fascia, but not as significantly as increasing loading on the Achilles tendon or the axial load. However, the strain with 5mm thick plantar fascia was measured much higher than other cases (Figure 13).

Further investigation of the characterization of soft tissue in this model must be conducted to analyze the plantar pressure and stress on hindfoot and forefoot. This model was also limited because it was only axially loaded and should be tested with off axis loads, and with non-linear and pathology specific material properties.

## 2.6 CONCLUSION

A 3D finite element model with varying plantar fascia thicknesses was developed to understand the effect of plantar fascia thickness for a patient with plantar fasciitis and diabetes because a thicker plantar fascia was measured from the patients. Results indicated that, plantar fascia strain increased with thicker the plantar fascia, which suggests that this should be further investigated while examining aspects such as plantar pressure and peak stress on the soft tissue. In

future iterations of the model, plantar soft tissues will be included as well as non-linear and pathology specific material properties.

## CHAPTER III

### THE EFFECT OF PLANTAR FASCIA THICKNESS AT VARIOUS FOOT POSITION IN A 3-D FINITE ELEMENT FOOT MODEL

#### 3.1 INTRODUCTION

The medial longitudinal arch of the foot supports body weight and absorbs ground reaction forces [31, 79]. The plantar fascia is one of major soft tissues that supports the medial longitudinal arch and transfers loads during gait, exercise, or running [79]. It is subjected to varying stresses such as the repeated tension loading and shear stress [76]. The repeated stresses increase the risk of injuries in foot such as plantar fasciitis which changes the properties of the plantar fascia [4]. Plantar fasciitis commonly causes inferior heel pain and Achilles tendon tightness, which limits the dorsiflexion of the foot [80]. Approximately, 2 million people suffer from plantar fasciitis annually in the United States [81]. Many clinical treatments such as stretching and orthosis like heel pad and arch supports are used to reduce the symptom of the plantar fasciitis. The surgical treatments like plantar fascia release are also used to reduce heel pain [80]. Simultaneously, many researchers have developed FE foot model to examine the strains or stresses distribution in plantar fascia during walking, standing, or under stretching using FE foot model [31, 36]. However, the effect of a thicken plantar fascia was not fully understood about the strains in plantar fascia because the FE foot model was simulated with one thickness of plantar fascia. Thus, we still need to learn about plantar fasciitis.

Patients with diabetes and/or plantar fasciitis have 15-100% higher plantar pressure than healthy subjects [4]. Additionally, the plantar fasciitis in people with diabetes or without diabetes affects the thickness of plantar fascia. Specifically, the healthy plantar fascia thickness has been reported 2.3 – 4.3 mm with an average of approximately 3.4 mm [66]. However, plantar fasciitis

patients without diabetes or with diabetes, the plantar fascial thickness measures approximately 4mm or greater [27, 66]. The patient with plantar fasciitis (PF) also measured 64% thicker in diabetic patients than patients without diabetes or control group [8, 66] (Table 6). However, the internal stress and strain measurement in plantar fascia have restrictively measured with in vivo study and in vitro study because of its intrinsic variability [36, 37].

Additionally, the peak plantar pressure of a diabetic foot was measured 50% higher at the 1<sup>st</sup> metatarsal head and 39% higher at the 5<sup>th</sup> metatarsal head than a healthy subject [82]. This increase in plantar pressure could be caused by reduced contact plantar surface [82], reduced range of joint motion, the incensement in stiffness of soft tissue and plantar fascia, and the deformations of foot morphology [20, 83-85]. However, in the studies, the thickness of plantar fascia and planta soft tissue were not evaluated and quantitative in the test.

As a result, in the other vivo and in the vitro studies were used to investigate the effect of plantar fasciitis and to improve our understanding of the functional behavior of the foot and ankle joints [78, 86]. The computational modeling of the foot and ankle were also used to figure out the relationship between the plantar fascia thickness or plantar pressure and plantar fasciitis. Nowadays, many studies have analyzed the relationship between plantar fasciitis and diabetes or plantar pressure [21, 87]. Also, some studies have examined foot deformities, degeneration, and injuries in patients with diabetes [32, 74]. In previous studies, the plantar pressure was collected at a neutral standing position or during gait, so the effect of thicken plantar fascia in the different foot positions (e.g., 10-degrees dorsiflexion and 10-degrees plantar flexion) have not been addressed yet.



Table 6 The thickness of plantar fascia between control group and patient with plantar fasciitis or diabetes, which was measured in Sonographic and MRI.

	Control subjects (mm)		Patient with plantar fasciitis or diabetes (mm)		Reference
Facia thickness measured by Sonographic	(n =66) 3.19 ± 0.43		(n=81) 5.61 ± 1.19		[88]
Facia thickness measured by Sonographic and MRI	MRI	Sonography	MRI	Sonography	[24]
	(n=154) 3.0 ± 0.5	3.2 ± 0.4	(n=68) 5.6 ± 1.3	4.9 ± 0.9	
Facia thickness measured by Sonographic	3.37 ± 1.0		4.75 ± 1.52		[23]
Fascia thickness measured by Sonographic	2.0 ± 0.5		2.9 ± 1.2 3.0 ± 0.8 3.1 ± 1.0		[20]
Fascia thickness measured by Sonographic	-		(n =39) 5.71 ± 1.33		[27]

### 3.2 STATEMENT OF PURPOSE

2-dimensional or 3-dimensional finite element method are popular methods to understand the internal stress and strains in plantar fascia in static conditions like standing [32, 34, 35, 37, 87, 89] and dynamic conditions such as walking [31, 36, 90, 91] and running [92]. Furthermore, the finite element analysis could help identify feet with increased risk for injury [34]. As aforementioned, the thickness of plantar fascia was affected by the foot pathologies and foot disease like plantar fasciitis and diabetes (Table 6). However, in previous literature, the thickness of plantar fascia was not considered or did not mention the thickness of plantar fascia in a finite element model of the human foot.

A 3D FE foot model with three different thickness of plantar fascia (e.g., 3mm, 4mm, and 5mm) in three different foot positions: such as neutral position, 10-degrees dorsiflexion, and 10-degrees plantar flexion to identify the plantar pressure with the different thickness of plantar fascia.

The 3D FE foot models were used to predict the effect of thickness of plantar fascia on plantar pressure and peak von Mises stress at bones. Furthermore, the plantar pressure of the 3D FE foot models was analyzed in different foot positions to examine the how much the foot positions affect the plantar pressure in forefoot and rearfoot.

### 3.3 METHODS

#### 3.2.1 Three-dimensional FE foot model including plantar fascia and plantar soft tissue

A 3D FE foot model was developed based on the CT images of a cadaver foot, including tibia, fibula, talus, calcaneus, navicular, cuboid, three cuneiforms, metatarsals, and phalanges. Also, the cartilage at each foot joint was created as single segment that filled the space between the bones based on CT images. However, the cartilages of the ankle joint for tibia, fibula, and talus were created separately (Figure 14 and 15). The thickness of cartilage was designated based on the distance between tibia and talus or talus and fibula (Figure 14). After creating a solid model of cartilage, it exported into Geomagic Design X (3D Systems) and Hypermesh (Altair) to create geometric model and FE model (Figure 15). The plantar fascia was also created as a solid model. In the CT images of a cadaver foot, it was hard to figure out the thickness, morphology, and length of plantar fascia, so the thickness of plantar fascia was created from calcaneus to metatarsal head for length, and the morphology and thickness of plantar fascia were developed based on the published literature (Table 6). The three different thickness of plantar fascia, 3mm, 4mm, and 5mm, were created for each foot position. Thus, a total of 9 plantar fascia were created in this research (Figure 17, 18, and 19). Four-node tetrahedral solid elements were used to mesh the bones, cartilage, plantar fascia, and plantar soft tissue (Table 7).

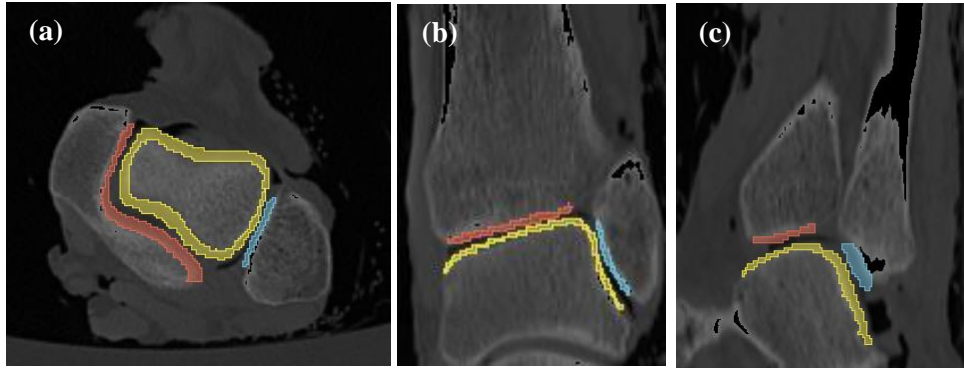


Figure 14 The CT scan images in three views show cartilages (yellow for talus; red for tibia; blue for fibula) at ankle joint. (a) the axial view; (b) coronal view; (c) sagittal view.

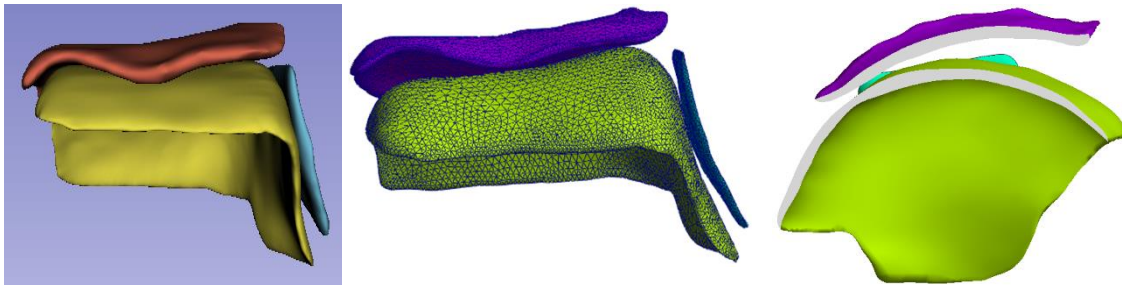


Figure 15 The 3D solid cartilages were created in 3D Slicer (a), and exported into Geomagic Design X and Hypermesh to create geometric model (b). The FE model was imported into FEBio (c).

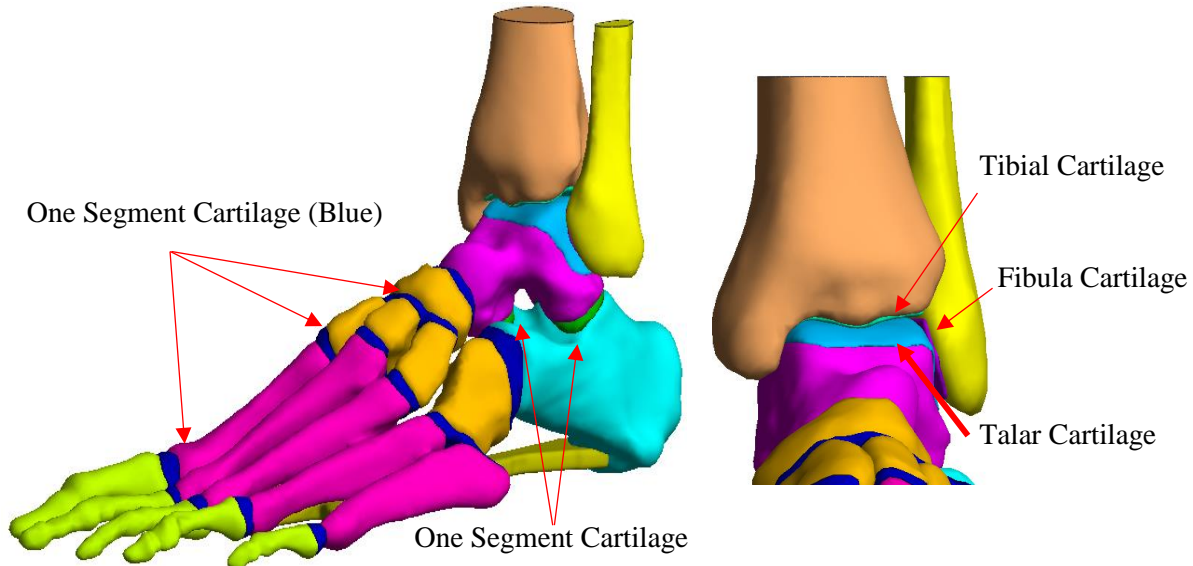


Figure 16 3D FE foot model including tibia, fibula, talus, calcaneus, cuboid, three naviculars, metatarsals, phalange is consisted of a one segment cartilage at each joint and plantar fascia. The cartilages at the ankle joint were created separately.

Table 7 The 3D FE foot model contained a total of 542595 elements. The Each segment showed a different number of elements.

Name of segments	Number of Elements	Type of Element
Tibia with tibial cartilage	27127	4-node tetrahedral solid (TET4)
Talus with talus cartilage	8855	
Fibula with cartilage	32840	
Calcaneus	23503	
Navicular	4513	
Three Cuneiforms	7254	
Cuboid	4500	
Metatarsal	23160	
Phalanges	47912	
other cartilages	37142	
3mm Plantar fascia	75930	
4mm Plantar fascia	83610	
5mm Plantar fascia	89887	
Soft tissue (Fat)	249859	

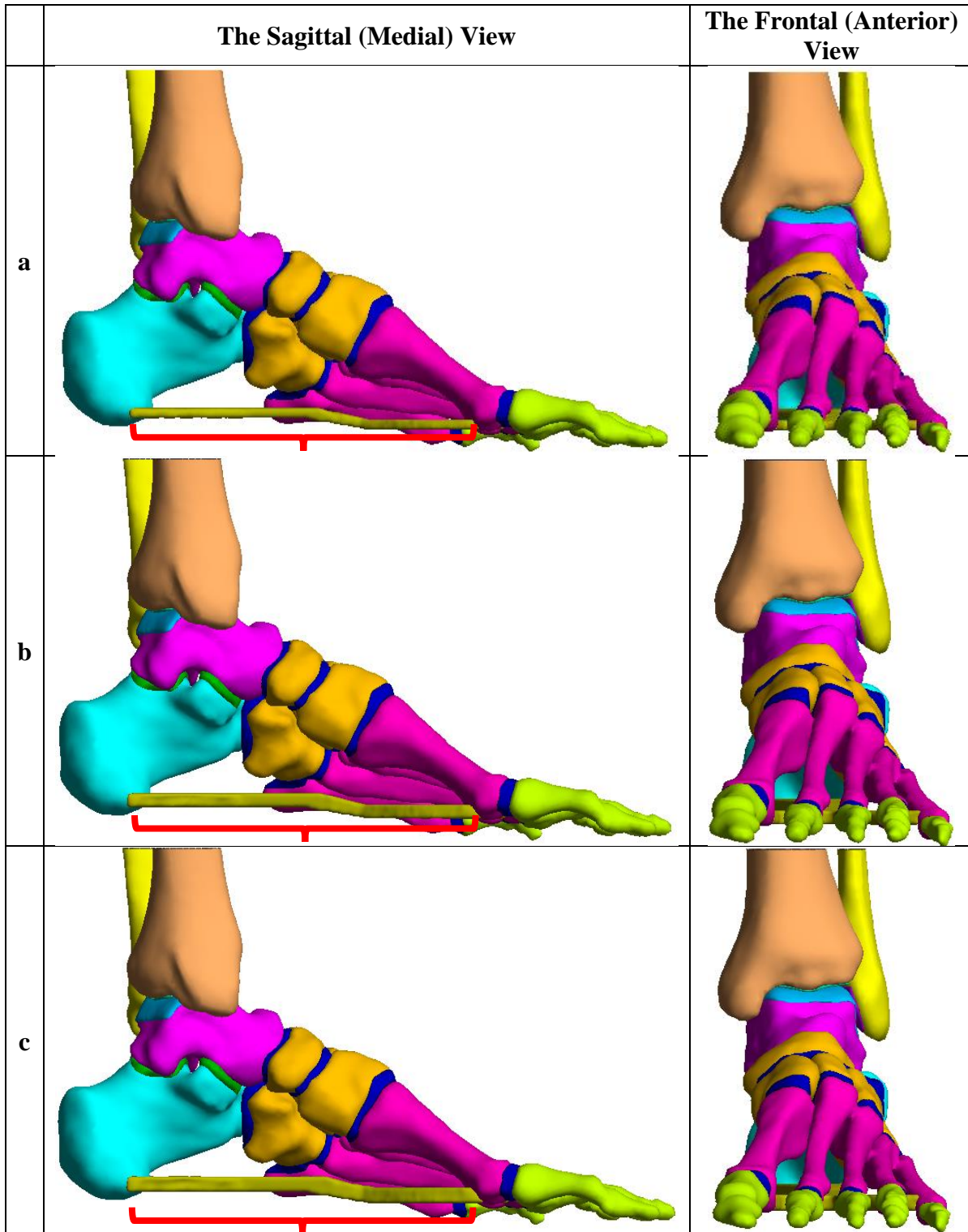


Figure 17 The 3-dimensional FE foot model at neutral position in sagittal and frontal view with a) 3mm, b) 4mm, and c) 5mm thick plantar fascia.

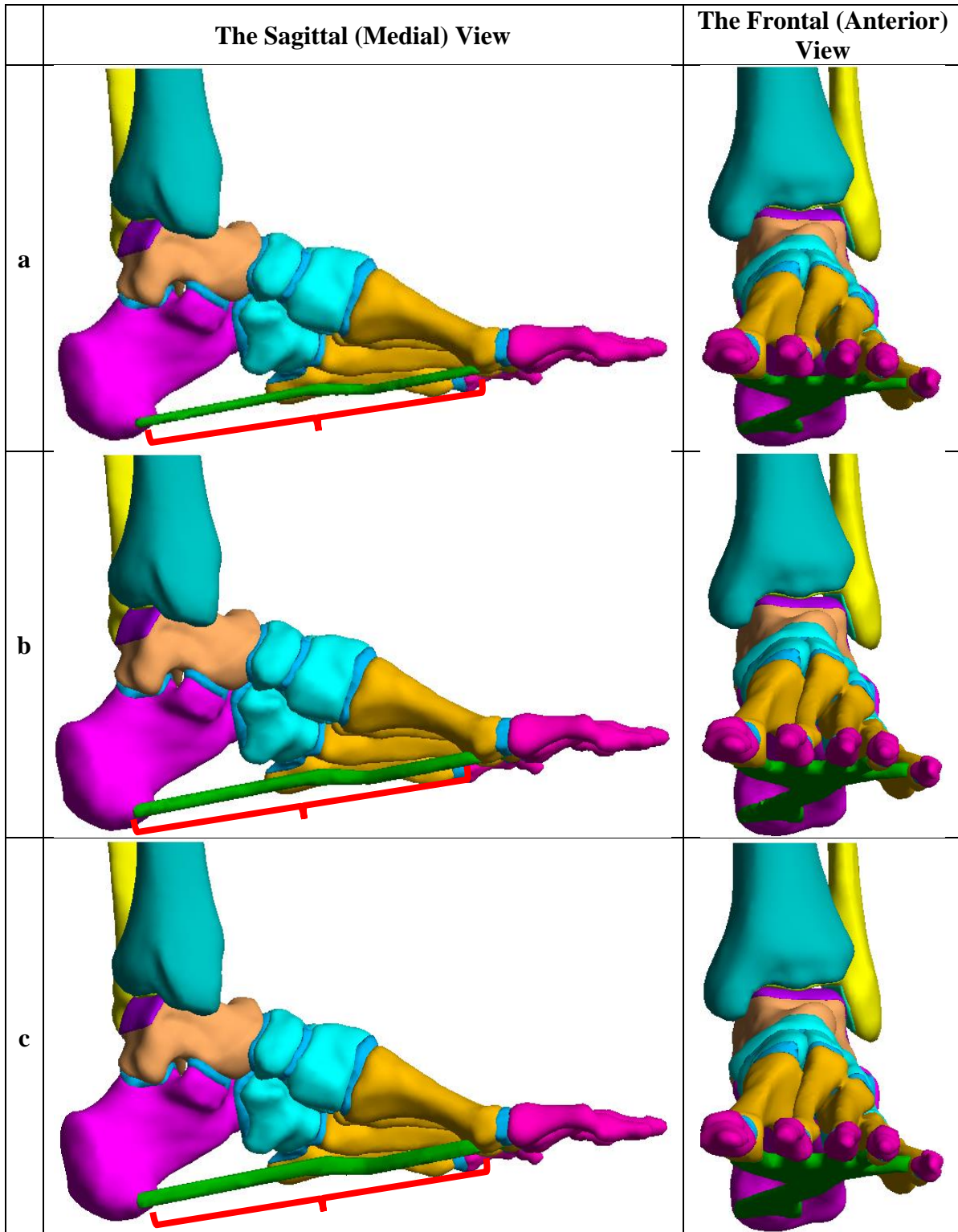


Figure 18 The 3-dimensional FE foot model at 10 degree dorsiflexion in sagittal and frontal view with a) 3mm, b) 4mm, and c) 5mm thick plantar fascia.

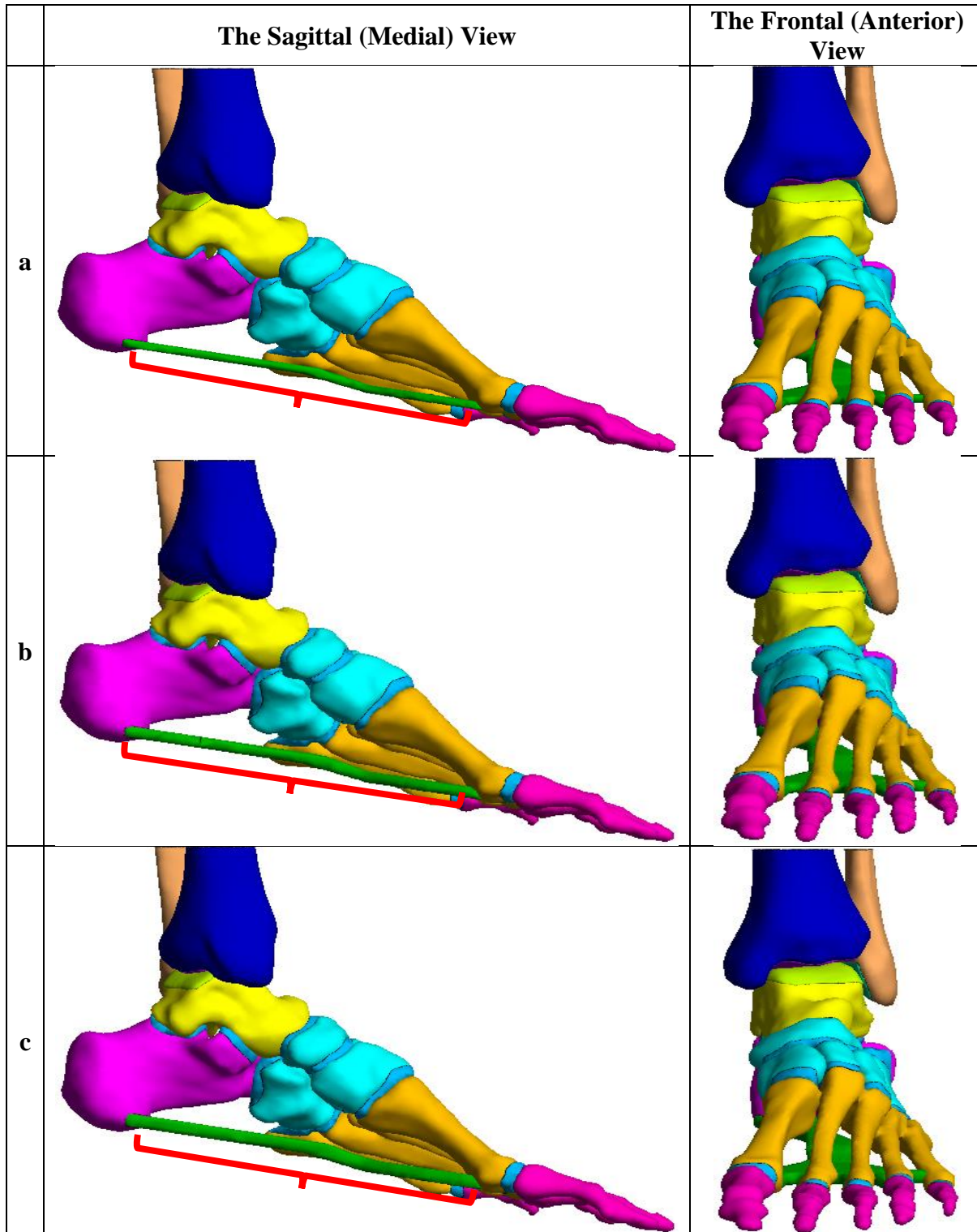


Figure 19 The 3-dimensional FE foot model at 10 degree plantar flexion in sagittal and frontal view with a) 3mm, b) 4mm, and c) 5mm thick plantar fascia.

For this research, CT scan was used to build the 3-dimensional (3D) geometric model for the foot and ankle. CT scans were obtained from the lower limb of a death male cadaver (unknown age) at three different foot positions neutral position, 10-degrees plantar flexion, and 10-degrees dorsiflexion (Figure 20).




	<b>Dorsiflexion</b>	<b>Plantar flexion</b>
<b>Neutral Position</b>		
<b>10-Degrees</b>		

Figure 20 The Computed Tomography (CT) scan was taken with lower limb cadaver in the three different foot angle like neutral position, 10-degrees dorsiflexion, and 10-degrees plantarflexion.

The plantar soft tissue was also developed based on the CT images as a 3D solid model (Figure 21). After that, the foot model was imported into Geomagic Design X to create as solid geometric model and Hypermesh to create FE model like creating bone and cartilage. Before FE model was created, the solid foot model was removed the intersection area between bones, cartilages, and soft tissue (Figure 22 and 23).



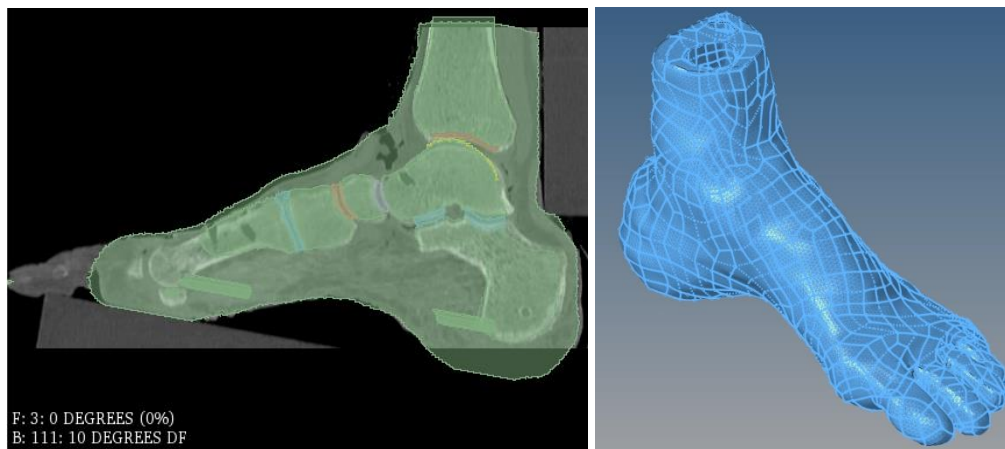


Figure 21 The 3D soft tissue of foot created on 3D Slicer (left). After that the 3D Solid foot model was imported into Geomagic Design X for creating geometric model and boolean intersection area between bones, cartilage, plantar fascia and soft tissue and Hypermesh for creating FE model (right).

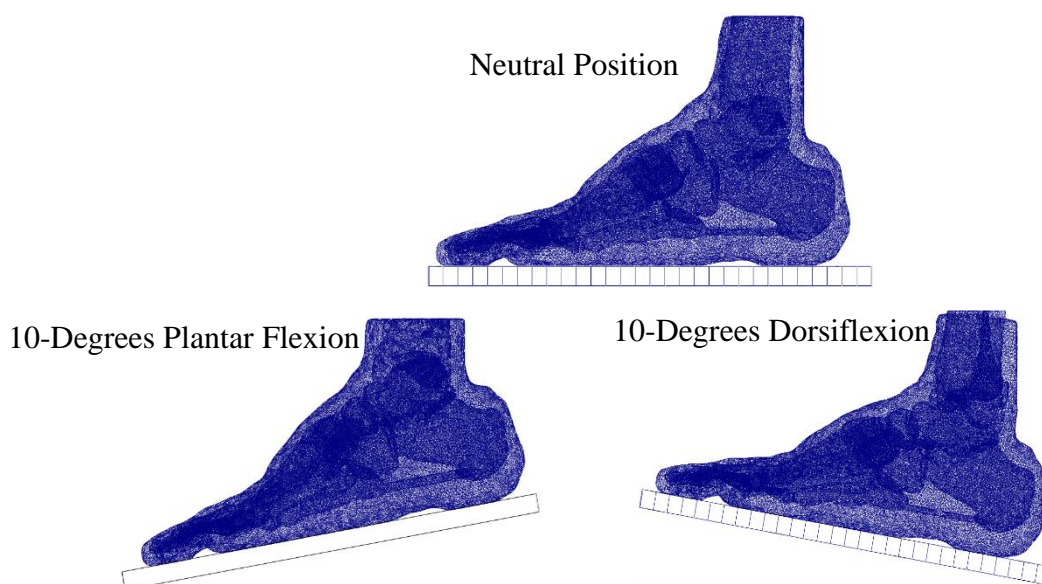


Figure 22 The 3D soft tissue foot with Boolean intersection area between bones, cartilage, plantar fascia, and soft tissue.

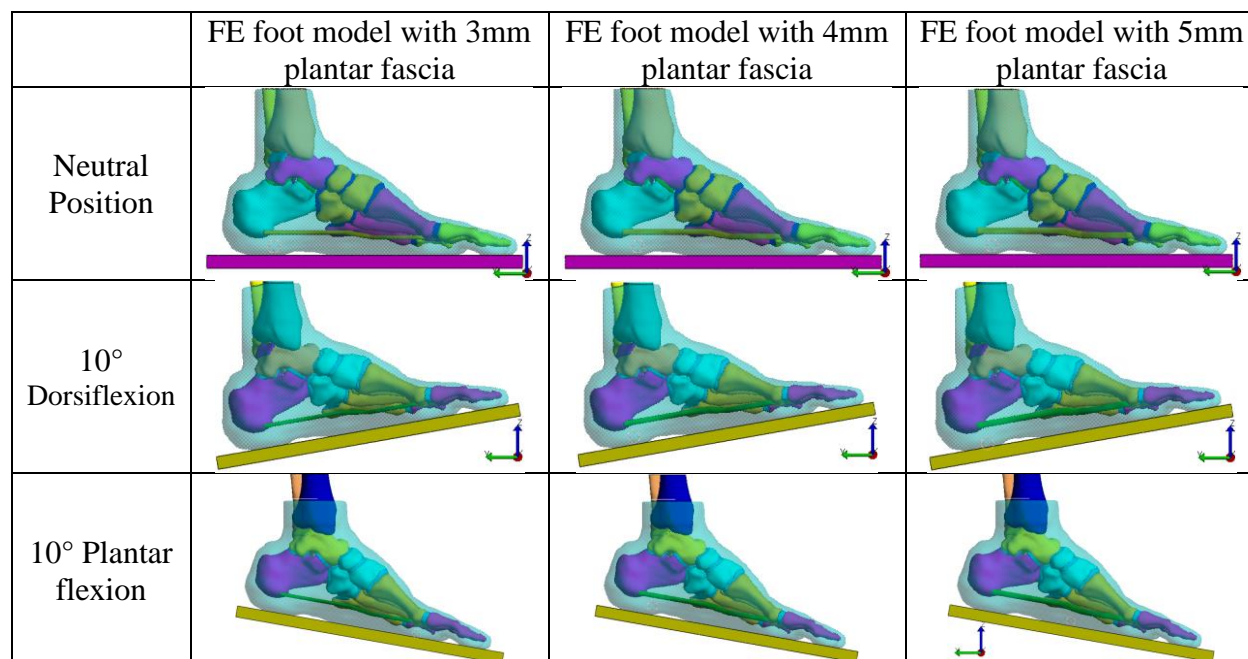


Figure 23 The 3D FE foot model in various foot positions were developed with three different thickness of plantar fascia.

The 3D finite element (FE) models including plantar soft tissue and plantar fascia were developed using Hypermesh (Altair), and FEBio (FEBio). Homogeneous isotropic elastic materials reported in the literature were used (Table 8) [31, 35, 36, 75, 93].

Table 8 Material properties and element types for bone, cartilage, plantar fascia, and plantar soft tissue

	Young's modulus (MPa)	Poisson's ratio	Element type	Reference
Bone	7300	0.3	3D-Tetrahedral solid	[35, 36]
Cartilage	100	0.4	3D-Tetrahedral solid	[31]
Plantar fascia	350	0.3	3D-Tetrahedral solid	[75]
Soft tissue	2.49	0.49	3D-Tetrahedral solid	[93]
Plate	Rigid body			

### 3.2.2 Numerical simulations

To evaluate the effect of thickness of plantar fascia in various thickness of plantar fascia and various combination of foot positions on plantar pressure responses, a 700 N axial load was applied to the top surface of tibia and fibula. Only vertical movement was allowed at the top surface of the tibia and fibula (Figure 24). The five phalanges were also fixed in all six degrees of freedom (DoF). The sole of the foot contacted to the top surface of a rigid plate (Figure 25). At the ankle joint, the tied surface to surface methods was used. Total 9 FE foot models simulated under the given conditions (Figure 23).

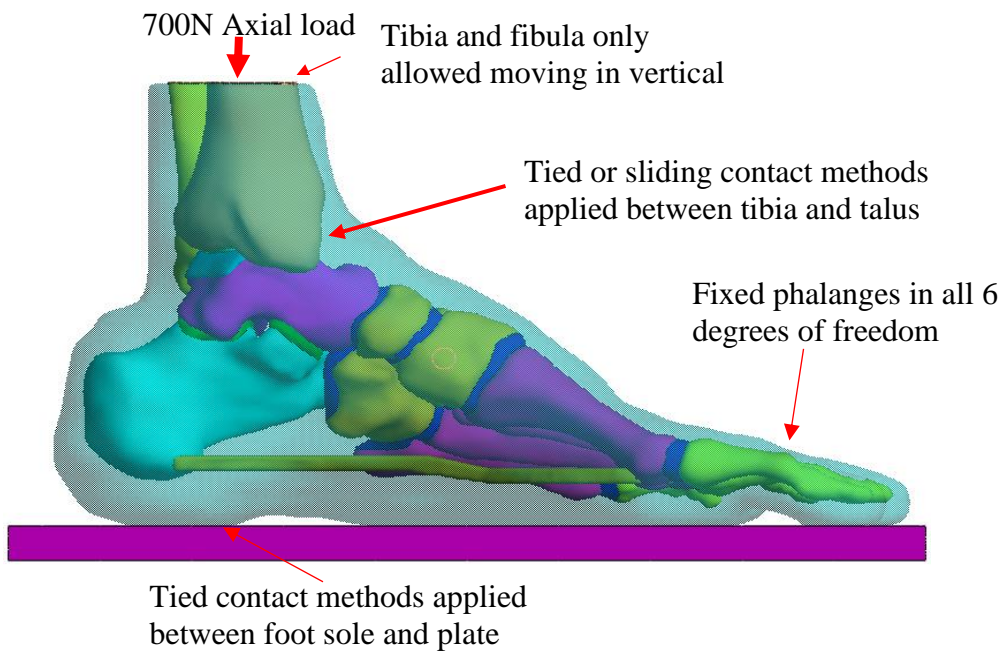


Figure 24 The 3D FE foot model was simulated under 700N axial load. The tibia and fibula only allowed to move in vertical movement. The phalanges were also fixed in all 6 degrees of freedom.

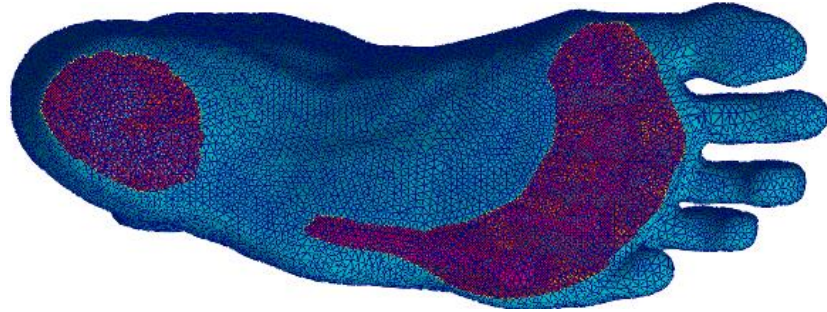


Figure 25 The tied contact method applied between foot and plate. The contact area was selected like the highlighted area on foot sole.

### 3.4 RESULTS

In the neutral position, the max stress ranged from 0.11104 – 0.11192 MPa at heel and from 0.10597 – 0.10628 MPa at forefoot in 3mm thick plantar fascia. At 10-degrees dorsiflexion, the peak stress ranged from 0.12713 – 0.12875 MPa at heel and 0.14709 – 0.14845 MPa at forefoot. At 10-degrees plantar flexion, the peak stress ranged from 0.13131 – 0.13283 MPa at heel and 0.15783 – 0.15891 MPa at forefoot. The plantar pressure was a tendency for an increase at forefoot and rearfoot areas at two different foot positions. Thus, while changing the foot position, the plantar peak stress at heel and at forefoot was also increased to 10% between neutral and 10° dorsiflexion, measured 14% higher stress between neutral and 10° plantar flexion at heel. The stress increased up to 32% between neutral and 10° dorsiflexion and up to 42% between neutral and 10° plantar flexion at forefoot (Table 9, Figure 26, 27, and 28).

Table 9 The peak stress at heel and at forefoot with three different thickness of plantar fascia in various foot positions

Foot positions	Thickness of plantar fascia	Peak Stress at heel (MPa)	Peak Stress at forefoot (MPa)
Neutral Position	3 mm	0.11192	0.10597
	4 mm	0.11144	0.10613
	5 mm	0.11104	0.10628
10-degrees of dorsiflexion	3 mm	0.12875	0.14709
	4 mm	0.12758	0.14807
	5 mm	0.12713	0.14845
10-degrees of plantar flexion	3 mm	0.13283	0.15783
	4 mm	0.13210	0.15835
	5 mm	0.13131	0.15891

The internal stress at the bone was not only affected by the thickness of plantar fascia but also affected by the position of foot (Table 10). The peak stress in neutral position ranged from 1.54 MPa to 6.64 MPa with 3mm plantar fascia, from 1.47 MPa to 6.03 MPa with 4mm plantar fascia, and from 1.39 MPa to 5.52 MPa with 5mm plantar fascia (Figure 29). The peak stress of 6.64 MPa measured at cuboid with 3mm plantar fascia (Figure 29). In 10-degree dorsiflexion, the peak stress also predicted from 1.49 MPa to 9.31 MPa with 3mm plantar fascia, from 1.35 MPa to 7.97 MPa with 4mm plantar fascia, and from 1.30 MPa to 7.93 MPa with 5mm plantar fascia (Figure 30). The peak stress of 9.31 MPa measured at the cuboid (Figure 30). In 10-degree plantar flexion, the peak stress measured from 1.55 MPa to 3.99 MPa with 3mm plantar fascia, from 1.62 MPa to 4.10 MPa with 4mm plantar fascia, and from 1.59 MPa to 3.90 MPa with 5mm plantar fascia (Figure 31). The peak stress of 4.10 MPa measured at the head of the 2<sup>nd</sup> metatarsal (Figure 31). While reducing the thickness of plantar fascia, the peak stress was gradually decreased up to 98% at calcaneus or increased up to 63% at 5<sup>th</sup> metatarsal, but the peak stress at some of bone segment such as talus, cuboid, 2<sup>nd</sup> metatarsal, 4<sup>th</sup> metatarsal, and 5<sup>th</sup> metatarsal with 4mm plantar fascia was shown a little bit different peak stress.

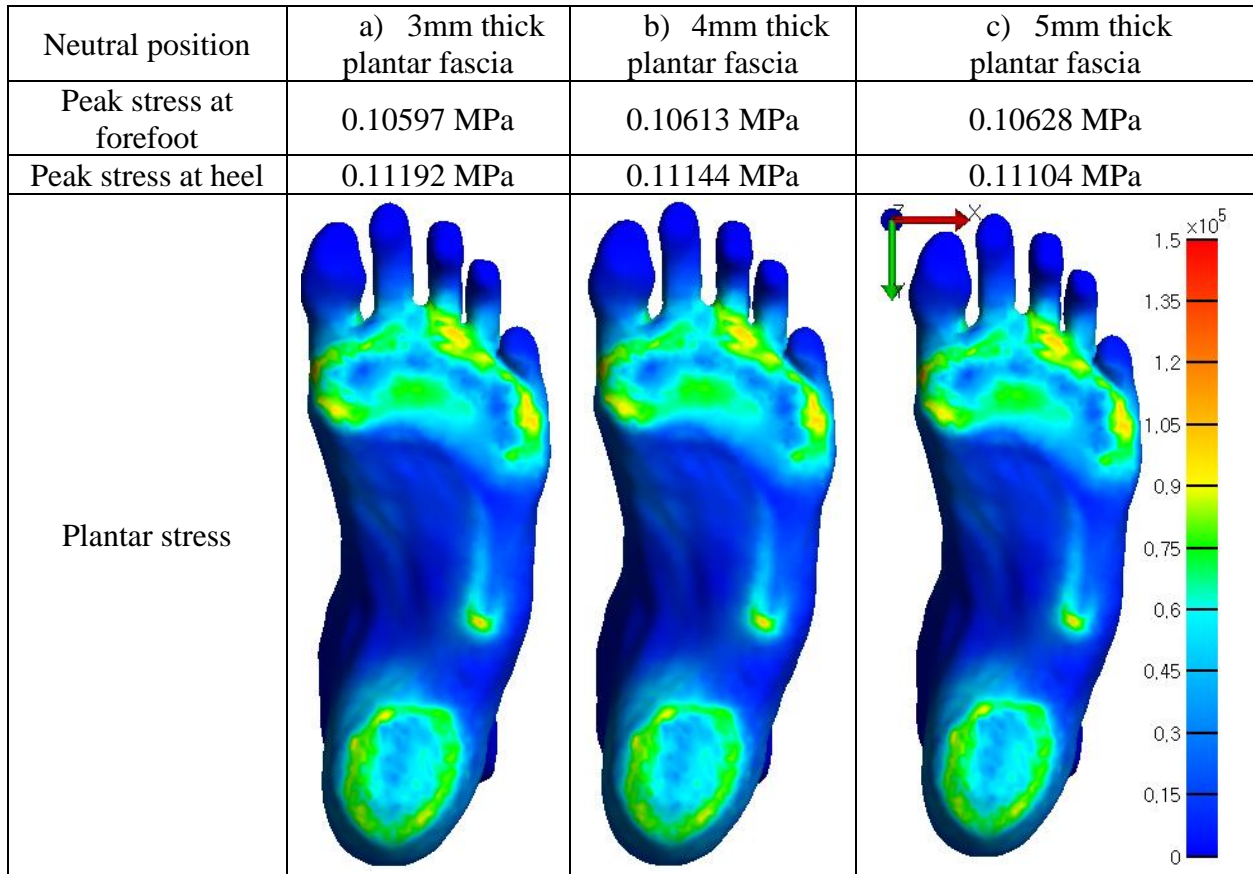


Figure 26 The plantar stresses at neutral position in axial views with a) 3mm, b) 4mm, and c) 5mm thick plantar fascia.

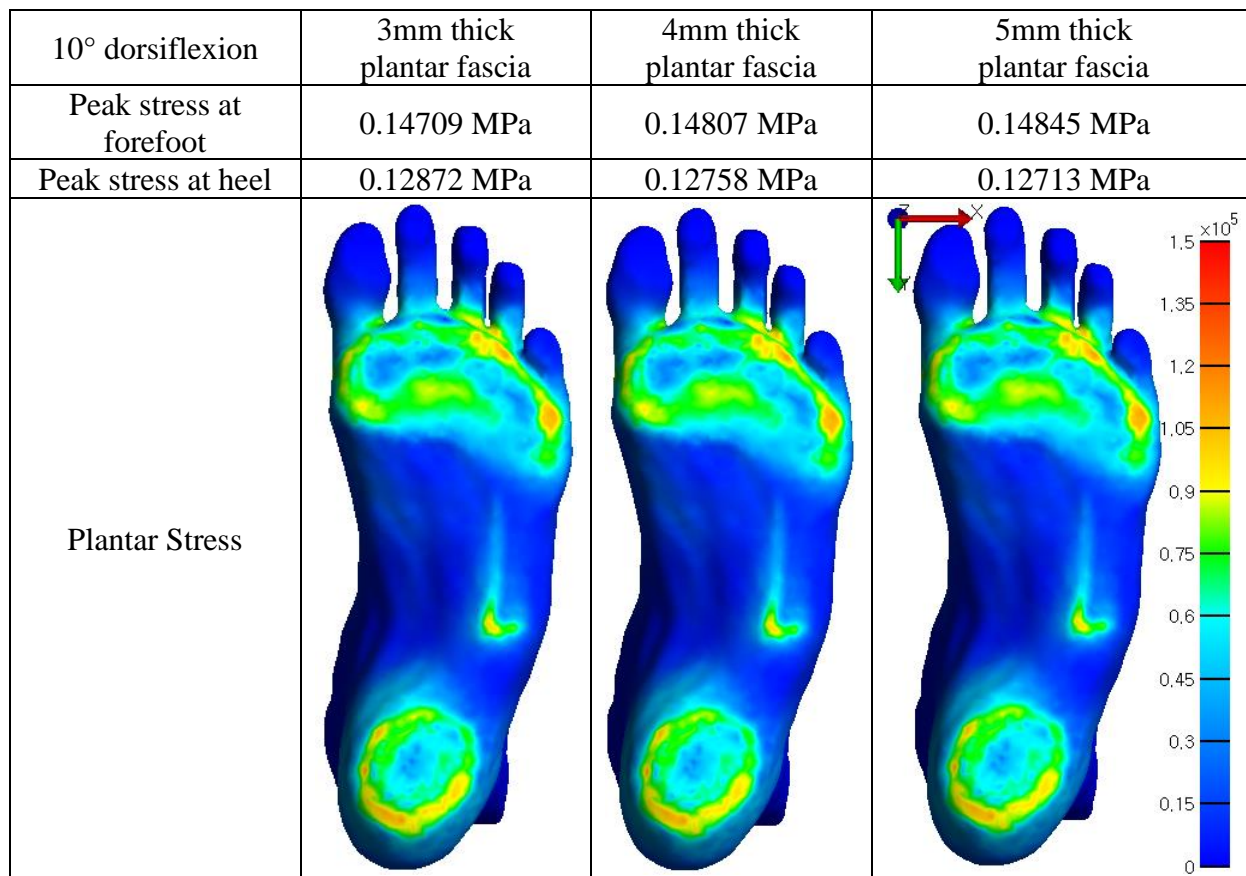


Figure 27 The plantar stresses at 10° dorsiflexion in axial views with a) 3mm, b) 4mm, and c) 5mm thick plantar fascia.

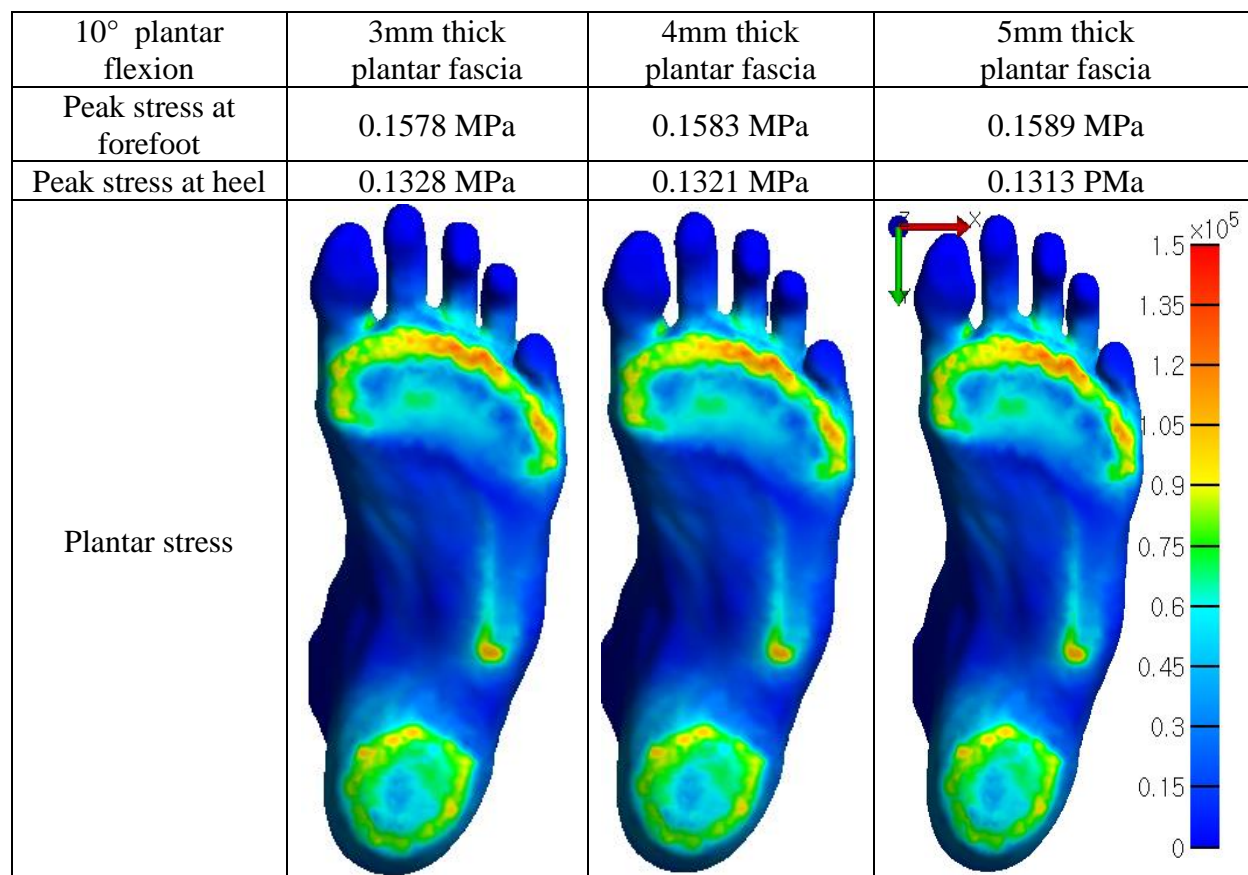


Figure 28 The plantar stresses at 10° dorsiflexion in axial views with a) 3mm, b) 4mm, and c) 5mm thick plantar fascia.

Table 10 The peak stresses in the segments of FE foot model with three different thickness of plantar fascia (e.g., 3mm, 4mm, and 5mm) in three different foot positions

Bone	Peak von Mises Stress (MPa)								
	Neutral Position			10° Dorsiflexion			10° Plantar Flexion		
	3mm	4mm	5mm	3mm	4mm	5mm	3mm	4mm	5mm
Talus	2.36	2.45	2.37	2.28	2.12	2.50	3.05	2.99	2.88
Calcaneus	1.70	1.67	1.64	5.99	2.14	2.08	3.87	2.43	2.50
Navicular	1.54	1.47	1.39	1.49	1.35	1.30	1.84	1.78	1.69
Cuboid	6.64	6.03	5.52	9.31	7.97	7.93	1.55	1.62	1.59
1 <sup>st</sup> Metatarsal	1.53	1.62	1.64	2.35	2.25	1.56	2.14	1.92	1.69
2 <sup>nd</sup> metatarsal	2.27	2.48	2.62	4.04	3.01	2.44	3.89	4.10	3.86
3 <sup>rd</sup> metatarsal	2.73	3.10	2.95	2.71	2.81	3.54	2.77	2.79	3.22
4 <sup>th</sup> metatarsal	1.95	1.87	1.81	2.43	2.11	2.12	2.82	1.84	1.87
5 <sup>th</sup> metatarsal	1.86	3.21	3.58	4.86	4.56	4.22	3.99	3.54	3.90



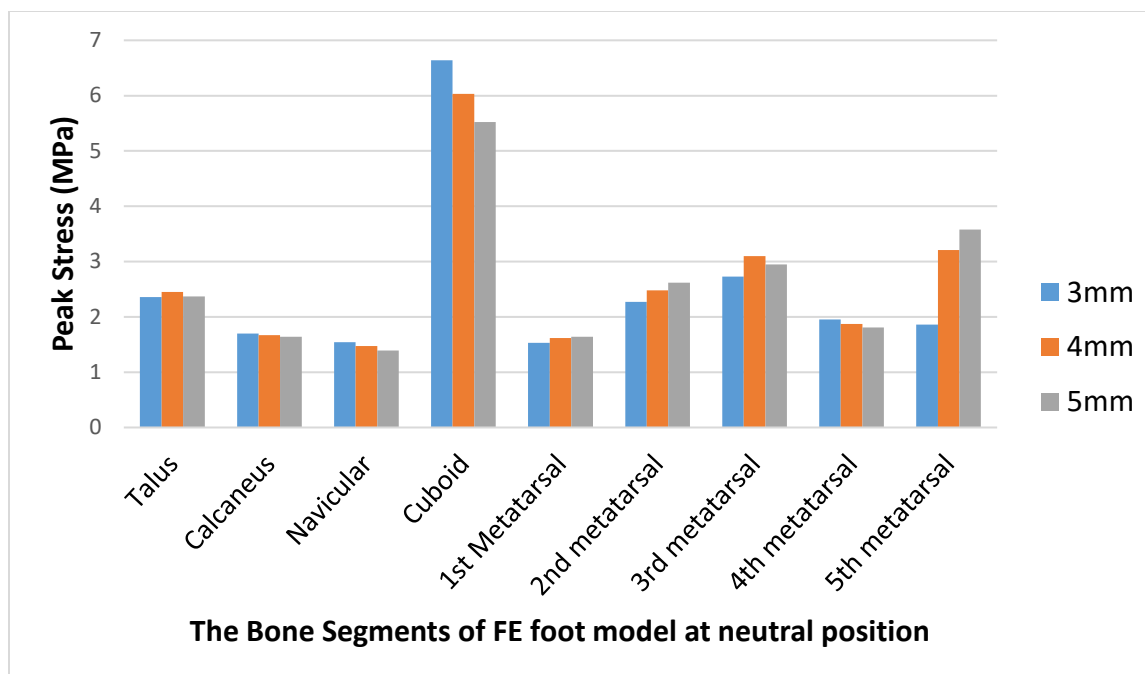


Figure 29 The peak von Mises stress of bones in 3D FE foot model at neutral position with three different thickness plantar fascia.

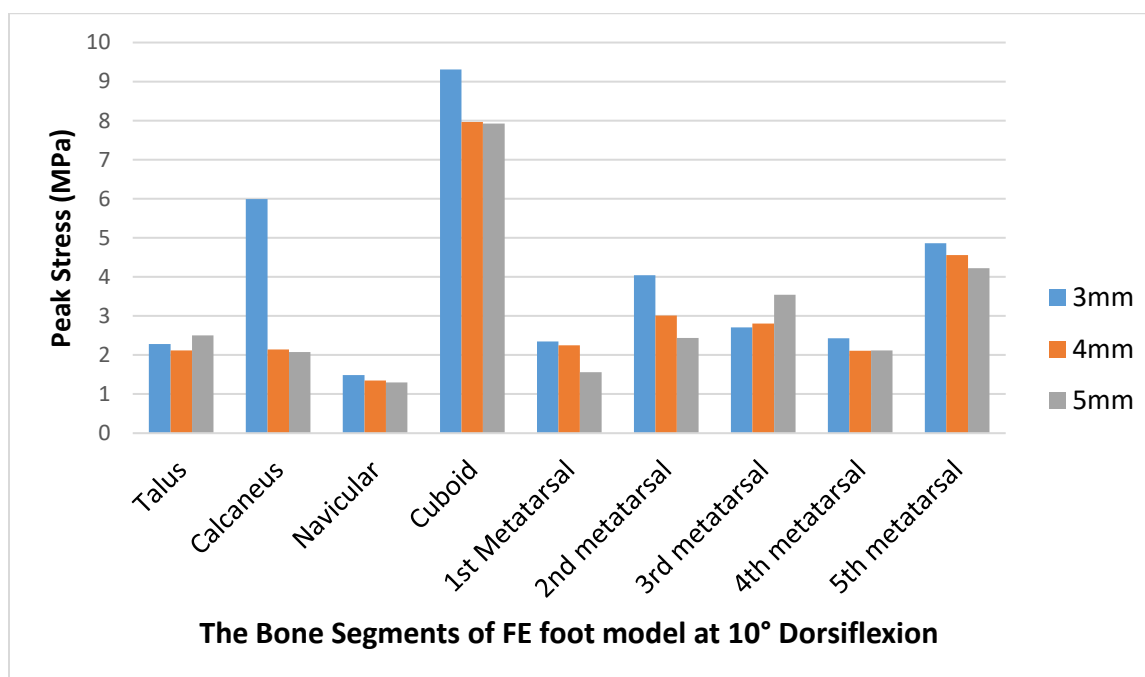


Figure 30 The peak von Mises stress of bones in 3D FE foot model at 10° dorsiflexion with three different thickness plantar fascia.

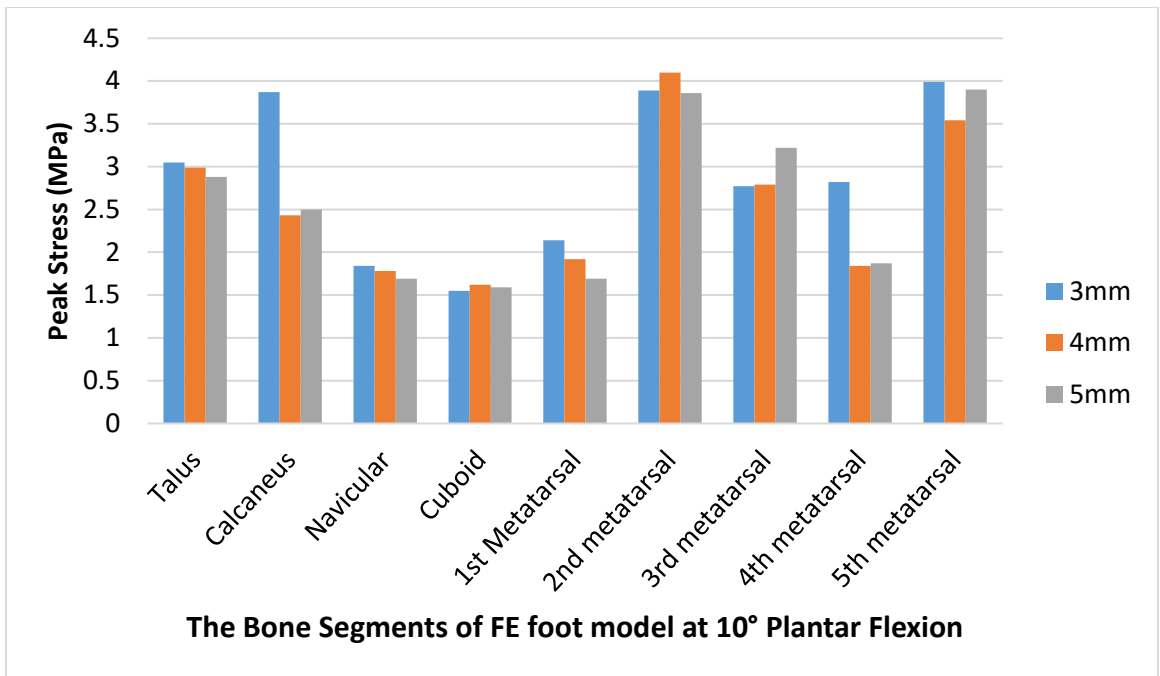


Figure 31 The peak von Mises stress of bones in 3D FE foot model at 10° plantar flexion with three different thickness plantar fascia.

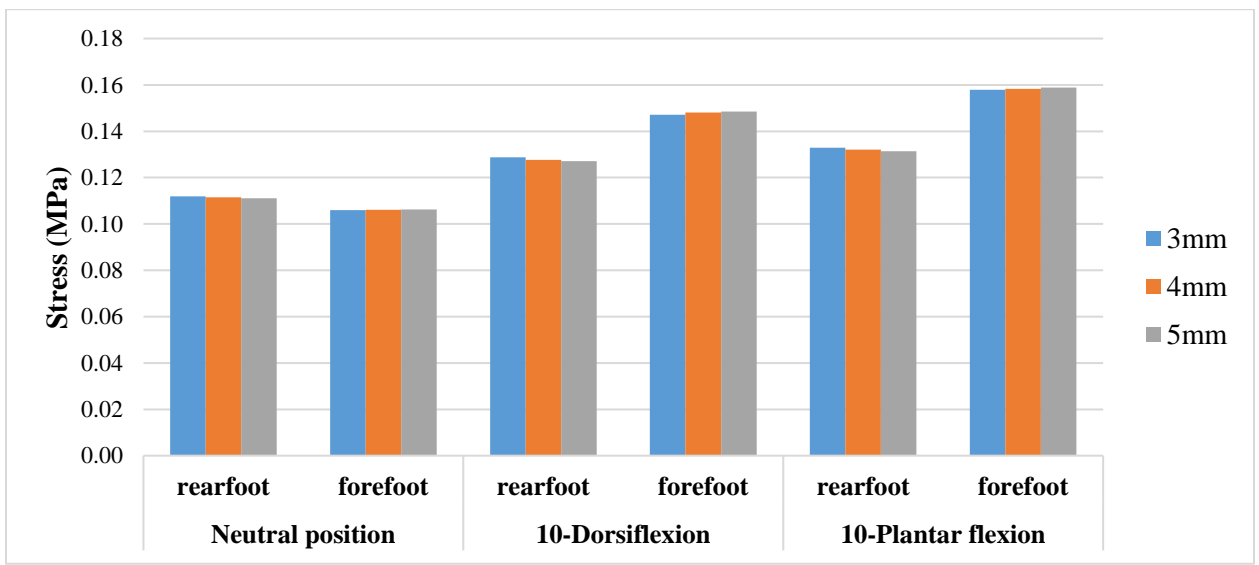


Figure 32 The stresses at rearfoot and forefoot area are measured in various foot positions with three different thickness of plantar fascia.

### 3.5 DISCUSSION

The finite element foot and ankle model were developed to study the effect of the stiffness of plantar fascia in various foot positions on the internal stress at bones and the plantar pressure. The predicted plantar pressure and plantar pressure distribution were in general comparable to the experimental measurement or the previous published research [4, 32, 34]. In current study, the current predicted plantar stress and internal stress at bone were compared with the simulated data which was from the previous published research. Thus, the difference between the current study and the previous published literature may be caused by the loading conditions, material properties, and the different morphology of foot.

The simulated peak plantar pressure of the two models at static standing measured 0.11 MPa for healthy FE foot model and 0.237 MPa for diabetic FE foot model in [4]. In the current study, the peak stress measured 0.111 MPa at neutral positions, 0.1478 MPa at 10-degrees of dorsiflexion, and 0.159 MPa at 10-degrees of plantar flexion. The peak plantar pressure of [4]'s study in diabetic data showed 72% higher than the current simulated data. The difference may be caused by the material properties of plantar soft tissue, because second order hyperelastic polynomial parameter was used for plantar soft tissue in [4]. Also, the loading conditions were not same. In [4], the specific loading conditions were applied to the FE model, but the 700N axial load applied in the top surface of tibia and fibula in current FE foot model.

The peak plantar pressure also measured 0.168 MPa for the FE foot model and 0.130 MPa for the F-scan during standing in [34]. The FE model predictions between [34] and the current study showed a 40% difference, but the difference between the current plantar stress and the F-scan data of [34], showed 16% different. The difference may be also caused by the non-linear and linear material properties and loading conditions (365N ground reaction force and 165N Achilles

tendon loading in [34]'s study) in predicted measurement and F-Scan data. Furthermore, the difference may be caused by the material properties of soft tissue. The second order polynomial was applied to plantar soft tissue, but linear elastic material property was applied in the current study.

The plantar pressure in the current 3D FE foot model ranged from 0.10597 MPa to 0.15891 MPa, which was similar the results of the predicted peak pressure at forefoot area [76]. The difference between the current study and [76] may be caused by the material properties of soft tissue. The hyperelastic polynomial material properties were applied in the plantar soft tissue in [76]. In the current study, when increased the thickness of plantar fascia, the peak plantar stress at forefoot area was increased, but the peak plantar stress at heel was decreased. However, the plantar pressure in [76] in rearfoot was increased when increased the stiffness of plantar soft tissue.

The stance phase of gait can be divided three different positions, i.e., heel strike, midstance, and push-off [94]. The peak force in stance phase of gait showed two peak forces at midstance and push-off, so the shape of stance phase of gait in the peak force showed M curve. In the normal walking, the peak force at midstance was higher than the peak stress at push-off. However, in the pathological walking, the peak stress at push-off was higher than the peak stress at midstance [94]. In the current study, while the thickness of plantar fascia and the foot positions was changed, the stress distribution was not changed much each other's. However, the peak plantar stress at the forefoot was increased, but the peak plantar stress at rearfoot was decreased when increasing thickness of plantar fascia. Also, when changing the foot position and increasing the thickness of plantar fascia at the same time, the higher peak stress measured at forefoot area than neutral position of FE foot model. Also, the peak plantar pressure tended to increase at 10 degrees dorsiflexion and 10 degrees plantar flexion and especially 10 degrees plantar flexion. Furthermore,

the plantar stress distribution at neutral position and 10-degrees dorsiflexion was widely spread out at rear foot and forefoot. In the other research, the distribution of stress showed similar pattern with the current study [32, 95, 96]. The stress was not measured under five phalanges area because the tied contact method was not applied in the area. However, In [86] the plantar pressure measured by F-scan (Tekscan Inc., Boston, MA) measured stress at rearfoot and forefoot including toe [86]. The peak stress in [86] at 1<sup>st</sup> toe. In [34], the peak stress measured by F-scan during standing measured around the center of heel. The stress distribution could be affected by the experimental environment. In the current study, with increased the thickness of plantar fascia, the peak stress was moving from 1<sup>st</sup> metatarsal to 5<sup>th</sup> metatarsal, so the stress distribution was also slightly moved to 5<sup>th</sup> metatarsal. Also, the peak stress was distributed around 3<sup>rd</sup>, 4<sup>th</sup>, and 5<sup>th</sup> metatarsal head in neutral position and 10-degrees dorsiflexion. However, peak stress in the 10-degrees plantar flexion was distributed widely from 1<sup>st</sup> metatarsal to 5<sup>th</sup> metatarsal. As a result, it was necessary to look at different foot positions.

### 3.6 CONCLUSION

3D finite element foot models with varying foot positions and plantar fascia thicknesses were created to examine changes that may occur in pathologies and injuries such as diabetes and plantar fasciitis. Because less flexible feet lead to higher plantar pressures the thicker plantar fascia that is measured in people with diabetes and plantar fasciitis, may contribute to foot ulceration, foot injury, or foot pain. In [97], the peak plantar pressure was significantly increased in all diabetic groups. Furthermore, the contact time between foot and ground was increased in diabetic group in [82]. In [37], the plantar pressure also was increased when increased the stiffness of plantar fascia. In the current study, the peak plantar pressures were also affected by the changing foot position.

The higher peak plantar pressure measured at 10° dorsiflexion and 10° plantar flexion than neutral position. As a results, the peak plantar pressure may have been affected by the diabetes, the stiffness of plantar fascia, and foot positions in 3D FE foot model. Thus, FE foot models should consider the range of foot positions.

To simplify the analysis in this study, the homogeneous linear elastic material properties were assigned to the bony and soft tissue structures including plantar fascia and plantar soft tissue. FE analysis was performed in FEBio (version 2.7), but the version of FEBio didn't support the second order polynomial material properties. As a results, linear elastic material properties were applied instead of the polynomial material property. Moreover, the plantar fascia only supported the structure modelled. The long plantar ligament and short plantar ligament were not included. In future iterations of the model, the two plantar ligaments will be conducted with non-linear material properties. Furthermore, the other major ligaments should also be added to the ankle joints.

## CHAPTER IV

### THE EFFECT OF PATIENT SPECIFIC BONE GEOMETRY ON CONTACT STRESS IN 3D-FINITE ELEMENT HINDFOOT MODEL

#### 4.1 INTRODUCTION

Foot injuries (e.g., ankle sprains and fractures) and disease (e.g., diabetes) can alter the mechanics of the hindfoot. These alterations increase your risk of developing ankle osteoarthritis over just normal aging. Also, the bone morphologies and the cartilage thickness can change with how to use foot like professional athletes (e.g., soccer players and runners). Previous research has studied the difference of foot morphology between barefoot and shod in running or between normal people and soccer group [98, 99].

The density of the articular surface of ankle joint was measured and compared between control group and soccer group in [99]. The density at ankle joint was measured differently between soccer group and control group. In the soccer group, the higher density measured than control group. The higher articular contact stress also measured in soccer group. In [98] studied about foot morphology between barefoot and shod in running. The feet morphology between unshod feet and shod feet measured significantly different with foot length and foot width [98]. In the different foot types such as planus, neutrally aligned, and cavus, the foot morphology in each foot type is shown different foot morphology . Specially, the dimension of bones (e.g., calcaneus, talus, navicular, and cuboid) measured significantly differently in each model [100].

Furthermore, the thickness of cartilage may also affect the articular contact stress at the ankle joint. In the previous study, the cartilage thickness was measured to identify the effect of pathological degeneration, the difference between healthy individual and ankle instability, and inflammatory joint disease. [101] measured the thickness of cartilage with 35 ankle cadavers

measured in the ranges 1.54 to 2.53mm at the former and the latter 2.07 to 2.98mm [101]. They measured the cartilage thickness separately in four distinct areas on each segment square using Swann and Seedhom technique. [102] measured the cartilage thickness of 16 healthy volunteers using MRI. The thickness of cartilage measured from 0.57mm to 0.89mm. According to the previous studies, the cartilage thickness is affected by the age, foot pathology, or foot disease (Table 11 and Table 12).

Table 11 The thickness of cartilage at ankle including the measurement methods.

Author	Talus					Methods
[103]	Control Group	Chronic ankle Injured Group		Age	21.0±2.5 years 21.2±1.8 years	LOGIQe system - Ultrasound
	0.45±0.083mm	0.427±0.094mm				
Author		Fibula (mm)	Tibia (mm)	Talus (mm)	Age (mean)	Methods
[104]	mean	0.85	1.16	1.10	61.5 years	Stereophotography system - ATOS
	max	2.06	2.18	2.38		
[102]	mean	x	0.89	0.72	22-27 years	MR images
	max	x	1.54	1.30		
[101]	mean	x	1.35	1.16	65.1 years	in Vitro needle force probe technique
[105]	mean	x	1.14	1.22	51 years	in Vitro needle force probe technique

Table 12 The mean thickness of cartilages in two groups, healthy and patient with ankle injuries.

	Healthy Group		Patient Group	
	Model 1 healthy cadaver	Model 2 from web	Model 3 patient- total ankle replacement	Model 4 patient- fuse ankle joint
The cartilage thickness (mm)	1.5	0.55	0.5	0.85
Age	Over 70 years	Unknown	72 years	72 years



## 4.2 STATEMENT OF PURPOSE

The thickness of cartilage was not considered in the previous 3D FE models. Also, the previous studies were conducted to investigate the difference between shod and unshod foot and between athletes and normal group concerning different foot width and length, density at the distal tibia and proximal talus. However, the mechanical analysis like the contact stress and the contact stress distribution has not widely studied. Thus, the aim of this study was to figure out the relationship between the bone morphology and cartilage thickness in the peak stress and the stress distribution in the talocrural joint.

## 4.3 METHODS

### 4.3.1 Development of the 3D FE model of bone

The 3D finite element models of the talocrural joint including tibia, talus, and cartilage were developed based on three different computed tomographic (CT) scans (Figure 33) (one death of the male cadaver in which the age was unknown and two for ankle patients before surgery) and one generated in MRI (BodyParts3D) which was taken from Japanese adult males and females of average height and weight. The geometries of two of the 3D FE models were constructed based on the CT scan images taken before surgery. One patient received a total ankle replacement (TAR) and the other received an ankle fusion. All CT images were imported into an open-source image computing platform called 3DSlicer (version 4.10.2) to create solid tibia and talus models, and the solid models were exported into Geomagic Design X (3D Systems) and Hypermesh (Altair) to generate geometric and solid finite element models. The 3D FE foot model were imported into FEBio (Figure 34). The linear elastic material properties for the bones were assigned as 17000 MPa for Young's modulus and 0.3 for the Poison's ratio. The cartilage was assigned isotropic linear elastic material properties ( $E = 12\text{MPa}$  and  $\nu=0.42$ ) [106].

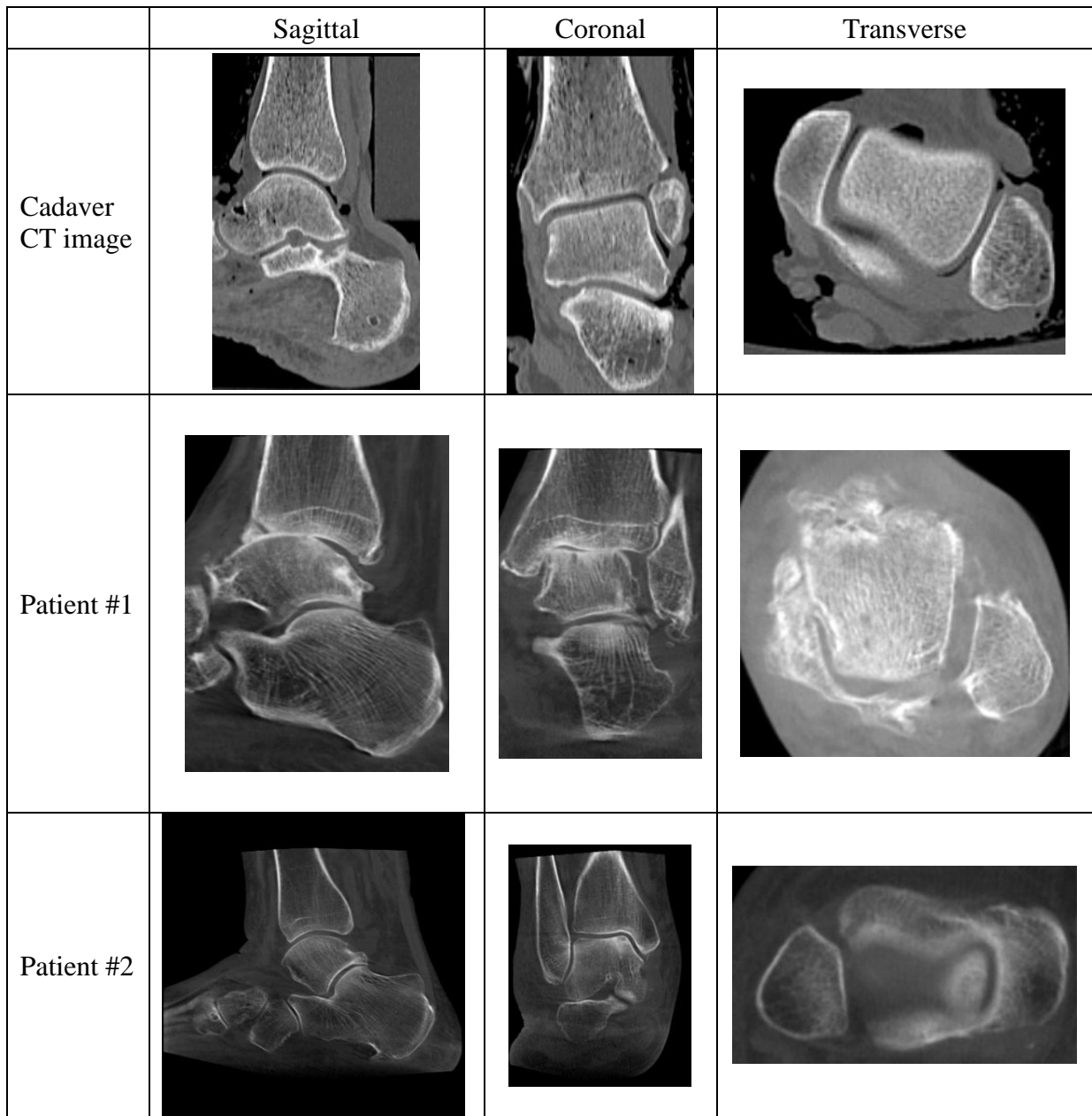


Figure 33 The three CT scan images. One is from a death male cadaver foot (unknown age) and another two CT scan images were from two patients before ankle surgery.

Table 13 The information about the two patients

	Patient #1, male	Patient #2, female
Age (years)	72.7	72
Weight (kg)	80.0	80
Height (cm)	165	165

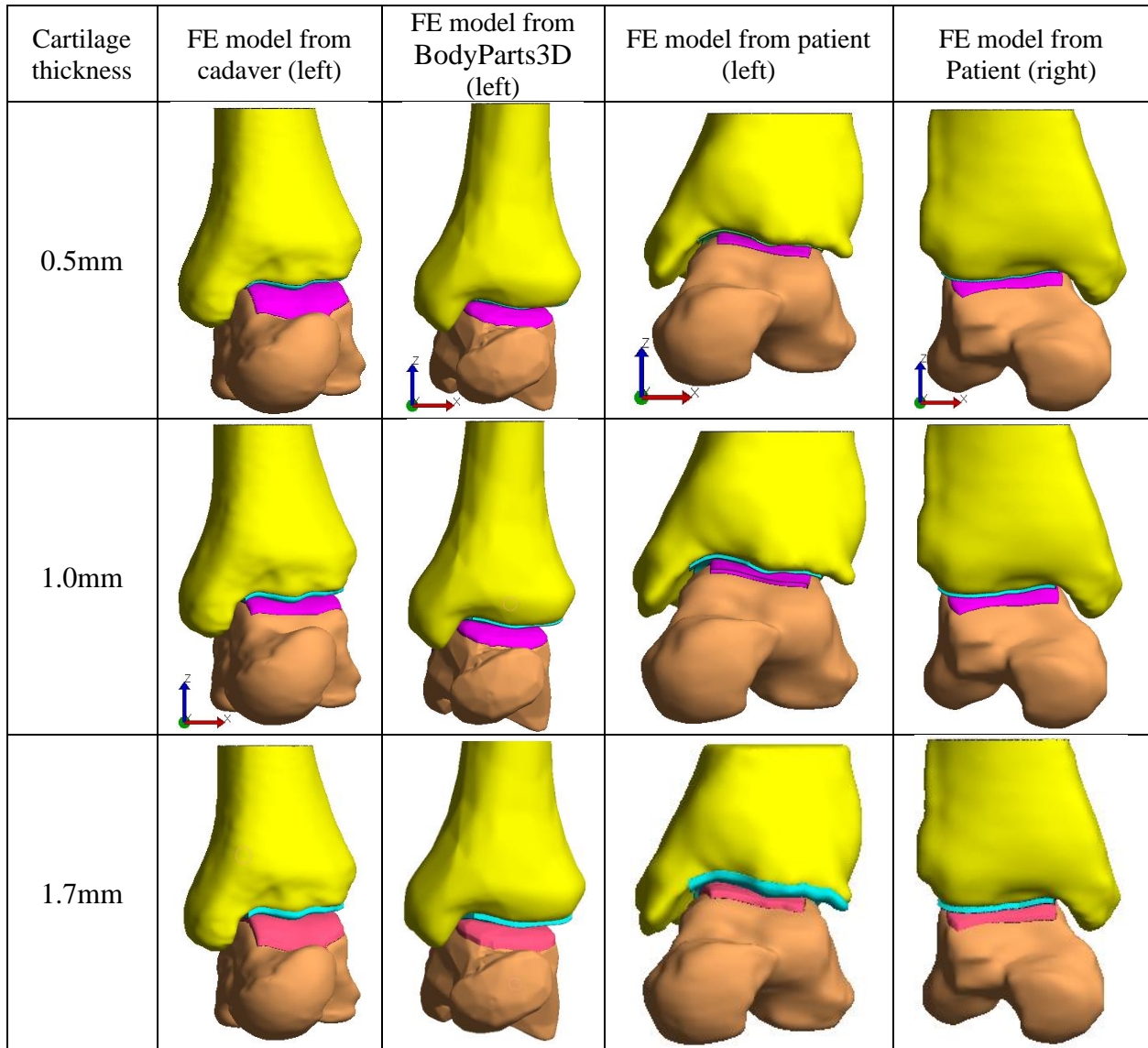


Figure 34 The 3D FE foot model including tibia, talus, and cartilage was created in three different thickness articular cartilage.

#### 4.3.2 Creating cartilage

The articular cartilage was added to the FE model by tracing the articular surface and extruding it to the desired thickness on the tibia and talus. In the published research, the cartilage thickness ranged from 1.06mm to 1.63mm at tibia, from 0.94mm to 1.62mm at talus, from 1.16 to 1.37mm at tibia, or 0.427 – 0.45mm, 0.85-2.38mm at talus (Table 11 and Table 14). In a computational model of the talocrural joint, cartilage was created to fill the joint space between

the tibia and talus, resulting in 1.7mm thickness of cartilage. Based on the prior literature, uniform cartilage thicknesses of 0.5mm, 1.0mm, and 1.7mm were created along the local bone surface (Figure 35). The cartilage was modeled as an isotropic linear elastic material property ( $E = 12\text{MPa}$  and  $\nu=0.42$ ) [106]. A single tension only linear spring ( $k=50\text{N/mm}$ ) placed to prevent anterior-posterior movement) [106] .

Table 14 The articular cartilage thickness at tibia and talus was measured in previous research.

Research	Tibia (mm)	Talus (mm)	Reference
Shepherd et al., 1999	1.06 – 1.63	0.94 – 1.62	[101]
Paschos et al., 2014	$1.07 \pm 0.15$	$1.57 \pm 0.16$	[107]
Cher et al., 2016	1.3 – 1.5	$1.6 \pm 0.1$	[108]
Millington et al., 2007	$1.16 \pm 0.14$	$1.1 \pm 0.18$	[104]
		$2.38 \pm 0.4$	

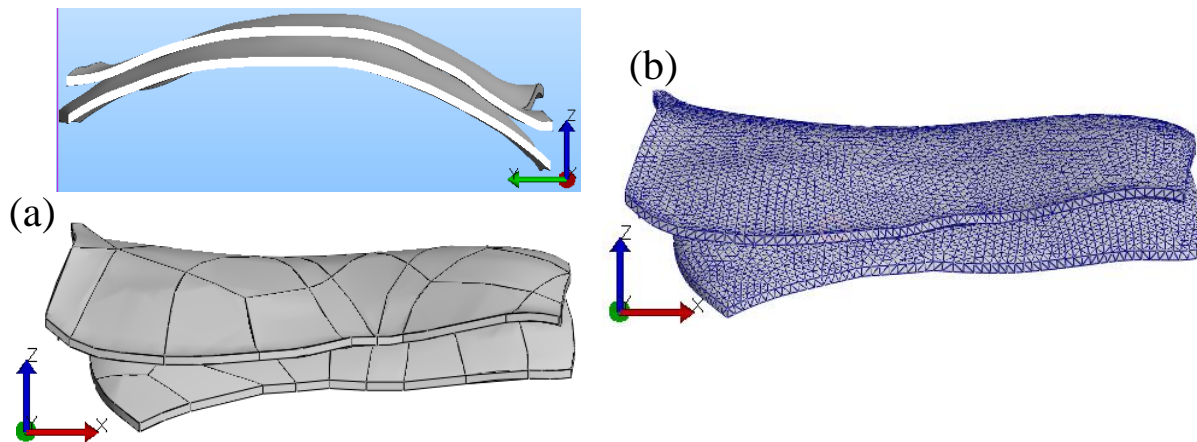


Figure 35 The articular cartilage was extruded along local bone surface normal between tibia and talus to a uniform thickness of 0.5mm, 1.0mm, and 1.7mm. (a) geometric model of the articular cartilage; (b) FE model of the articular cartilage.

### 4.3.3 Simulations

To evaluate the effect of thickness of articular cartilage in various foot models, the 700 N axial load on the top surface of tibia was applied, and the top surface of tibia only vertical movement was allowed (Figure 36). The single tension only linear spring ( $k=50\text{N/mm}$ ) was placed to prevent anterior-posterior movement between the tibia and talus [106]. The sliding element to element method was applied between tibial cartilage and talar cartilage. The contact area was also measured at tibial cartilage. The contact area was selected as the contact stress was higher than  $0.5\text{MPa}$  in tibial cartilage. The anterior and posterior of surfaces at the base of the talus were fully fixed in six degrees of freedom (DoF) (Figure 37).

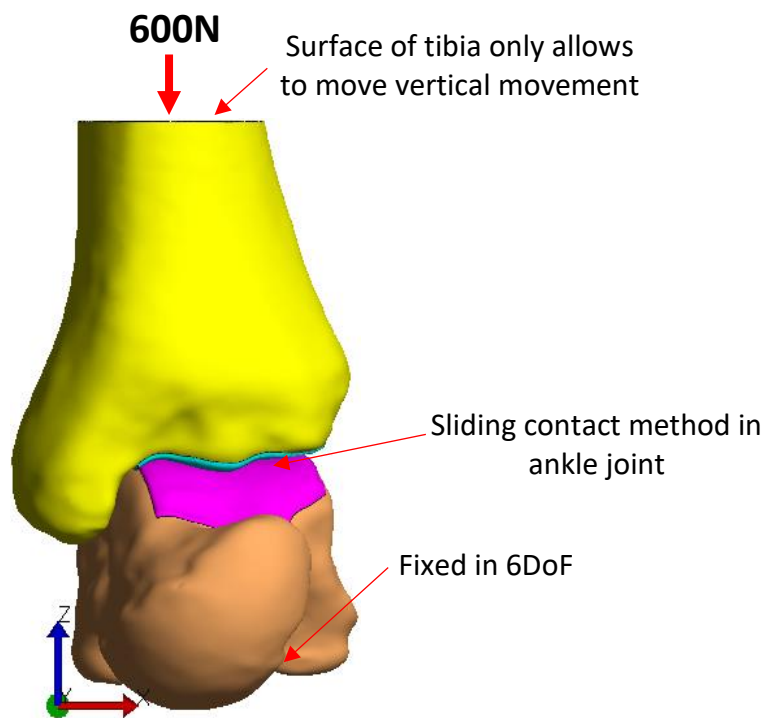


Figure 36 The 3D FE foot model was simulated under 600N axial load.

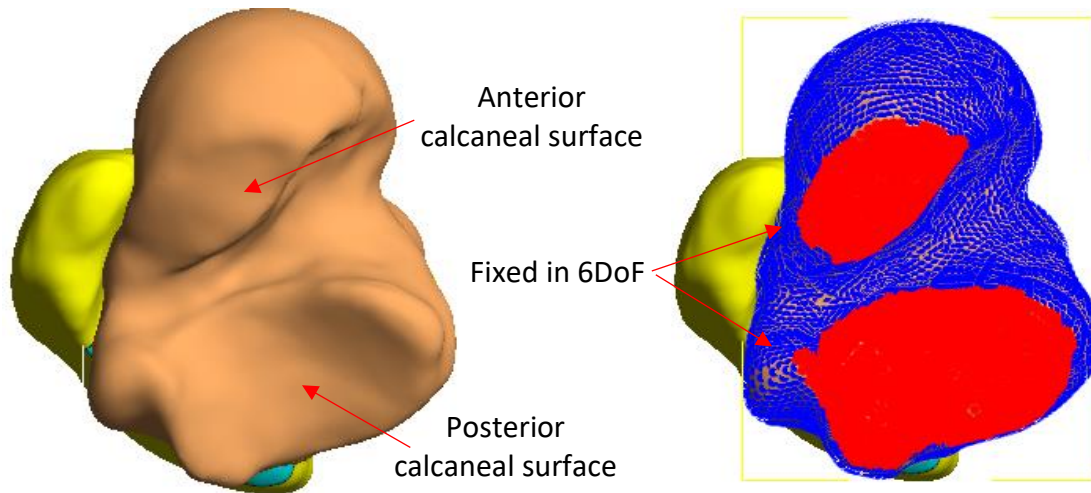


Figure 37 The inferior view of talus. The talus at anterior and posterior calcaneal surface was fixed in six degrees of freedom.

#### 4.4 RESULTS

In this research, four different foot models were built to understand the effect of foot bone morphology in the joint between tibia and talus. Furthermore, the three different thicknesses of cartilage were applied to analyze the stress distribution and the peak stress in the contact surface. The FE predictions characterized a peak von Mises stress and the stress distribution across the joint contact surface including contact area.

The peak talocrural contact stress in the healthy group ranged from 2.03 MPa to 6.16 MPa was similar between Model 1 and Model 2 (Figure 38). In the Model 1 and Model 2, the peak contact stress increased as the cartilage thickness decreased (Figure 38). In Model 3, before total ankle replacement, the peak contact stress increased from 1.05 MPa to 3.61 MPa as cartilage thickness decreased from 1.7mm to 0.5mm. However, the peak contact stress did not increase as much as it did in the healthy models. Further, in Model 4, the peak contact stress decreased from 2.41 MPa to 1.93 MPa when the cartilage was thinner (Figure 38). The differences between the

peak stress trends in the healthy versus. injured models may be explained by contact area and the stress distribution across the joint contact surface. Specifically, in Model 1 and Model 2, the contact areas decreased from  $491\text{mm}^2$  to  $263\text{mm}^2$  and from  $413\text{mm}^2$  to  $138\text{mm}^2$  as the thickness of cartilage decreased, respectively (Figure 39, 40, and 41). The contact area in Model 3 and Model 4 did not decrease as much as in Model 1 and Model 2 (Figure 39). The contact stress area was decreased from  $454\text{mm}^2$  to  $302\text{mm}^2$  in model 3 and from  $490\text{mm}^2$  to  $421\text{mm}^2$  in Model 4 (Figure 42 and 43). As well, the stress distribution in all models was spread widely in the contact area when increased thickness of cartilage. However, the shape of stress distribution showed differently in each FE talocrural joint model.

FE predicted contact stress distributions is shown in Figure 40, Figure 41, Figure 42, and Figure 43. The contact stress distribution was spread out from the middle of medial area to the lateral side while increasing the thickness of cartilage in Model 1 (Figure 40). The contact stress distribution in Model 2 was concentrated at the corner of posterior and lateral side in both 0.5mm and 1.0mm thick cartilage. However, the contact stress distribution with 1.7mm thick cartilage was mostly spread out at the corner of the anterior/medial side and lateral side (Figure 41). The stress distribution of the Model 3 had total ankle replacement surgery scattered in anterior and medial side in 0.5mm and 1.0mm thick cartilage. However, with the 1.7mm thick cartilage in Model 3, the stress distribution spread out in all over the contact surface (Figure 42), and the lowest peak contact stress measured in all four-foot models. The contact stress distribution in Model 4 was similar to Model 3. However, the area of stress distribution was shown changed by increasing the thickness of cartilage (Figure 43).

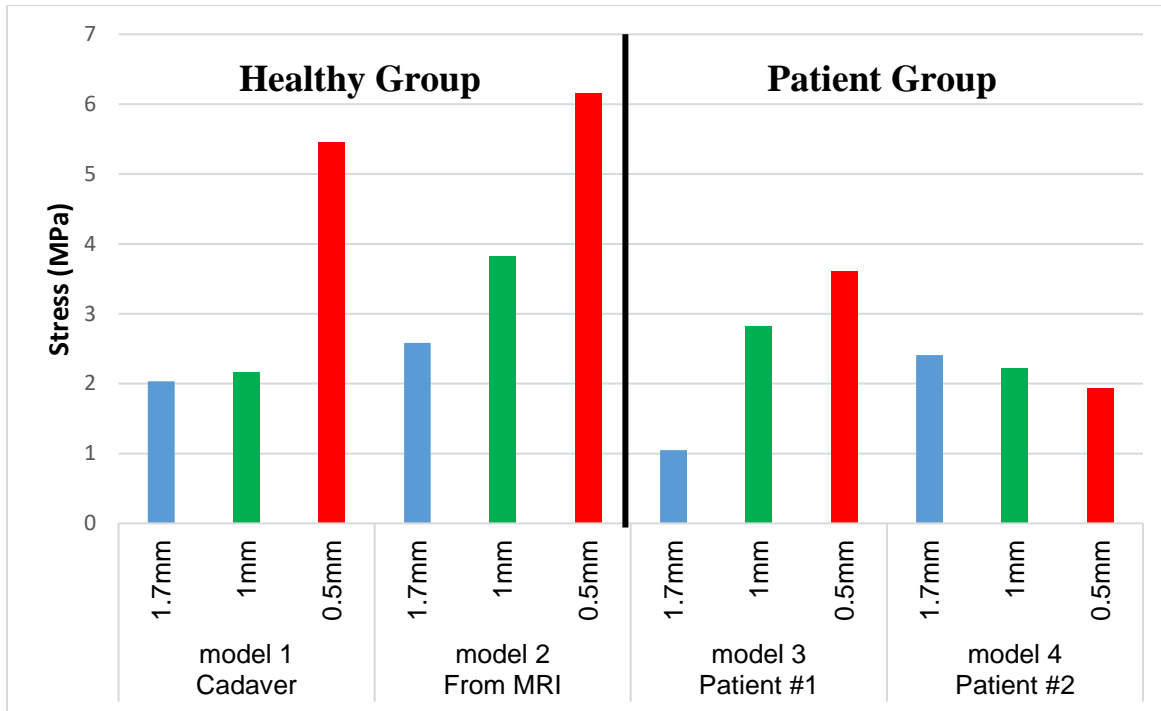


Figure 38 The peak stress at the tibial cartilage surface. The peak stress measured in two different group such as healthy group and patient group.

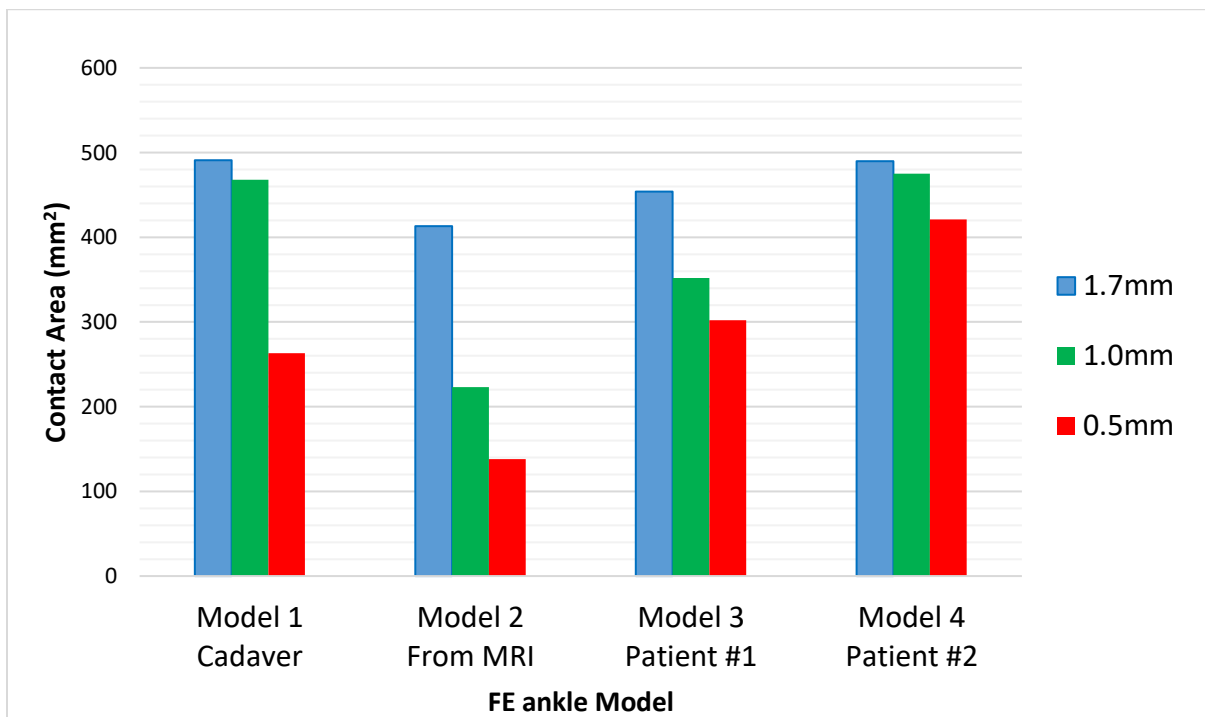


Figure 39 The contact areas in various thickness of cartilage in the FE ankle models including tibia and talus.



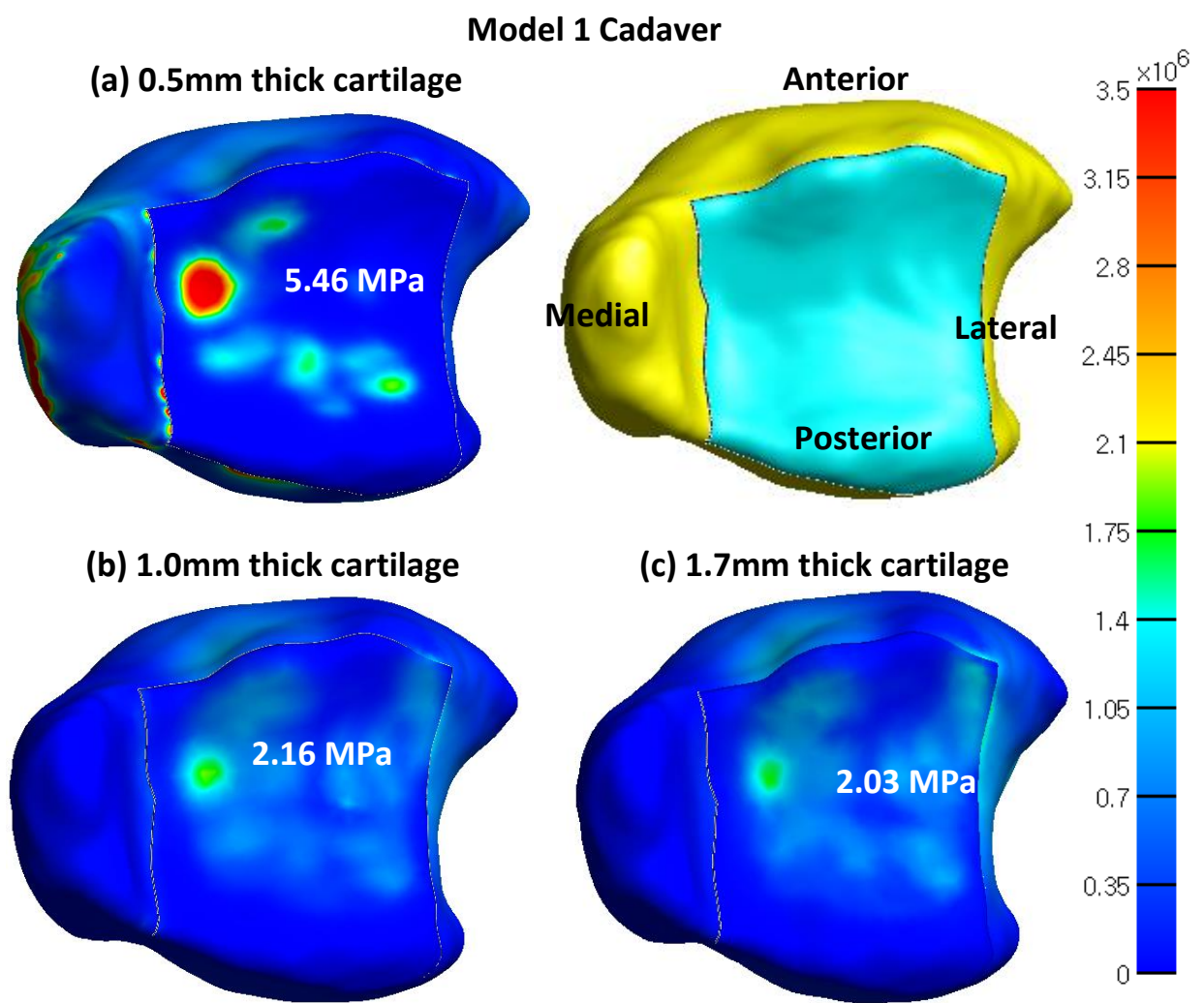


Figure 40 The distal view of the tibial articular cartilage in Model 1. The three different stress distributions showed similar stress distribution, but the peak stress was decreased when the thickness of cartilage increased.

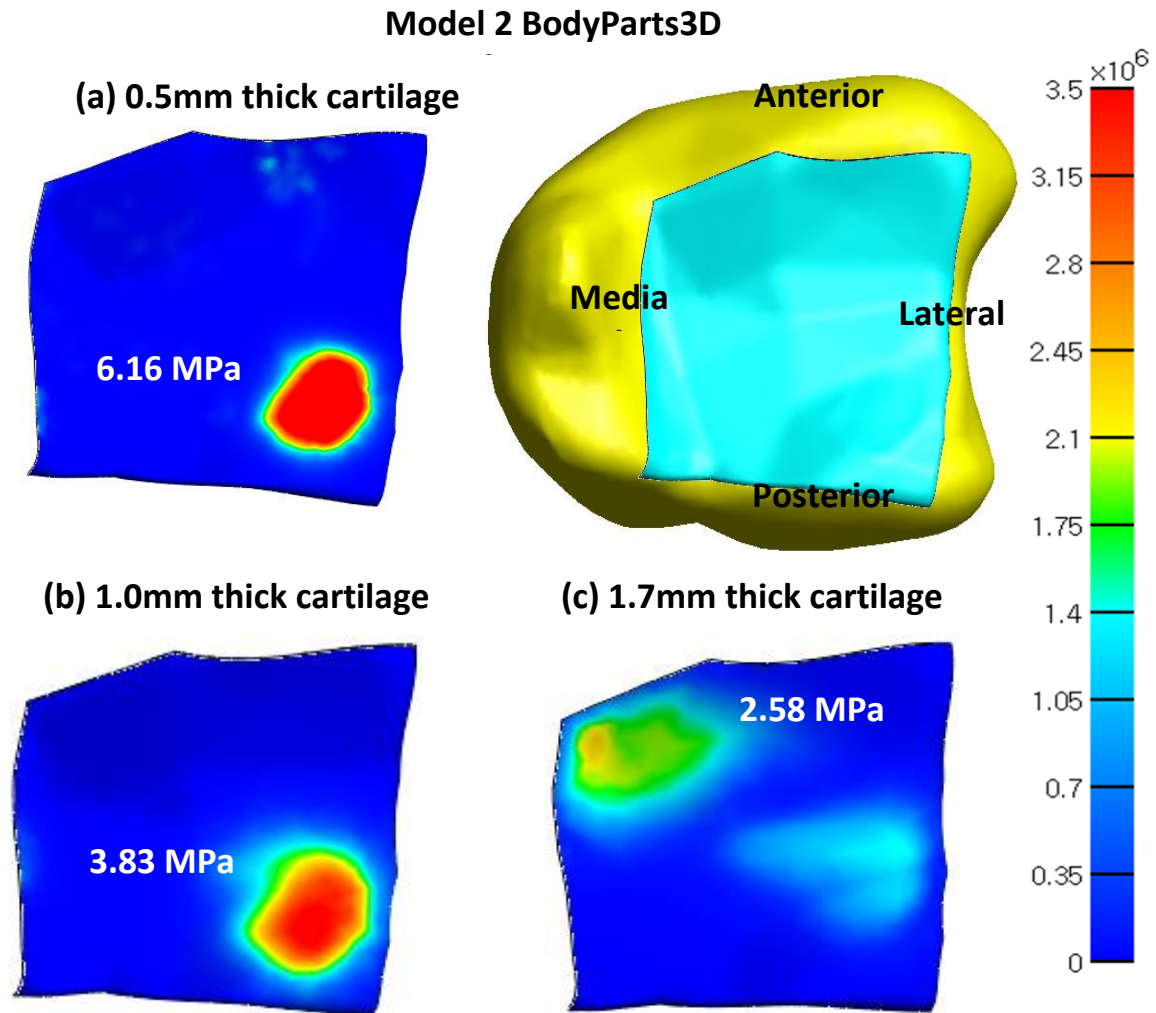


Figure 41 The distal view of the tibial articular cartilage in Model 2. The peak stress and the stress distribution with 0.5mm and 1.0mm thick cartilage measured on the tibial articular cartilage.

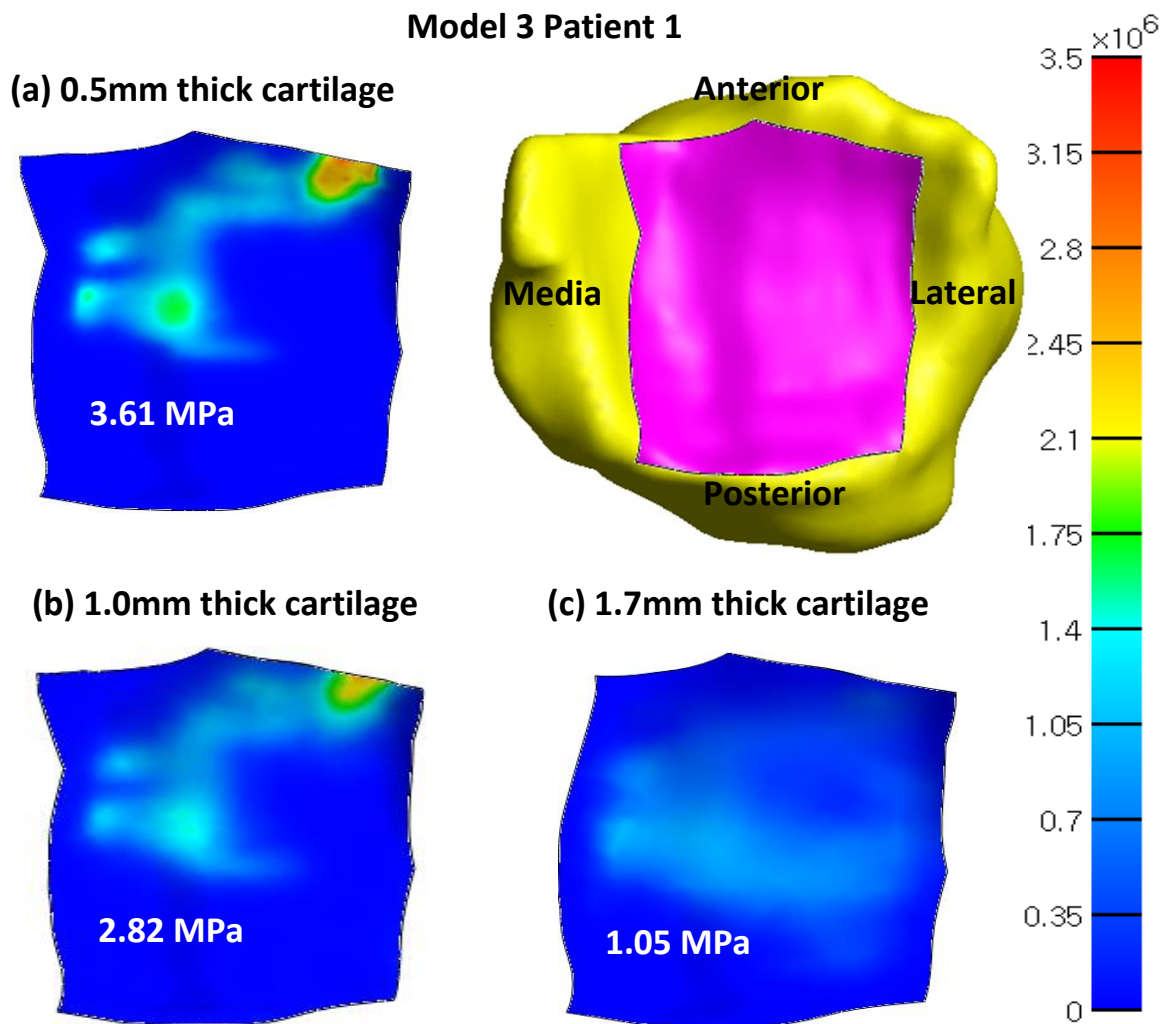


Figure 42 The distal view of the tibial articular cartilage in Model 3. The peak stress and the stress distribution with 0.5mm and 1.0mm thick cartilage measured on the tibial articular cartilage.

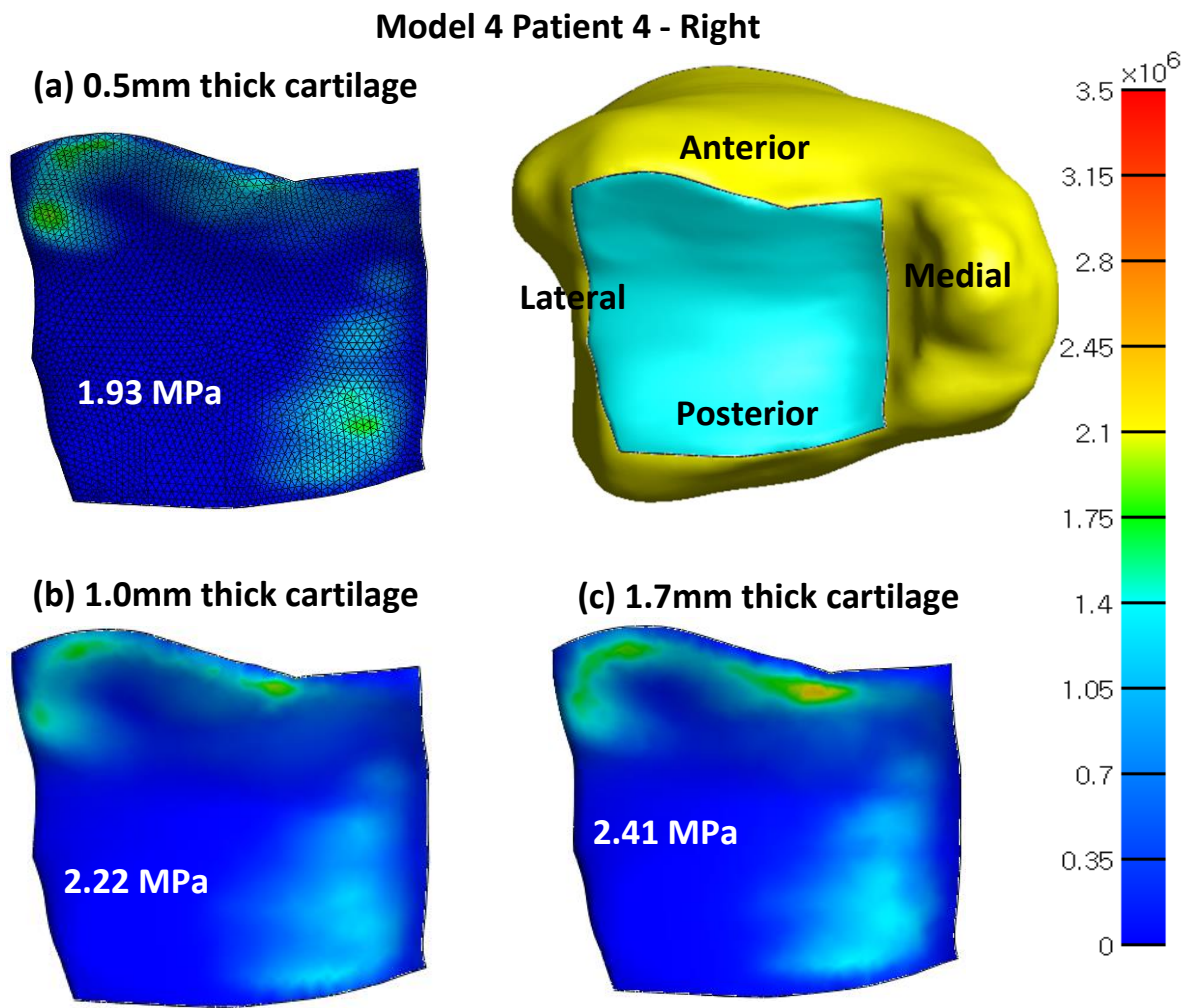


Figure 43 The distal view of the tibial articular cartilage in Model 4. The peak stress and the stress distribution with 0.5mm and 1.0mm thick cartilage measured on the tibial articular cartilage.

## 4.5 DISCUSSION

The computational model like FE model has widely used to compare the physical measurement and the predicted data from the FE model [106]. The FE model was also used to understand inner stress for total ankle replacement in the foot [54]. The current FE models were developed to understand the effect of foot injuries and pathologies on ankle contact stress. The FE models were simulated to figure out the contact peak stress and the contact stress distribution for both healthy subjects including one death male cadaver with unknown age and BodyParts3D which was created from MRI and two patients with ankle injuries. The peak contact stress ranged from 1.05 MPa to 6.16 MPa with the various thickness of cartilage in all models.

The 3D FE talocrural joint models of cadaver and MRI model were developed from Geomatic Design X for geometric model and Hypermesh software for finite element model. And the FE models were simulated in FEBio. However, the FE ankle model of [106] was developed and simulated in ABAUQS (ABAQUS Inc.) and the contact stress results were imported into MATLAB. The contact stress with 1.7mm thick cartilage was measured from 2.92 MPa to 3.69 MPa in physical measurements and from 2.47 MPa to 3.74 MPa in FE model [106]. Also, the stress distribution showed very similar each other in previous study [106]. The current peak stress with 1.7mm thick cartilages ranged from 1.05 MPa to 2.58 MPa. Additionally, the stress distribution also showed very different pattern of the stress distribution. Thus, the peak stress showed over 80% difference between the current results and the published literature. In the model of [43], the FE ankle models were developed like model1 including tibia, fibula, talus, ankle ligament, and 1.7mm cartilage and Model 2 including tibia, fibula, talus, calcaneus, ankle ligaments, and 1.7mm cartilage. In [43], the predicted contact stress from 2.05 MPa to 2.31 MPa [43]. Thus, the FE foot model also affected by the number of bone segment.

The contact stress and distribution were affected by the bone morphology or thickness of the cartilage. The stress distribution may have been affected by the foot position while taking CT scan images (Figure 44). As shown in Figure 44b, the anterior area of tibia contacted the talus, and the angle of tibia was perpendicular to the talus. However, in the Model 4 (Figure 44c), the angle of tibia was not perpendicular to the talus as Model 3. The stress distribution was also affected by the smoothing of the segments. Also, the CT scans for Model 3 and Model 4 were not taken with high resolution, so the solid model which was created based on CT scan was not smooth as much as a real bone segment.

In the future, the effect of bone smooth should be compared to know how much smoothing influences results. Because the FE model was segmented from CT scan, so when creating the smooth FE model from CT scan, it required a 4-step processes as showed in Figure 45.

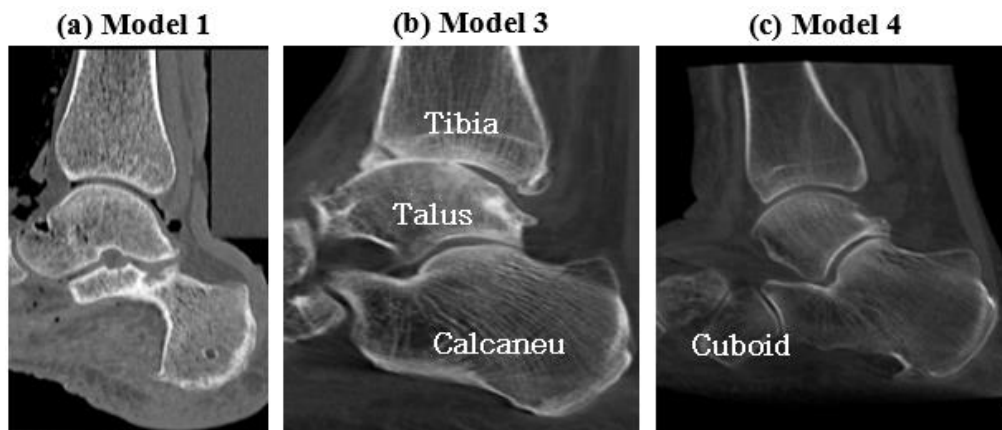


Figure 44 The lateral view of CT scan. (a) CT scan taken from a death cadaver (Model 1); (b) the angle of tibia was perpendicular to the talus but bone spur was on the tibia (Model 3); (c) but the tibia in this picture was not perpendicular to the talus (Model 4)

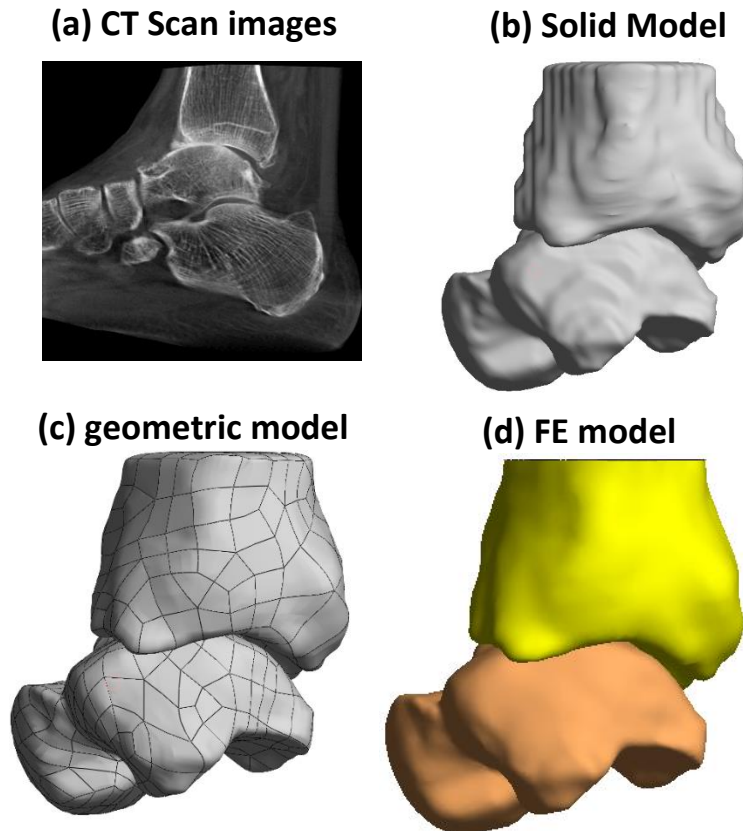


Figure 45 The FE model was developed based on CT scan images. As a first step, the rough solid model created in Slicer, then the geometric model developed by the Geomagic Design X software. Finally, the smooth FE model was created in Hypermesh.

#### 4.6 CONCLUSION

Stress distributions at the talocrural joint vary based on cartilage thickness and bony morphology. Therefore, when creating patient specific models including the hindfoot these parameters should not be generalized. Also, when taking the CT scan image, the foot position should be considered because the location of peak contact stress could be affected by the angle of tibia and talus. Furthermore, the resolution of CT scan should be considered because the bone shape and contact surface at a joint

## CHAPTER V

### DISCUSSION AND CONCLUSION

Foot and ankle are the one of critical structures in the lower limb. The ankle joint consists of the lower leg like the load-bearing for gait and other activities like running and jumping [109]. As a results, a large force of around five times body weight in normal gait and up to thirteen times body weight during running and jumping is acting on the foot and ankle [109]. Thus, the foot and ankle are surrounded by many muscles, tendons, and ligaments to generate propulsion, to absorb the ground reaction force, to consist of the foot structure like the longitudinal arch (Figure 46).

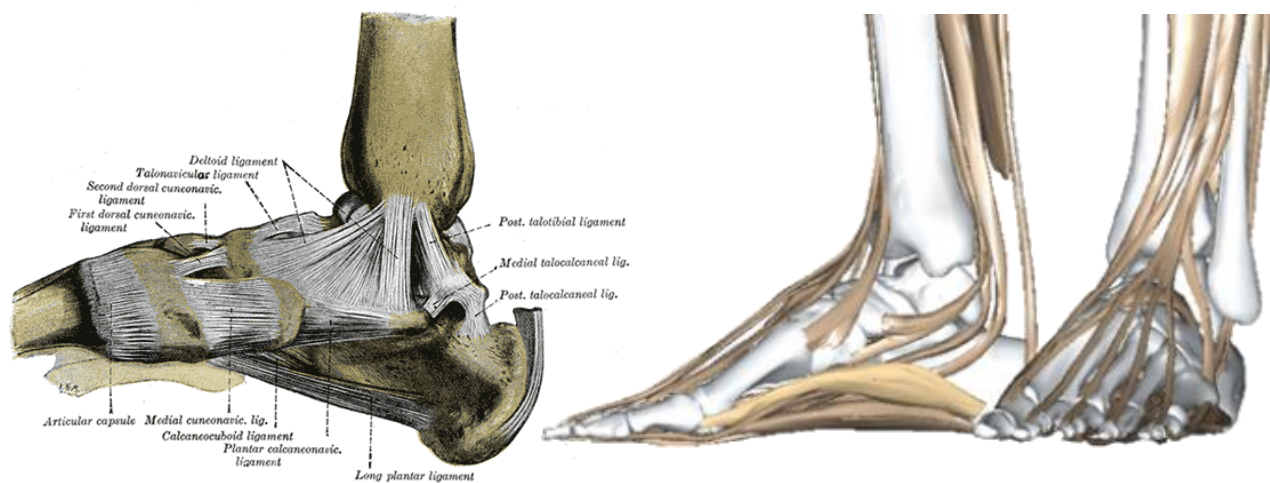


Figure 46 The medial view of tibiotalar joint with ligaments (left) [110]. The medial and anterior view of foot with muscles.

As previously mentioned, the foot construction consists of 26 bones and 33 joints. In the current model, the bony structure consisted of 15 segments including the tibia, fibula, talus, calcaneus, navicular, cuboid, three cuneiforms, single segment metatarsal, and 5 segment phalanges. Also, the cartilage was created as a single segment in all foot joints except the ankle joints between tibia, fibula, and talus.



The plantar fascia is frequently a source of foot pain when people have injuries, like plantar fasciitis and in people with foot problems caused by diabetes mellitus. Thus, the plantar fascia and plantar soft tissue were also created using an open-source image computing platform called 3DSlicer.

3D finite element foot and ankle models including three different thickness of 3D solid plantar fascia (i.e., 3mm, 4mm, and 5mm) and different ankle positions (i.e., neutral position, 10° dorsiflexion, and 10° plantar-flexion) was developed to figure out the effect of different thicknesses of plantar fascia and ankle positions to peak plantar pressure and plantar pressure distribution. Additionally, 3D FE model of the talocrural joint was investigated to analyze the thickness of cartilage (i.e., 0.5mm, 1.0mm, and 1.7mm) and bone morphology in healthy and injured ankle.

All tissues were idealized as linear elastic, homogenous and isotropic. The material properties were adopted form previous literature (Table 15).

Table 15 The material properties for all tissues

	Young's modulus (MPa)	Poisson's ratio	Element type	Reference
Bone	7300	0.3	3D-Tetrahedral solid	[35, 36]
Cartilage	100	0.4	3D-Tetrahedral solid	[31]
	12	0.42	3D-Tetrahedral solid	[106]
Plantar fascia	350	0.3	3D-Tetrahedral solid	[75]
Soft tissue	2.49	0.49	3D-Tetrahedral solid	[93]
Ligament	50N/mm		1D tension only	[106]
Plate	Rigid body			

When the thickness of plantar fascia increased, the peak plantar pressure (PP) moved from hindfoot to forefoot. Also, the peak stress was also affected by the foot positions. The peak plantar stress ranged from 0.106 MPa to 0.112 MPa at neutral position. However, when changed the foot position, the peak stress ranged from 0.127 MPa to 0.148 MPa at 10° dorsiflexion, and from 0.131 MPa to 0.159 MPa at 10° plantar flexion. Finally, the contact stress at the ankle joint was affected by the bone morphologies. The peak contact stress ranged from 2.03 MPa to 6.16 MPa in the healthy group and from 1.05 MPa to 3.61 MPa in the patient group.

The conclusion of this dissertation, plantar fascia thickness does impact both the strain in the plantar fascia and the plantar pressure, especially, when the plantar fascia is greater than 4mm. The different foot positions could show greater plantar pressure, thus FE foot models should consider the range of foot positions. Moreover, the bone morphology and cartilage thickness do effect contact stresses in the ankle, therefore, those parameters should be considered when using models to answer clinical questions.

## 5.1 LIMITATIONS

The flexible links like ligament, muscles, and tendons were not included in the 3D FE foot model because the foot joints were fully connected without any movements and rotation in the joints (Figure 16).

One of thick and strong ligaments, the plantar fascia, was constructed between the calcaneus and the metatarsals, having a uniform thickness of 3mm, and 4mm, and 5mm in the current model. The plantar fascia was one of the important ligaments to support the medial longitudinal arch. Hence, many researchers have studied about the role of plantar fascia [111], the stiffness of plantar soft tissue to the diabetic foot [32], the stiffness of plantar fascia [37], and the

effects of plantar fasciitis and diabetes to the foot [4, 82, 112]. However, in the previous studies, it was focused on plantar soft tissue in the foot with diabetes and plantar fasciitis, so the plantar fascia was modeled as 1D tension only spring or 3D solid model without mention the thickness of plantar fascia. Even though, the different stiffness of plantar fascia was tested in [37], but the plantar fascia was developed as 1D spring. The morphology and mechanical material properties of plantar fascia in patients and in healthy subjects was also studied [2, 67, 113]. As a results, linear and non-linear material properties for plantar fascia were simulated in a finite element analysis [4, 37, 38, 64, 83]. However, in this study, the non-linear material properties were not applied in the FE foot model because FEBio didn't support the 5 terms incompressible Mooney-Rivlin Hyperelastic material property (Table 16). As a result, the linear material properties for the plantar fascia were only simulated in the current 3D FE foot model (Table 16).

Table 16 Linear and non-linear material properties for plantar fascia.

Linear Material Properties				
	Thickness	Young's modulus, E (MPa)	Poisson's ratio, $\nu$	Reference
Plantar fascia	-	350	0 - 0.45	[4, 32, 54, 75, 96]

5-term Incompressible Mooney-Rivlin Hyperelastic (MPa)					Reference
$C_{10}$	$C_{01}$	$C_{20}$	$C_{11}$	$C_{02}$	[64]
-222.1	290.97	-1.1257	4.7267	79.602	

Furthermore, the plantar fascia was developed based on the CT scan images. The CT scan images were taken with 0.484mm increments in a neutral and unloaded position. However, the morphology and thickness of plantar fascia was not possible to measure out in the CT scan images. Thus, the morphology of plantar fascia was developed based on the other literature and anatomy of plantar fascia.

## 5.2 PILOT WORKED TOWARD FUTURE WORK

For future work, the ankle ligaments such as tibiocalcaneal ligament and anterior tibiotalar ligament, posterior tibiotalar ligament should be included to represent ankle joint movement such as dorsiflexion and plantar flexion (Figure 47). Furthermore, the metatarsal and sesamoid were also developed as a foot anatomy. In the current 3D FE model, the metatarsal segment was developed as a single segment in current research (Figure 48), and the sesamoid was not included in the 3D FE model. As a result, the highest stress concentrated at 5<sup>th</sup> metatarsal head. However, the metatarsal was created as an individual segment as shown in Figure 48 and the sesamoids were developed like Figure 47, the peak stress on metatarsals was measured 1<sup>st</sup> metatarsal head. As well, the plantar stress distribution was also affected by the metatarsal and sesamoid structure (Figure 50). Thus, the sesamoid model should be included.

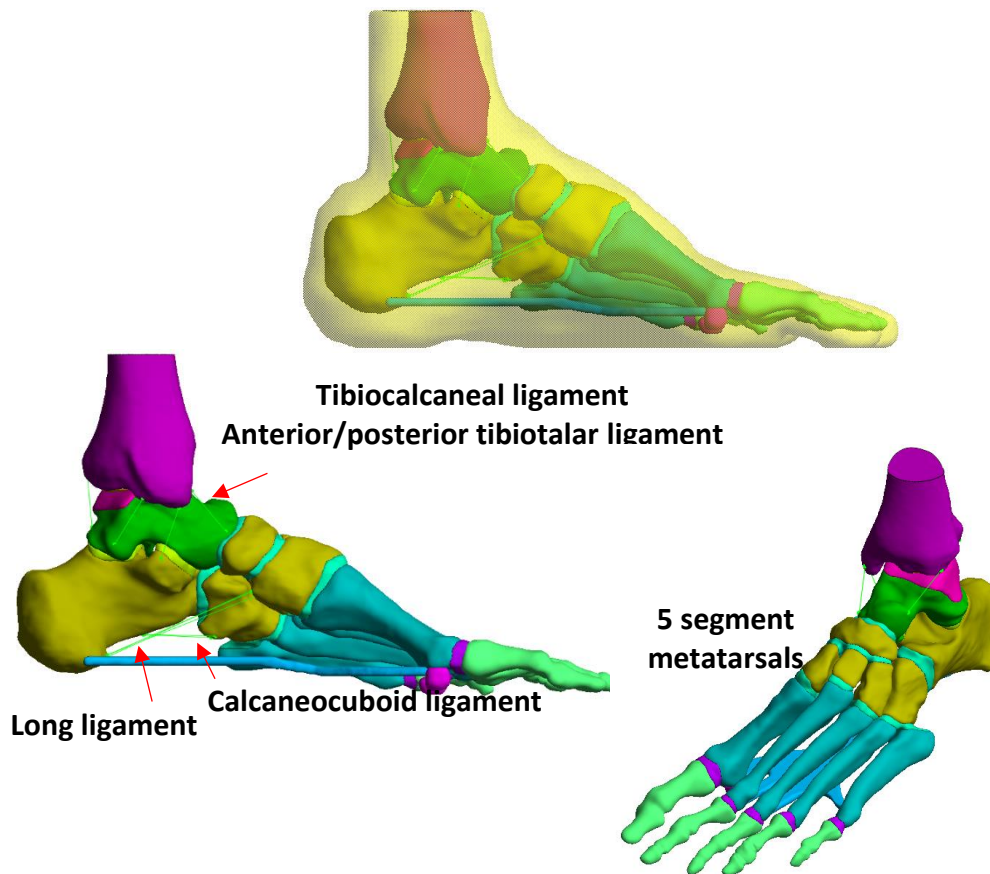


Figure 47 The 3D FE foot model including 18 bone segment, plantar fascia, ankle ligaments, short and long ligaments, soft tissue.

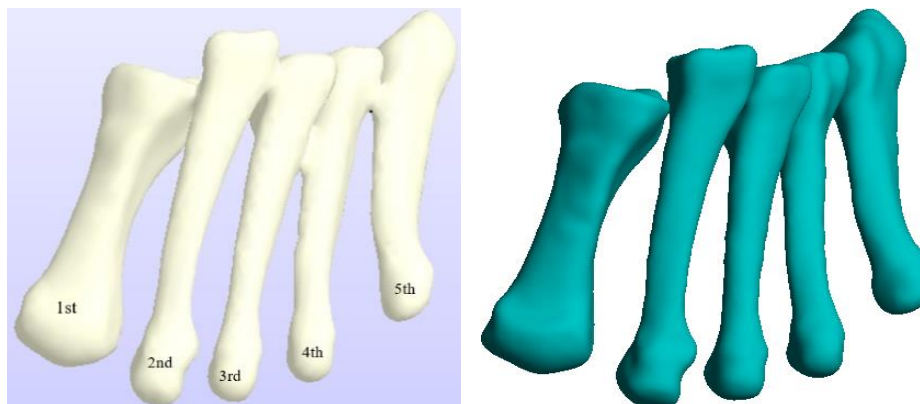


Figure 48 The axial view of the metatarsal. The metatarsal consists of 5 segments, but one of metatarsal was developed as a single segment (left). Another metatarsal developed as individual segment (right)

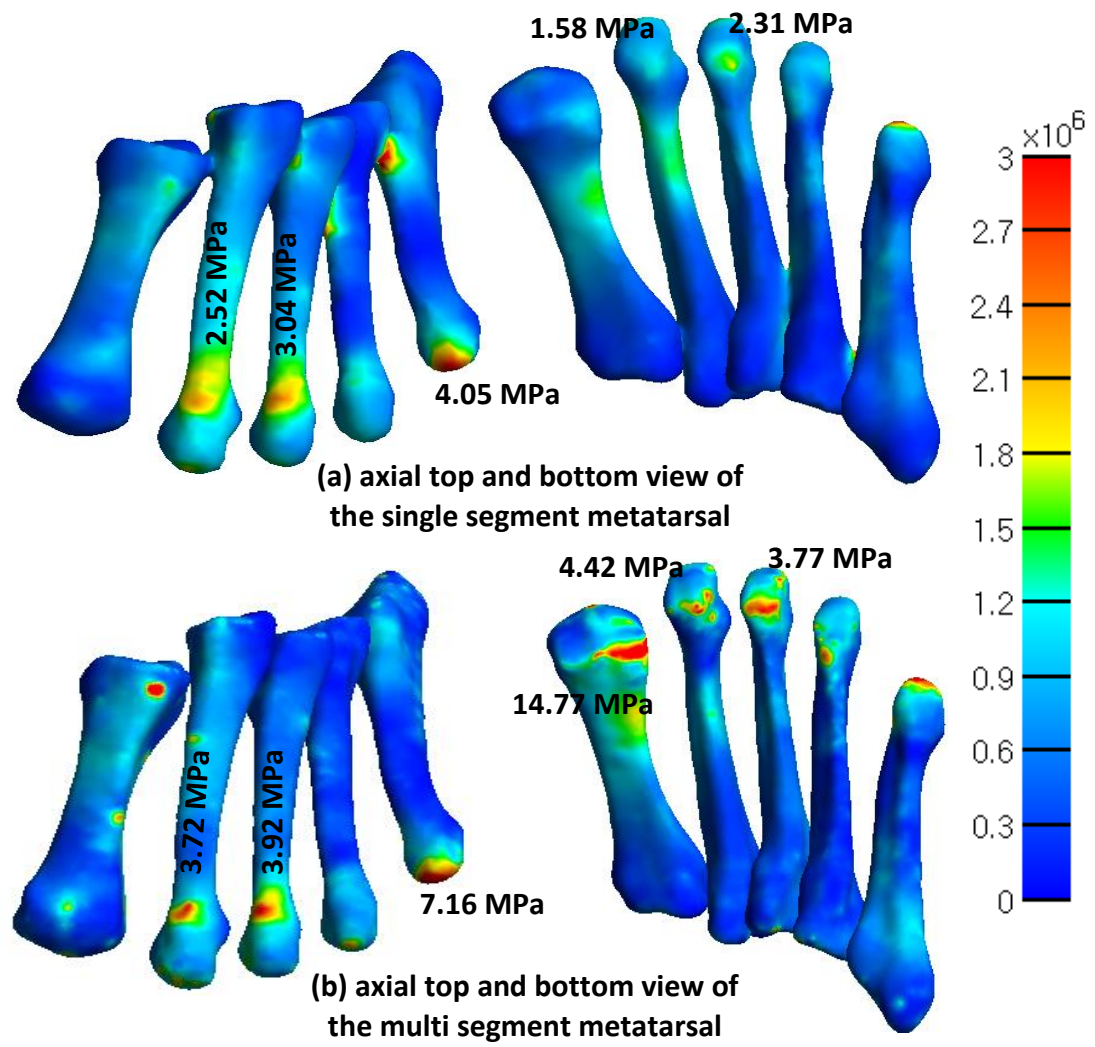


Figure 49 The stress at metatarsal was changed by the metatarsal structure.

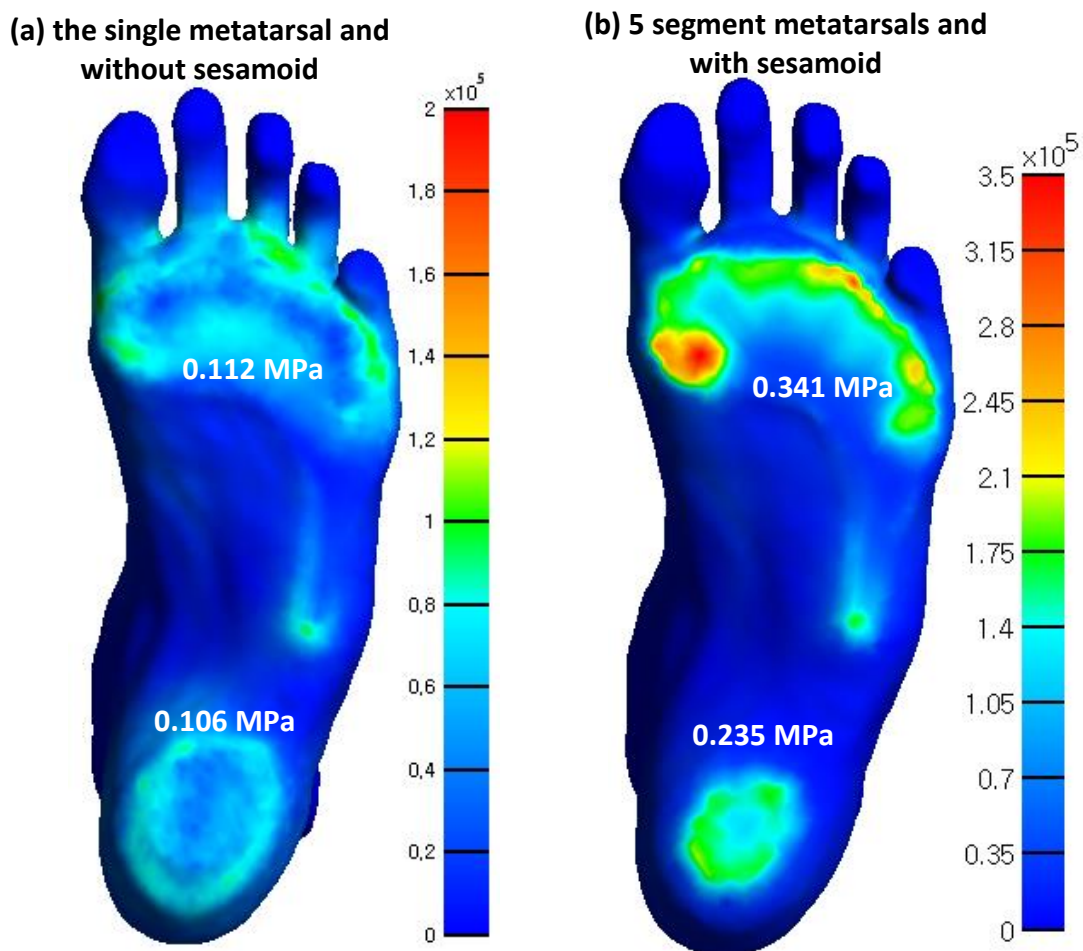


Figure 50 The plantar stress distribution and the peak plantar stress was affected by the bone structure like metatarsal and sesamoids.

To validate this model, in vitro experiments are required. A six degree of freedom closed kinetic chain device was designed and prototyped to collect the experimental data. The 1<sup>st</sup> generation device was developed to control the angle of a cadaver using two servo motors (Figure 51). After preliminary testing with a cadaver (Figure 52) the motors could not move the foot through its range of motion smoothly.

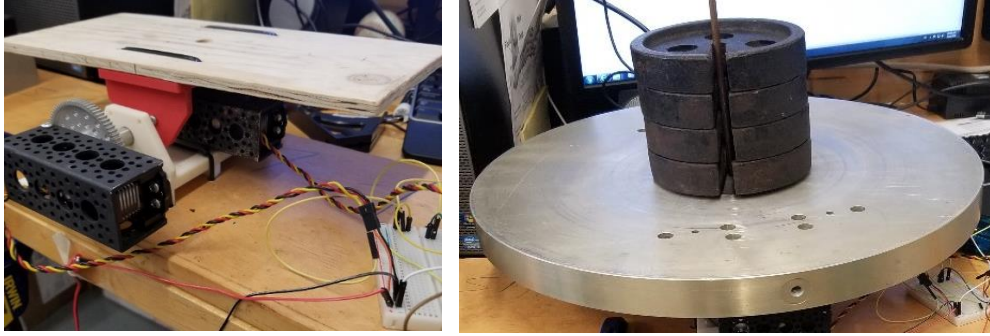


Figure 51 The single position control device developed using two servo motors and it tested under 66.6 lb.

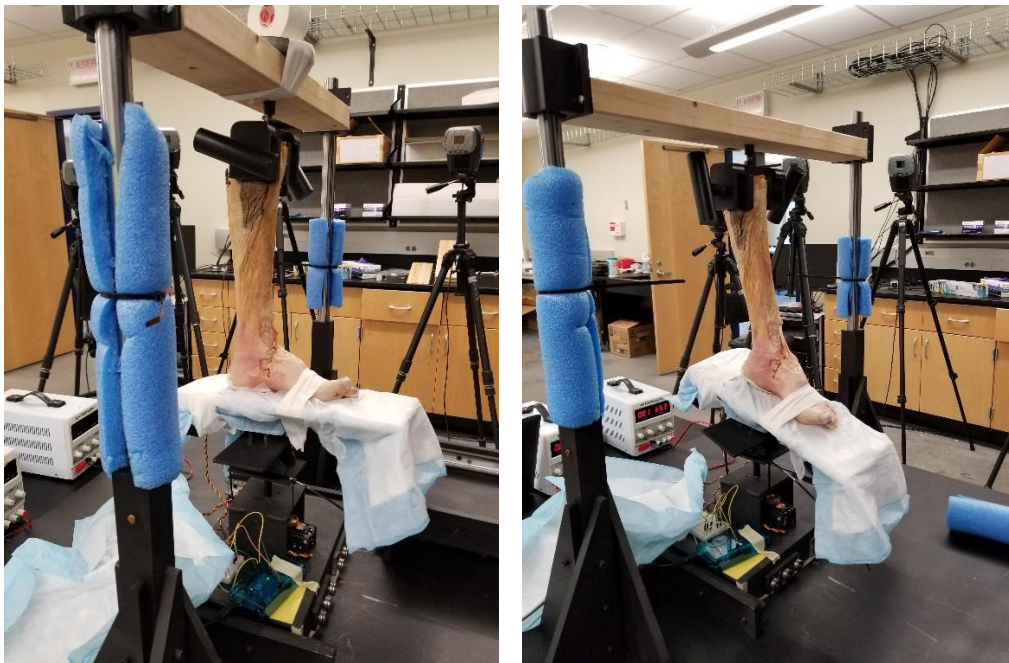


Figure 52 The device tested with the cadaver. The device was operated from neutral position (left) to 20° plantar flexion (right)

Therefore, the second load device was designed and developed with a high torque servo motor (Figure 53 and 54). After building the device, it was tested with a 15lb 3D printer (Figure 54). However, the angular velocity was too fast, and the coupling shaft could not fully hold the top plate. Thus, the 3rd generation device was designed with worm gear and spur gear to reduce the angular velocity and increase the torque on the top plate (Figure 55 and 56).



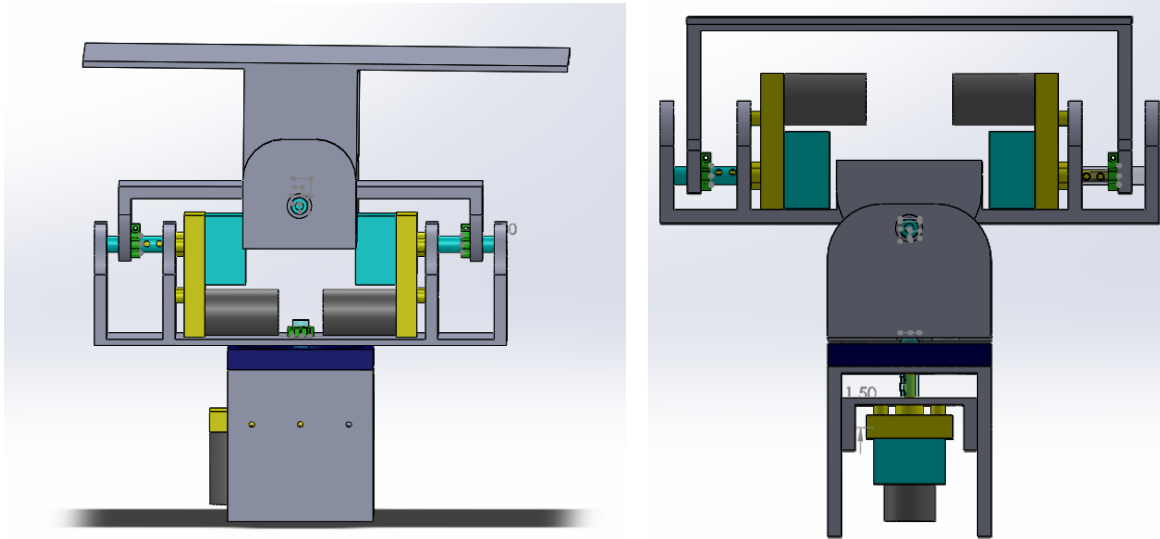


Figure 53 The 2nd generation foot and ankle positioning device designed with the five-servo motors.

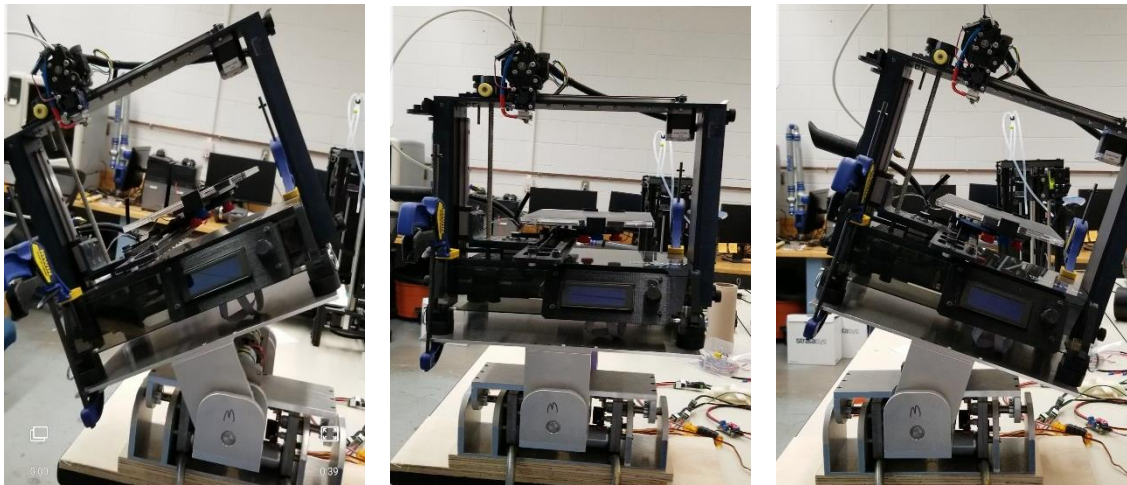


Figure 54 The 2nd generation device tested with 25lb 3D printer.

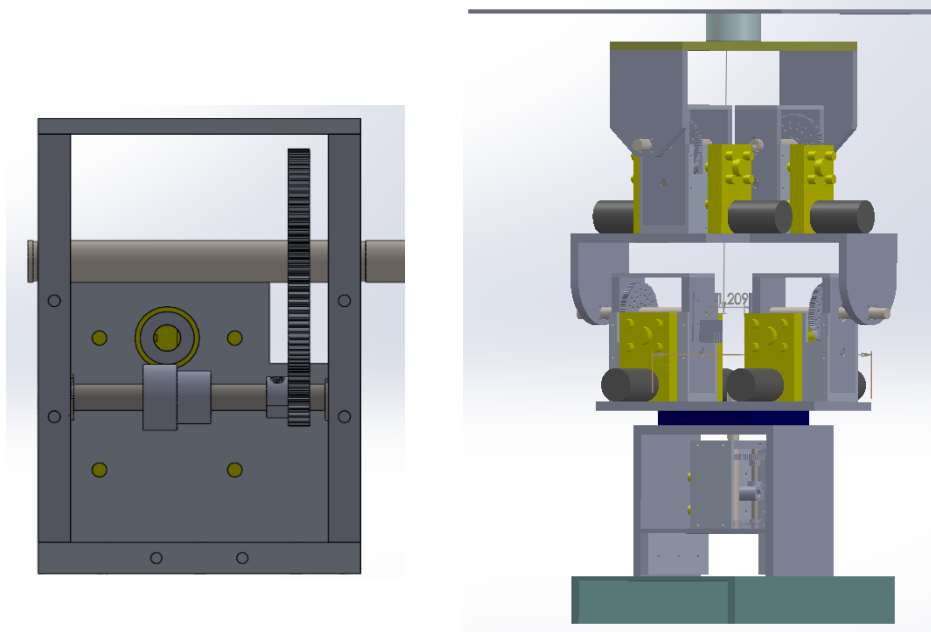


Figure 55 The 3D design device of the gear box including 25:1 worm gear and 1:7 spur gear box (Left) and the 3rd generation ankle positioning device with 5 gear boxes (Right).

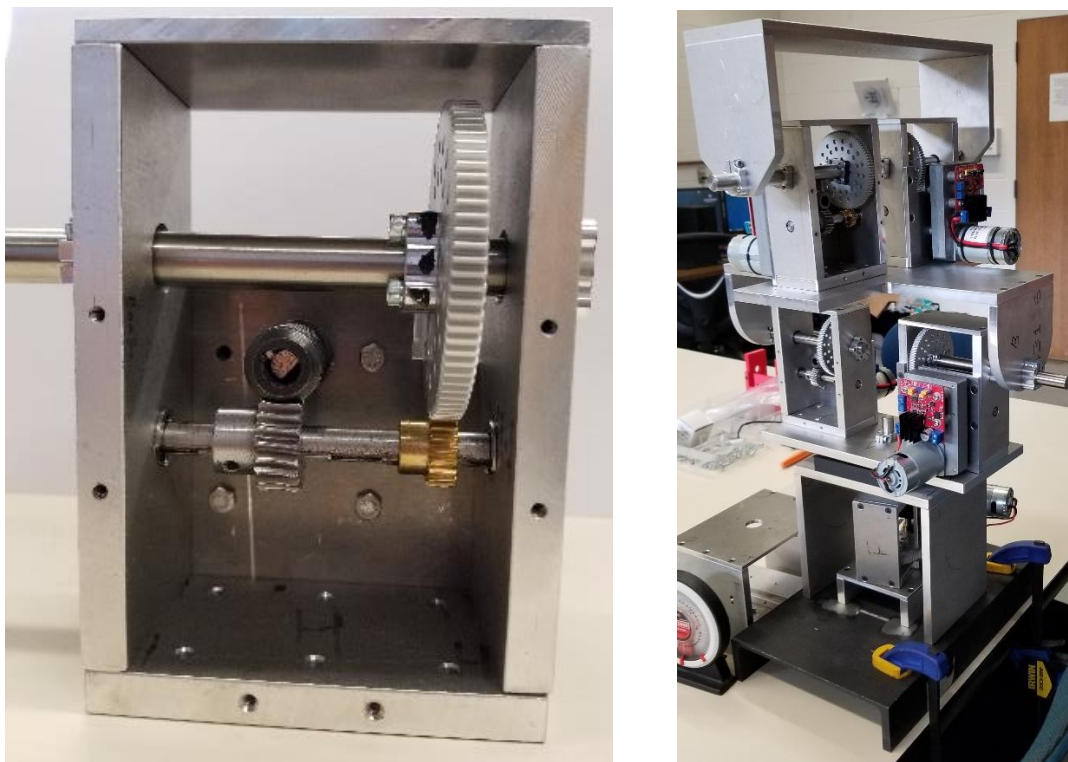


Figure 56 The real 3rd generation gear box (left) and the fully assembled foot and ankle loading device (right).

## REFERENCES

- [1] H. Gray, P. L. Williams, and L. H. Bannister, *Gray's anatomy the anatomical basis of medicine and surgery*. New York : Churchill Livingstone, 1995.
- [2] Z. Qian *et al.*, "Morphology and mechanical properties of plantar fascia in flexible flatfoot: A noninvasive in vivo study," *Frontiers in Bioengineering and Biotechnology*, vol. 9, p. 9, 2021.
- [3] W.-M. Chen, J. Park, S.-B. Park, V. P.-W. Shim, and T. Lee, "Role of gastrocnemius-soleus muscle in forefoot force transmission at heel rice-A 3D finite element analysis," *Journal of Biomechanics*, vol. 45, pp. 1783-1798, 2012.
- [4] A. Guiotto, Z. Sawacha, G. Guarneri, A. Avogaro, and C. Cobelli, "3D finite element model of the diabetic neuropathic foot:Agait analysis driven approach," *Journal of Biomechanics*, vol. 47, pp. 3064-3071, 2014.
- [5] A. Guiotto, A. Scarton, Z. Sawacha, G. Guarneri, A. Avogaro, and C. Cobelli, "Gait analysis driven 2D finite element model of the neuropathic hindfoot," *Journal of Mechanics in Medicine and Biology*, vol. 16, no. 2, pp. P1-P18, 2016, doi: 10.1142/S0219519416500123.
- [6] "25 fun foot facts." <https://www.profootcenter.com/contents/25-fun-foot-facts> (accessed 7/30, 2020).
- [7] M. J. Thomas, R. Whittle, H. B. Menz, T. Rathod-Mistry, M. Marshall, and E. Roddy, "Plantar heel pain in middle-aged and older adults: population prevalence, associations with health status and lifestyle factors, and frequency of healthcare use," *BMC Musculoskeletal Disorders*, vol. 20, p. 8, 2019.
- [8] M. A. Tahririan, M. Motififard, M. N. Tahmasebi, and B. Siavashi, "Plantar fasciitis," *Journal of Research in Medical Sciences*, vol. 17(8), pp. 799-804, 2012.
- [9] K. Rome and T. E. Howe, "Risk factors associated with the development of plantar heel pain in athletes," *Physical Therapy Reviews*, vol. 11, 2001.
- [10] C. L. Hill, T. K. Gill, H. B. Menz, and A. W. Taylor, "Prevalence and correlates of foot pain in a population-based study: the North West Adelaide health study," *BioMed Central*, 2008.
- [11] J. Anderson and J. Stanek, "Effect of foot orthoses as treatment for plantar fasciitis or heel pain," *Journal of Sport Rehabilitation*, vol. 22, pp. 130-136, 2013.
- [12] D. A. Lawrence, M. F. Rolen, K. A. Morshed, and H. Moukaddam, "MRI of heel pain," *American Journal of Roentgenology*, vol. 200, p. 11, 2012.
- [13] A. P. Ribeiro, S. M. A. João, R. C. Dinato, V. D. Tessutti, and I. C. N. Sacco, "Dynamic patterns of forces and loading rate in runners with unilateral plantar fasciitis: A cross-sectional study," *PLOS ONE*, vol. 10(9), 2015.
- [14] R. Chang, P. A. Rodrigues, R. E. A. V. Emmerik, and J. Hamill, "Multi-segment foot kinematics and ground reaction forces during gait of individuals with plantar fasciitis," *Journal of Biomechanics*, vol. 47, 2014.
- [15] L. H. Gill, "Plantar fasciitis diagnosis and conservative management," *Journal of the American Academy of Orthopaedic Surgeons*, vol. 5, no. 2, p. 9, 1997.
- [16] A. M. McMillan, K. B. Landorf, J. T. Barrett, H. B. Menz, and A. R. Bird, "Diagnostic imaging for chronic plantar heel pain: a systematic review and meta-analysis," *Journal of Foot and Ankle Research*, 2009, doi: 10.1186/1757-1146-2-32.
- [17] P. Jayaprakash, S. Bhansali, A. Bhansali, P. Dutta, and R. Anatharaman, "Magnitude of foot problems in diabetes in the developing world: a study of 1044 patients," *Diabetic Medicine*, vol. 26, p. 4, 2009, doi: 10.1111/j.1464-5491.2009.02781.x.
- [18] A. Agić, V. Nikolić, B. Mijović, and U. Reischl, "Biomechanical model of the diabetic foot," *Collegium Antropologicum*, vol. 32, p. 6, 2008.
- [19] "Diabetes Programme." [https://www.who.int/diabetes/action\\_online/basics/en/index3.html#:~:text=Complications%20of%20diabetes&text=Microvascular%20complications%20include%20damage%20to,severe%20infections%20leading%20to%20amputation](https://www.who.int/diabetes/action_online/basics/en/index3.html#:~:text=Complications%20of%20diabetes&text=Microvascular%20complications%20include%20damage%20to,severe%20infections%20leading%20to%20amputation). (accessed 8/18, 2020).

- [20] E. D'Ambrogi *et al.*, "Contribution of plantar fascia to the increased forefoot pressures in diabetic patients," *Pathophysiology/Complications*, vol. 26, pp. 1525-1529, 2003.
- [21] E. D'Ambrogi, C. Giacomozzi, V. Macellari, and L. Uccioli, "Abnormal foot function in diabetic patients: the altered onset of Windlass mechanism," *Diabetic Medicine*, vol. 22, pp. 1713-1719, 2005.
- [22] A. C. Duffin, A. Lam, R. Kidd, A. K. F. Chan, and K. C. Donaghue, "Ultrasonography of plantar soft tissues thickness in young people with diabetes," *Diabetic Medicine*, vol. 19, pp. 1009-1013, 2002.
- [23] M. Akfirat, C. Sen, and T. Günes, "Ultrasonographic appearance of the plantar fasciitis," *Clinical Imaging*, vol. 27, no. 5, p. 5, 2003.
- [24] N. Sabir, S. Demirlenk, B. Yagci, N. Karabulut, and S. Cubukcu, "Clinical utility of sonography in diagnosing plantar fasciitis," *J Ultrasound Med*, vol. 24, pp. 1041-1048, 2005.
- [25] H. R. Osborne, W. H. Breidahl, and G. T. Allison, "Critical differences in lateral X-rays with and without a diagnosis of plantar fasciitis," *J Sci Med Sport*, vol. 9, no. 3, p. 6, 2006.
- [26] J. F. Berkowitz, R. Kier, and S. Rudicel, "Plantar fasciitis: MR imaging," *PMID*, vol. 179, no. 3, p. 3, 1991.
- [27] S. Mahowald, B. S. Legge, and J. F. Grady, "The correlation between plantar fascia thickness and symptoms of plantar fasciitis," *Journal of the American Podiatric Medical Association*, vol. 101, no. 5, p. 5, 2011.
- [28] C. Stecco *et al.*, "Plantar fascia anatomy and its relationship with Achilles tendon and paratenon," *Journal of Anatomy*, vol. 223, p. 12, 2013.
- [29] A. Gefen, "The in vivo elastic properties of the plantar fascia during the contact phase of walking," *Foot & Ankle Int*, vol. 24, no. 3, p. 7, 2003.
- [30] D. G. Wright and D. C. Rennels, "A study of the elastic properties of plantar fascia," *The Journal of Bone & Joint Surgery*, p. 11, 1964.
- [31] H.-Y. K. Cheng, C.-L. Lin, H.-W. Wang, and S.-W. Chou, "Finite element analysis of plantar fascia under stretch—The relative contribution of windlass mechanism and Achilles tendon force," *Journal of Biomechanical Engineering*, vol. 41, p. 9, 2008.
- [32] J. T.-M. Cheung, M. Zhang, A. K.-L. Leung, and Y.-B. Fan, "Three-dimensional finite element analysis of the foot during standing—A material sensitivity study," *Journal of Biomechanics*, vol. 38, p. 10, 2005, doi: 10.1016/j.jbiomech.2004.05.035.
- [33] W. Aerts *et al.*, "Validation of plantar pressure simulations using finite and discrete element modelling in healthy and diabetic subjects," *Computer Methods in Biomechanics and Biomedical Engineering*, vol. 20, no. 13, p. 11, 2017.
- [34] W.-M. Chen, T. Lee, P. V.-S. Lee, J. W. Lee, and S.-J. Lee, "Effects of internal stress concentrations in plantar soft-tissue—A preliminary three-dimensional finite element analysis," *Medical Engineering & Physics*, vol. 32, no. 4, p. 8, 2010.
- [35] C. A. Costa, V. V. Lain, A. L. Godoy-Santos, V. G. d. Antoni, P. R. Linzmaier, and F. A. Costa, "Analysis of pressure distribution in the foot using finite elements," *Journal of Foot and Ankle*, vol. 14, no. 2, p. 4, 2020.
- [36] Y.-N. Chen, C.-W. Chang, C.-T. Li, C.-H. Chang, and C.-F. Lin, "Finite element analysis of plantar fascia during walking: A quasi-static simulation," *American Orthopaedic Foot & Ankle Society*, vol. 36(1), p. 8, 2015.
- [37] J. T.-M. Cheung, M. Zhang, and K.-N. An, "Effects of plantar fascia stiffness on the biomechanical responses of the ankle-foot complex," *Clinical Biomechanics*, vol. 19, p. 8, 2004.
- [38] R. L. Actis *et al.*, "Numerical simulation of the plantar pressure distribution in the diabetic foot during the push-off stance," *Medical & Biological Engineering & Computing*, vol. 44, p. 11, 2006, doi: 10.1007/s11517-006-0078-5.
- [39] W.-M. Chen, S.-J. Lee, and P. V. S. Lee, "Plantar pressure relief under the metatarsal heads – Therapeutic insole design using three-dimensional finite element model of the foot," *Journal of Biomechanics*, vol. 48, p. 7, 2015.

- [40] Y.-W. Chang, W. Hung, H.-W. Wu, Y.-C. Chiu, and H.-C. Hsu, "Measurements of foot arch in standing, level walking, vertical jump and sprint start," *International Journal of Sport and Exercise Science*, vol. 2, no. 2, p. 8, 2010.
- [41] S. H. Scott and D. A. Winter, "Biomechanical model of the human foot: Kinematics and kinetics during the stance phase of walking," *Journal of Biomechanics*, vol. 26, no. 9, p. 14, 1993.
- [42] Z. Qian, L. Ren, Y. Ding, J. R. Hutchinson, and L. Ren, "A dynamic finite element analysis of human foot complex in the sagittal plane during level walking," *PLOS ONE*, vol. 8, no. 11, p. 10, 2013.
- [43] J. Kim, "The effect of bone and ligament morphology of ankle joint loading in the neutral position," Master of Science, Mechanical Engineering, Old Dominion University, 2007.
- [44] AclandAnatomy.com, "Acland's video atlas of human anatomy: Plantar fascia," ed. YouTube, 2014, p. <https://www.youtube.com/watch?v=3pWgieC3woU>.
- [45] A. Asghar and S. Naaz, "The transverse arch in the human feet: A narrative review of its evolution, anatomy, biomechanics and clinical implications," *Anatomy & Biological Anthropology*, vol. 34, no. 3, p. 2, 2021.
- [46] A. Erdemir, A. J. Hamel, A. R. Fauth, S. J. Piazza, and N. A. Sharkey, "Dynamic Loading of the Plantar Aponeurosis in Walking," *The Journal of Bone & Joint Surgery*, vol. 86-A, no. 3, p. 7, 2004.
- [47] D. J. Morton, "Evolution of the longitudinal arch of the human foot," *The Journal of Bone & Joint Surgery*, vol. 6, no. 1, p. 31, 1924.
- [48] D. T. Reilly and A. H. Burstein, "The elastic and ultimate properties of compact bone tissue," *Journal of Biomechanics*, vol. 8, no. 6, p. 9, 1975.
- [49] A. H. Franco, "Pes Cavus and Pes Planus: Analyses and treatment," *Physical Therapy Reviews*, vol. 67, no. 5, p. 7, 1987.
- [50] Y. Gu and Z. Li, "Mechanical information of plantar fascia during normal gait " *Physics Procedia*, vol. 33, p. 4, 2012.
- [51] J. H. Hicks, "The mechanics of the foot," *Journal of Anatomy*, vol. 88, p. 6, 1954.
- [52] L. A. Bolgla and T. R. Malone, "Plantar Fasciitis and the Windlass Mechanism: A Biomechanical Link to Clinical Practice," *Journal of Athletic Training*, vol. 39, p. 6, 2004.
- [53] Z. Jin, *Computational modelling of biomechanics and biotribology in the musculoskeletal system*. Woodhead Publishing, 2014, p. 9.
- [54] Y. Wang, Z. Li, D. W.-C. Wong, Cheng-Kung, and M. Zhang, "Finite element analysis of biomechanical effects of total ankle arthroplasty on the foot," *Journal of Orthopaedic Translation*, vol. 12, p. 11, 2017.
- [55] J. T.-M. Cheung and M. Zhang, "A 3-dimensional finite element model of the human foot and ankle for insole design," *Arch Phys Med Rehabil* vol. 86, p. 6, 2005.
- [56] S. Cutts, N. Obi, C. Pasapula, and W. Chan, "Plantar fasciitis," *Annals of The Royal College of Surgeons of England*, vol. 94, p. 4, 2012.
- [57] R. Periyasamy, Snehanand, and A. C. Ammini, "The effect of aging on the hardness of foot sole skin: A preliminary study," *The Foot*, vol. 22, no. 2, p. 5, 2012.
- [58] K. Rome, "Anthropometric and biomechanical risk factors in the development of plantar heel pain: A review of the literature," *Physical Therapy Reviews*, vol. 2, no. 3, p. 12, 1997.
- [59] J. B. J. Zwaferink, W. Custers, I. Paardekooper, H. A. Berendsen, and S. A. Bus, "Effect of a carbon reinforcement for maximizing shoe outsole bending stiffness on plantar pressure and walking comfort in people with diabetes at high risk of foot ulceration," *Gait and Posture*, vol. 86, 2021.
- [60] M. R. Zonfrillo *et al.*, "The association of overweight and ankle injuries in children," *Ambulatory Pediatrics*, vol. 8, no. 1, p. 4, 2008.
- [61] S. C. Wearing, J. E. Smeathers, P. M. Sullivan, B. Yates, S. R. Urry, and P. Dubois, "Plantar fasciitis: Are pain and fascial thickness associated with arch shape and loading?," *Physical Therapy*, vol. 87, no. 8, p. 8, 2007.

- [62] J. L. Crary, J. M. Hollis, and A. Manoli, "The Effect of plantar fascia release on strain in the spring and long plantar ligaments," *Foot & Ankle International*, vol. 24, no. 3, p. 6, 2003.
- [63] H. B. Kitaoka, Z. P. Luo, E. S. Growney, L. J. Berglund, and K.-N. An, "Material properties of the plantar aponeurosis," *Foot & Ankle*, vol. 15, p. 4, 1994.
- [64] H. Y. Cheng, C. L. Lin, H. W. Wang, and S. W. Chou, "Finite element analysis of plantar fascia under stretch-the relative contribution of windlass mechanism and Achilles tendon force," *J Biomech*, vol. 41, no. 9, pp. 1937-44, 2008, doi: 10.1016/j.jbiomech.2008.03.028.
- [65] J. T.-M. Cheung and B. M. Nigg, "Clinical applications of computational simulation of foot and ankle," *Sport Orthopadie Traumatologie*, vol. 23, p. 8, 2007.
- [66] S. J. Priesand, B. M. Schmidt, L. Ang, J. S. Wrobel, and M. Munson, "Plantar fasciitis in patients with type 1 and type 2 diabetes: Acontemporary cohort study," *Journal of Diabetes and Its Complications*, vol. 33, p. 5, 2019.
- [67] B. Y. C. Khor, J. Woodburn, L. Newcombe, and R. Barn, "Plantar soft tissues and Achilles tendon thickness and stiffness in people with diabetes: a systematic review," *Journal of Foot and Ankle Research*, vol. 14, no. 35, p. 18, 2021.
- [68] C. C. Robinson, L. F. Balbinot, M. F. Silva, M. Achaval, and M. A. Zaro, "Plantar pressure distribution patterns of individuals with prediabetes in comparison with healthy individuals and individuals with diabetes," *Journal of Diabetes Science and Technology*, vol. 7, no. 5, p. 9, 2013.
- [69] C. Giacomozzi, E. D'Ambrogi, L. Uccioli, and V. Macellari, "Does the thickening of Achilles tendon and plantar fascia contribute to the alteration of diabetic foot loading?," *Clinical Biomechanics*, vol. 20, p. 8, 2005.
- [70] D. Baur *et al.*, "Shear wave elastography of the plantar fascia: Comparison between patients with plantar fasciitis and healthy control subjects," *Journal of Clinical Medicine*, vol. 10, no. 10, p. 9, 2021.
- [71] J. Acevedo and J. Beskin, "Complications of plantar fascia rupture associated with corticosteroid injection," *Foot & Ankle Int*, vol. 19, p. 7, 1998.
- [72] B. F. Digiovanni *et al.*, "Plantar fascia-specific stretching exercise improves outcomes in patients with chronic plantar fasciitis. A prospective clinical trial with two-year follow-up," *J Bone Joint Surg Am*, vol. 88, p. 4, 2006.
- [73] A. H. A. Razak, K. S. Basaruddin, A. F. Salleh, W. M. R. Rusli, M. S. M. Hashim, and R. Daud, "Finite element modelling of plantar fascia response during running on different surface types " *Journal of Physics*, vol. 908, p. 9, 2017.
- [74] F. Ursini, F. Arturi, K. Nicolosi, A. Ammendolia, and S. D'Angelo, "Plantar fascia enthesopathy is highly prevalent in diabetic patients without peripheral neuropathy and correlates with retinopathy and impaired kidney function," *PLOS ONE*, p. 12, 2017.
- [75] E. Morales-Orcajo, T. R. Souza, J. Bayod, and E. B. d. L. Casas, "Non-linear finite element model to assess the effect of tendon forces on the foot-ankle complex," *Medical Engineering and Physics*, vol. 49, p. 8, 2017.
- [76] J. T.-M. Cheung, M. Zhang, and K.-N. An, "Effect of Achilles tendon loading on plantar fascia tension in the standing foot," *Clinical Biomechanics*, vol. 21, p. 10, 2005, doi: 10.1016/j.clinbiomech.2005.09.016.
- [77] R. E. Carslon, L. L. Fleming, and W. C. Hutton, "The biomechanical relationship between the tendoachilles, plantar facia and metatarsophalangeal joint dorsiflexion angle," *Foot & Ankle Int*, vol. 21, p. 8, 2000.
- [78] S. Siegler, J. Block, and C. D. Schneck, "The mechanical characteristics of the collateral ligaments of the human ankle joint," *Foot & Ankle*, vol. 8, p. 9, 1988.
- [79] C. L. Saltzman, D. A. Nawoczenski, and K. D. Talbot, "Measurement of the medial longitudinal arch " *Arch Phys Med Rehabil* vol. 76, p. 5, 1995.
- [80] D. Singh, J. Angel, G. Bentley, and S. G. Trevin, "Fornightly review: plantar fasciitis," *British Medical Journal*, vol. 615, p. 5, 1997.

- [81] D. L. Riddle, M. Pulisic, and K. Sparrow, "Impact of demographic and impairment-related variables on disability associated with plantar fasciitis," *Foot & Ankle International*, vol. 25, no. 5, p. 7, 2004.
- [82] Z. Pataky, J.-P. Assal, P. Conne, H. Vuagnat, and A. Golay, "Plantar pressure distribution in Type 2 diabetic patients without peripheral neuropathy and peripheral vascular disease," *Diabetic Medicine*, vol. 22, pp. 762-767, 2005.
- [83] W. R. Ledoux, Y.-N. Wang, and K. Lee, "Histomorphological evaluation of diabetic and non-diabetic plantar soft tissue," *Foot & Ankle International*, vol. 32, pp. 802-810, 2011, doi: 10.3113/FAI.2011.0802.
- [84] W. R. Ledoux, J. B. Shofer, J. H. Ahroni, D. G. Smith, B. J. Sangeorzan, and E. J. Boyko, "Biomechanical differences among pes cavus, neutrally aligned, and pes planus Feet in subjects with diabetes," *Foot & Ankle Int*, vol. 24, pp. 845-850, 2003.
- [85] A. Guiotto, Z. Sawacha, G. Guarneri, G. Cristoferi, A. Avogaro, and C. Cobelli, "The role of foot morphology on foot function in diabetic subjects with or without neuropathy," *Gait and Posture*, vol. 37, pp. 603-610, 2013.
- [86] V. K. Nandikolla, R. Bochen, S. Meza, and A. Garcia, "Experimental gait analysis to study stress distribution of the human foot," *Journal of Mechanical Engineering*, vol. 2017, p. 3432074, 2017.
- [87] A. Gefen, "Plantar soft tissue loading under the medial metatarsals in the standing diabetic foot," *Medical Engineering Physics*, vol. 25, p. 9, 2003, doi: 10.1016/S1350-4533(03)00029-8.
- [88] W.-C. Tsai, M.-F. Chiu, C.-L. Wang, F.-T. Tang, and M.-K. Wong, "Ultrasound evaluation of plantar fasciitis," *Scandinavian Journal of Rheumatology*, vol. 29(4), pp. 255-259, 2000.
- [89] Y. Wang, D. W.-C. Wong, and M. Zhang, "Computational models of the foot and ankle for pathomechanics and clinical applications: A review," *Annals of Biomedical Engineering*, vol. 44, no. 1, p. 9, 2015.
- [90] A. Gefen, M. Megido-Ravid, Y. Itzchak, and M. Arcan, "Biomechanical analysis of the three-dimensional foot structure during gait: A basic tool for clinical applications," *American Society of Mechanical Engineers (ASME)*, vol. 122, p. 10, 2000.
- [91] C. G. Fontanella, E. L. Carniel, V. Macchi, A. Porzionato, R. D. Caro, and A. N. Natali, "Biomechanical response of the plantar tissues of the foot in healthy and degenerative conditions," *Muscles, Ligaments and Tendons Journal*, vol. 7, no. 4, pp. 503-509, 2017.
- [92] T. L.-W. Chen, D. W.-C. Wong, Y. Wang, J. Lin, and M. Zhang, "Foot arch deformation and plantar fascia loading during running with rearfoot strike and forefoot strike: A dynamic finite element analysis," *Journal of Biomechanics*, vol. 83, p. 13, 2019.
- [93] V. Isvilanonda, E. Dengler, J. M. Iaquinto, B. J. Sangeorzan, and W. R. Ledoux, "Finite element analysis of the foot: Model validation and comparison between two common treatments of the clawed hallux deformity," *Clinical Biomechanics*, vol. 27, p. 8, 2012, doi: 10.1016/j.clinbiomech.2012.05.005.
- [94] D. A. Winter, "Overall principle of lower limb support during stance phase of gait," *Journal of Biomechanics*, vol. 13, p. 5, 1980.
- [95] Z. Taha, M. S. Norman, S. F. S. Omar, and E. Suwarganda, "A finite element analysis of a human foot model to simulate neutral standing on ground," *Procedia Engineering*, vol. 147, p. 6, 2016.
- [96] K. Tao *et al.*, "An in vivo experimental validation of a computational model of human foot," *Journal of Bionic Engineering*, vol. 6, p. 11, 2009.
- [97] O. A. Fawzy, A. I. Arafa, M. A. E. Wakeel, and S. H. A. Kareem, "Plantar pressure as a risk assessment tool for diabetic foot ulceration in egyptian patients with diabetes," *Clinical Medicine Insights: Endocrinology and Diabetes*, vol. 7, p. 9, 2014.
- [98] Y. Shu, Q. Mei, J. Fernandez, Z. Li, N. Feng, and Y. Gu, "Foot morphological difference between habitually shod and unshod runners," *PLoS ONE*, vol. 10, p. 13, 2015.
- [99] J. Shiota, D. Momma, T. Yamaguchi, and N. Iwasaki, "Long-term stress distribution patterns across the ankle joint in soccer players," *The Orthopaedic Journal of Sports Medicine*, p. 6, 2020.

- [100] E. S. Moore, M. W. Kindig, D. A. McKearney, S. Telfer, B. J. Sangeorzan, and W. R. Ledoux, "Hind- and midfoot bone morphology varies with foot type and sex," *Journal of Orthopaedic Research*, p. 16, 2019.
- [101] D. E. Shepherd and B. B. Seedhom, "Thickness of human articular cartilage in joints of the lower limb," *Annals of the Rheumatic Diseases*, vol. 58, 1999.
- [102] D. Al-Ali, H. Graichen, S. Faber, K.-H. Englmeier, M. Reiser, and F. Eckstein, "Quantitative cartilage imaging of the human hind foot: precision and inter-subject variability," *Journal of Orthopaedic Reserach*, vol. 20, p. 8, 2002.
- [103] K. Song, B. G. Pietrosimone, and E. A. Wikstrom, "Comparision of talar cartilage thickness between those with and without chronic ankle instability: A ultrasonography study," *Osteoarthritis and Cartilage*, 2019.
- [104] S. A. Millington, M. Grabner, R. Wozelka, D. D. Anderson, S. R. Hurwitz, and J. R. Crandall, "Quantification of ankle articular cartilage topography and thickness using a high resolution stereophotography system," *OsteoArthritis and Cartilage*, vol. 15, p. 7, 2007.
- [105] K. A. Athanasiou, G. G. Niederauer, and J. R. C. Schenck, "Biomechanical topography of human ankle cartilage " *Annals of Biomedical Engineering*, vol. 23, p. 8, 1995.
- [106] D. D. Anderson, J. K. Goldsworthy, W. Li, M. J. Rudert, Y. Tochigi, and T. D. Brown, "Physical validation of a patient-specific contact finite element model of the ankle," *Journal of Biomechanics*, vol. 40, p. 8, 2007.
- [107] N. K. Paschos, E. A. Makris, J. C. Hu, and K. A. Athanasiou, "Topographic variations in biomechanical and biochemical properties in the ankle joint: An in vitro bovine study evaluating native and engineered cartilage," *Journal of Arthroscopic and Related Surgery*, vol. 30, no. 10, p. 10, 2014.
- [108] W. L. Cher, G. M. Utturkar, C. E. Spritzer, J. A. Nunley, L. E. DeFrate, and A. T. Collins, "An analysis of changes in in vivo cartilage thickness of the healthy ankle following dynamic activity," *Journal of Biomechanics*, vol. 49, p. 5, 2016.
- [109] C. L. Brockett and G. J. Chapman, "Biomechanics of the ankle," *Orthopaedics and Trauma* vol. 30, no. 3, p. 7, 2016.
- [110] H. Gray and W. H. Lewis, *Anatomy of the human body*. Philadelphia: Lea & Febiger, 1918.
- [111] W. Kim and A. S. Voloshin, "Role of plantar fascia in the load bearing capacity of the human foot," *Journal of Biomechanics*, vol. 28, p. 9, 1995.
- [112] K. Gariani, F. W. Waibel, A. F. Viehöfer, and I. Uçkay, "Plantar fasciitis in diabetic foot patients: Risk factors, pathophysiology, diagnosis, and management," *Dove Press Journal*, vol. 13, p. 9, 2020.
- [113] R. F. Ker, M. B. Bennett, S. R. Bibbyt, R. C. Kestert, and R. M. Alexander, "The spring in the arch of the human foot " *NATURE*, vol. 325, no. 8, p. 3, 1987.



## VITA

Jinhyuk Kim

### EDUCATION

<b>Ph.D. IN MECHANICAL ENGINEERING</b>	<b>AUGUST 2022</b>
Old Dominion University, Norfolk, VA	
<b>MASTER OF SCIENCE IN MECHANICAL ENGINEERING</b>	<b>AUGUST 2017</b>
Old Dominion University, Norfolk, VA	
<b>BACHELOR OF SCIENCE IN MECHANICAL ENGINEERING</b>	<b>MAY 2014</b>
Old Dominion University, Norfolk, VA	

### PUBLICATIONS

- [1] **Jinhyuk Kim**, (2022, August). The effect of bone geometry on contact stress in 3D-finite element hindfoot model, 2022 North American Congress of Biomechanics (NACOB) , Ottawa, Canada
- [2] Issac Kumi, Michael Polanco, **Jinhyuk Kim**, (2022, August). Comparison of a spine model between two finite element programs, 2022 North American Congress of Biomechanics (NACOB), Ottawa, Canada
- [3] **Jinhyuk Kim**, (2021, August). The effect of plantar fascia thickness at different foot position in a 3-D finite element foot model, 2021 American Society of Biomechanics (ASB) 45<sup>Th</sup> Annual meeting, Virtual
- [4] Issac Kumi, Michel Polanco, **Jinhyuk Kim**, (2021, August). Comparison of results from different finite element software used in spine modeling, 2021 American Society of Biomechanics (ASB) 45<sup>Th</sup> Annual meeting, Virtual
- [5] **Jinhyuk Kim**, (2020, August). Analysis the strain of plantar fascia with different plantar fascia thickness and tendon loading in 3-D finite element foot model, 2020 American Society of Biomechanics (ASB) 44<sup>th</sup> Annual Conference, Atlanta, GA
- [6] **Jinhyuk Kim**, (2018, August). Developing the sensitivity of a human ankle joint finite element model to the thickness of cartilage, 2018 American Society of Biomechanics (ASB) Annual Conference, Rochester, MN